Holographic Fluctuations at Finite Density

A Thesis

Submitted to the
Tata Institute of Fundamental Research, Mumbai
Subject Board of Physics
for the degree of Doctor of Philosophy

by

Shivam Kumar Sharma

International Centre for Theoretical Sciences,
Tata Institute of Fundamental Research
Bengaluru, India

December, 2025

Declaration

This thesis is a presentation of my original research work. Wherever contributions of others are involved, every effort is made to indicate this clearly, with due reference to the literature, and acknowledgement of collaborative research and discussions.

The work was done under the guidance of Professor **R. Loganayagam**, at the International Centre for Theoretical Sciences of the Tata Institute of Fundamental Research, Bengaluru, India.

Shivam Kumar Sharma

Date: Dec 2, 2025

In my capacity as the formal supervisor of record of the candidate's thesis, I certify that the above statements are true to the best of my knowledge.

R. Loganayagam

Date: Dec 2, 2025

Acknowledgements

As I reflect on my PhD journey, I am deeply grateful to all those who have guided, supported, and inspired me — both academically and personally. The knowledge shared, experiences lived, people met, places visited, collaborations formed, and friendships built have all become an inseparable part of my life.

While it is impossible to thank everyone individually, I will do my best to acknowledge those who played a significant role in helping me navigate and complete this journey.

First and foremost, I would like to thank my advisor, R. Loganayagam, for his unwavering support over the years. He encouraged me to approach physics with both openness and independence. From shaping the thesis problem to guiding me through its complexities, his insights and deep understanding of the literature were invaluable. I learned from him not only how to tackle difficult problems but also when to let go of ones that weren't progressing. I fondly recall our early sessions working through Mathematica files, and his patient support as I struggled with writing. Working as his teaching assistant was also a valuable experience, even as we held different views on pedagogy. In hindsight, I wish I had interacted with him even more.

I am also deeply grateful to my collaborators — R. Loganayagam, Godwin Martin, Krishnendu Ray, and Akhil Sivakumar. In my first year, I began working with Akhil during the nationwide COVID lockdown. At a time when interactions were limited, his guidance helped me understand a project that later evolved into my thesis. I also thank my junior, Godwin, from whom I learned a great deal.

I am thankful to everyone in the string theory group at ICTS — Rajesh Gopakumar, Gautam Mandal, Raghu Mahajan, Suvrat Raju, Ashoke Sen, Spenta Wadia, and many others — for the numerous stimulating discussions. I am especially grateful to my batchmates Omkar Shetye, Priyadarshi Paul, and Tuneer Chakraborty for the discussions and learning we shared. I also deeply appreciate Bhanu, Harshit, Ankush, Uddeepta, Mahaveer, Sparsh, Ashik, Anup, Akash, and many more with whom I shared meals, games, and laughter. Life during the PhD would not have been nearly as enjoyable without them.

I would also like to thank other past and present members of the string theory group

— including Avi, Kaustubh, Joydeep, Chandramouli, Victor, Anurag, Naveen, Anupam, Athira, Rishabh, Pronobesh, Shridhar, Jyotirmoy, Shanmugapriya, and Muktajyoti — for the invaluable discussions throughout my PhD. I am also grateful to Gautam Mandal and Subhro Bhattacharjee for serving on my thesis monitoring committee and for their helpful feedback from time to time. I would further like to thank many professors from other institutes with whom I have had many discussions — including Shiraz, Alok, Ronak, Amitabh, Sandip, and Dileep — as well as other members of the Indian string theory community with whom I have interacted.

I gratefully acknowledge the broader ICTS community — the academic office, accounts office, establishment office, IT and AV teams, gardeners, canteen staff, cleaning staff, and security team — for their contributions to creating such a vibrant research environment. I am also thankful to members of other research groups, including Souvik, Aditya, Saikat, Jigyasa, Divya, Srishti, Irshad, Prateek, Shalabh, Atharva, and many others, with whom I have enjoyed my time at ICTS.

Outside of my ICTS family, I would like to thank my friends and family who supported me, directly or indirectly, throughout my PhD. I am especially thankful to my parents, Prachi and Vivek, for their unwavering support, and to my friends Banashree, Akash, Rohan, Priyanka, Diksha, and Sachin for many on- and off-topic conversations, random chats, and their steady encouragement

Finally, I would like to thank my thesis reviewers, Prof. Amos Yarom and Prof. Arnab Kundu, for their time and effort in providing comments on my thesis. I acknowledge the support of the Department of Atomic Energy, Government of India, under project no. RTI4001. I am sincerely grateful to the people of India for their continued and generous support of research in the basic sciences.

List of Figures

List of Publications

Works that are included in the thesis:

1. R. Loganayagam, Krishnendu Ray, Shivam K. Sharma, Akhil Sivakumar, *Holographic KMS relations at finite density*, JHEP 03 (2021) 233, [2011.08173].

2. Shivam K. Sharma, *Holographic Fluctuation-Dissipation Relations in Finite Density Systems*, [2501.17852], *Accepted in JHEP*.

Works that are not included in the thesis but related:

1. Godwin Martin, Shivam K. Sharma, *Open EFT for Interacting Fermions from Holography*, [2403.10604].

2. R. Loganayagam, Godwin Martin, Shivam K. Sharma, *Loops Outside a Black Hole*, [2509.03656].

Abbreviations

GR : General Relativity

AdS/CFT : Anti-de Sitter/Conformal Field Theory

AdS/CMT : Anti-de Sitter/Condensed Matter Theory

CPT : Charge-Parity-Time reversal

EFT : Effective Field Theory

SK : Schwinger-Keldysh

grSK : Gravitational Schwinger-Keldysh

RNSK : Reissner-Nordström Schwinger-Keldysh

KMS : Kubo-Martin-Schwinger

FDR : Fluctuation-Dissipation Relation

FDT : Fluctuation-Dissipation Theorem

QGP: Quark-Gluon Plasma

QFT: Quantum Field Theory

IF: Influence Functional

EF : Eddington-Finkelstein

Notations

$g_{\mu\nu}$: Metric

$\mathcal{R}_{\mu\nu}$: Ricci tensor

$\mathcal{R}$: Ricci scalar

G_N : Newton's gravitational constant

$T_{\mu\nu}$: Energy-momentum tensor of matter

$x = (t, \mathbf{x})$: Spacetime point

β : Inverse temperature

μ : Chemical potential

ζ : Mock tortoise coordinate on grSK contour

$Z_{\rm SK}$: Schwinger-Keldysh generating functional

$S_{\rm IF}$: Influence Phase

$S_{\rm os}$: On-shell action

$G^{\rm in}$: Ingoing boundary-to-bulk propagator

$G^{\rm out}$: Outgoing boundary-to-bulk propagator

$\mathbb{G}_{\rm ret}$: Retarded bulk-to-bulk propagator

$\mathbb{G}_{\rm adv}$: Advanced bulk-to-bulk propagator

$\mathbb{G}$: Bi-normalisable bulk-to-bulk propagator

Contents

Abstract

Strongly coupled quantum systems at finite density exhibit fluctuation and dissipation phenomena that are difficult to access using conventional field–theoretic techniques. This thesis employs real-time holography to develop a framework for understanding these effects through their gravitational duals. Using the AdS/CFT correspondence, we construct an open Effective Field Theory (EFT) describing probes interacting with finite-density holographic media, clarifying the interplay between Hawking fluctuations and quasinormal-mode dissipation near charged black holes that underlies fluctuation–dissipation relations (FDRs). On the gravitational side, we analyze the scattering of charged scalar fields in the AdS Reissner–Nordström background and obtain an effective exterior field theory that captures both infalling-mode dissipation and Hawking-induced fluctuations. We further develop a real-time Witten diagrammatic framework for computing n-point functions of interacting charged scalars, providing real-time correlation functions of the dual finite-temperature, finite-density CFT. Using this exterior field theory, we derive—for the first time—both linear and non-linear holographic FDRs at small but finite density, which reduce to the expected behavior in the zero-density limit. Overall, this thesis offers a comprehensive holographic description of fluctuations and dissipation in strongly coupled finite-density systems and introduces new tools for studying open quantum dynamics in gravity and holography.

Chapter 1

Introduction

1.1 Background

Not so long ago, gravity and condensed matter physics were considered entirely separate domains. Many viewed them as unrelated — each could be studied without reference to the other. While the separation is largely true, recent developments in theoretical physics suggest a deeper connection between the two than previously assumed.

Gravity is governed by Einstein's theory of General Relativity (GR) — a classical framework in which spacetime is modelled as a smooth manifold equipped with a metric. This metric defines the curvature of spacetime, which determines how matter/light moves. In turn, matter influences this curvature via its energy and momentum. As John Wheeler famously summarised:

"*Spacetime tells matter how to move; matter tells spacetime how to curve.*"[1]

The first part of this statement — how matter moves — can be derived from the appropriately generalised Newton's laws or from the principle of stationary action, both of which lead to the same equations of motion (geodesic equations). The second part, however, is what makes General Relativity unique: it treats spacetime as dynamic, and its geometry is determined by matter through Einstein's field equations:

$$\mathcal{R}_{\mu\nu} - \frac{1}{2} g_{\mu\nu} \mathcal{R} = 8\pi G_N \, T_{\mu\nu} \ , \tag{1.1}$$

[1] Quoted from *Geons, Black Holes, and Quantum Foam: A Life in Physics* by John A. Wheeler and Kenneth Ford.

where $g_{\mu\nu}$ is the metric, $\mathcal{R}_{\mu\nu}$ the Ricci tensor, and $\mathcal{R}$ the Ricci scalar, respectively. On the right-hand side, G_N is Newton's gravitational constant and $T_{\mu\nu}$ is the energy-momentum tensor of matter. This fundamental interaction between geometry and matter is beautifully illustrated in the figure 1.1 below.

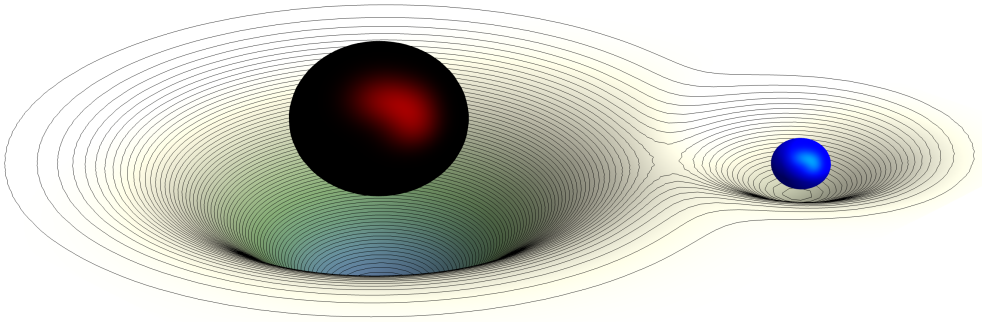

Figure 1.1: Spacetime curvature due to the presence of matter, with black and blue blobs representing massive objects that warp the surrounding geometry.

In contrast, modern condensed matter physics is deeply rooted in quantum theory, which is fundamentally different from classical physics. Despite both quantum mechanics and General Relativity emerging around the same era, gravity has eluded its incorporation into the quantum framework. Reconciling the two remains one of the biggest challenges in theoretical physics. Various approaches, such as string theory and loop quantum gravity, aim to address this.

String theory replaces point particles with extended one-dimensional objects called *strings*. It is a complete quantum theory that describes the dynamics of strings in higher-dimensional spacetime ($D > 4$). It offers a unified framework that includes gravity and quantum physics. In the last five decades, string theory has evolved into a mathematically rich structure characterised by various dualities and symmetries. However, its major weakness remains the lack of experimental validation.

Meanwhile, condensed matter physics has advanced rapidly through experimental breakthroughs, revealing a wide range of new complex materials. Theoretical progress, however, has often struggled to keep the pace — especially in understanding strongly correlated quantum many-body systems, such as those found in high-T_c superconductors and non-Fermi liquids. This began to shift when physicists started applying concepts from string theory, particularly dualities, to these systems. Most notably, the AdS/CFT

correspondence — a celebrated example of *holographic duality* — has been increasingly used to study such systems. Over the past two decades, it has offered valuable insights into the behaviour of strongly coupled quantum matter [1–3].

The AdS/CFT correspondence [4–6] is a concrete realisation of holographic duality that relates a $(d+1)$-dimensional Anti-de Sitter (AdS) spacetime to a conformal field theory (CFT) defined on its d-dimensional boundary. A schematic representation of this correspondence is shown in the figure 1.2 below.

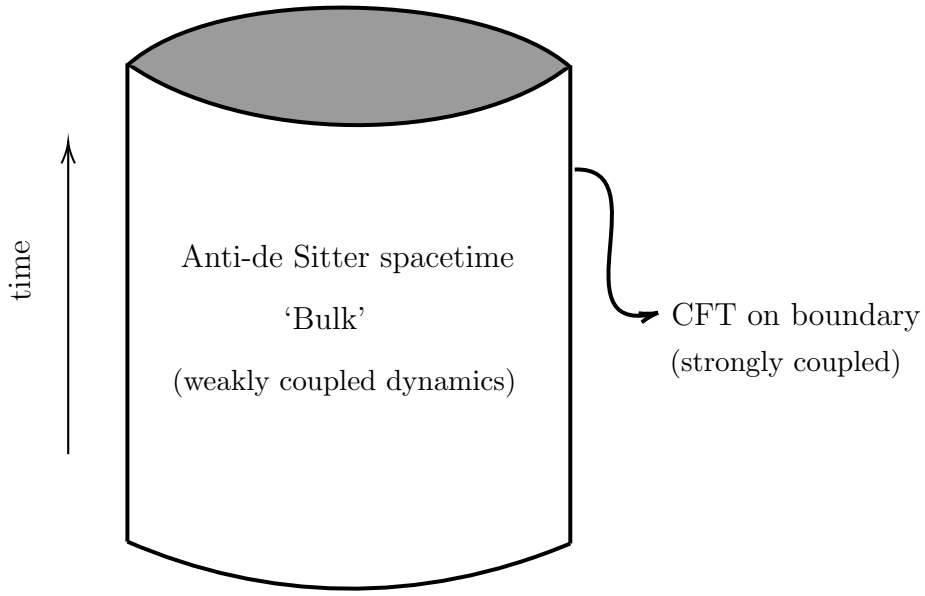

Figure 1.2: Schematic representation of the AdS/CFT correspondence. The bulk of the cylinder represents AdS spacetime, while the CFT resides on its boundary.

The most prominent example is $\mathcal{N}=4$ $SU(N)$ Super Yang–Mills (SYM) theory in $(3+1)$-dimensions and type IIB superstring theory on $\mathrm{AdS}_5 \times S^5$.[2] The parameters on the 'AdS' side are string coupling g_s and string length l_s, and the parameters on the 'CFT' side are rank N and gauge coupling constant g_{YM}. Then, these parameters under the correspondence are identified as:

$$2\pi g_s = g_{YM}^2 \ , \qquad \text{and} \qquad \left(\frac{l_{\mathrm{AdS}}}{l_s}\right)^4 = 2g_{YM}^2 N \equiv 2\lambda \ , \tag{1.2}$$

where λ is called 't Hooft coupling, given by $\lambda = g_{YM}^2 N$. These identifications provide just a glimpse into the rich structure of the correspondence. We direct the readers to look [7–9] for a detailed review on the AdS/CFT correspondence.

[2]The radius of sphere S^5 is same as that of AdS_5 and denoted by l_{AdS}.

Depending on the restriction on parameters, there exist many forms of AdS/CFT correspondence, as shown in the table (taken from [1]) below–

AdS/CFT	$\mathcal{N}=4$ **SYM theory**	**IIB theory on** $AdS_5 \times S^5$
Strongest form	any N and λ	Quantum string theory, $g_s \neq 0$, $\frac{l_s}{l_{\text{AdS}}} \neq 0$
Strong form	$N \to \infty$, λ fixed but arbitrary	Classical string theory, $g_s \to 0$, $\frac{l_s}{l_{\text{AdS}}} \neq 0$
Weak form	$N \to \infty$, λ large	Classical supergravity, $g_s \to 0$, $\frac{l_s}{l_{\text{AdS}}} \to 0$

In the 't Hooft limit ($N \to \infty$ with fixed λ), the strongly coupled SYM theory (regime where $\lambda \to \infty$) is mapped to weakly coupled classical supergravity in AdS. This is the essence of what makes the AdS/CFT correspondence a *strong/weak duality*, often also referred to as *gauge/gravity duality*, as illustrated in figure 1.2.

While the duality was originally formulated within the framework of string theory, much of its structure is more general and can be expressed in the language of boundary quantum field theory (QFT) and bulk gravitational physics. A central feature of the correspondence is the one-to-one mapping between single-trace primary operators $\mathcal{O}$ in the boundary theory and dynamical fields ϕ in the bulk. This mapping enables the computation of boundary correlation functions by studying the dynamics of bulk fields.

This relationship is formalised in the *holographic dictionary*, as first introduced by Gubser, Klebanov, Polyakov, and Witten (and hence referred to as the GKPW dictionary) [5, 6], which asserts:

$$\left\langle \exp\left(\int d^d x\, J(x)\mathcal{O}(x)\right)\right\rangle_{\text{QFT}} = Z_{\text{grav}}\left[\phi\big|_{\partial\text{AdS}} = J\right], \tag{1.3}$$

where $J(x)$ is a source coupled to the boundary operator $\mathcal{O}(x)$, and Z_{grav} is the gravitational partition function evaluated with the boundary condition $\phi|_{\partial\text{AdS}} = J$.

In the semiclassical (large-N, strong-coupling) limit, the Z_{grav} is well-approximated by its saddle point,

$$Z_{\text{grav}}[\phi|_{\partial\text{AdS}} = J] \approx \exp\left(iS_{\text{on-shell}}[\phi]\right), \tag{1.4}$$

where $S_{\text{on-shell}}$ is the classical bulk action evaluated on the solution ϕ that satisfies the prescribed boundary condition.

This correspondence forms the foundation for computing correlation functions in strongly coupled boundary theories via classical gravitational dynamics in the bulk.

Specifically, the generating functional for correlators of a boundary operator $\mathcal{O}$ is given by the on-shell value of the dual bulk action evaluated with appropriate boundary conditions. This principle will be used extensively throughout this work.

More broadly, holography maps strongly coupled boundary dynamics to weakly coupled bulk gravity, offering a powerful framework to study otherwise intractable quantum systems. The GKPW prescription enables the computation of boundary correlators from the bulk on-shell action. Notably, black holes in the bulk are dual to thermal states on the boundary [10], allowing the study of finite-temperature, strongly correlated systems via classical gravity [11–15]; for reviews, see [16–20]. As a result, gravity and condensed matter theory (CMT) — once seen as disconnected to one another — are now linked through holography, giving rise to the emerging subfield known as AdS/CMT (Anti-de Sitter/Condensed Matter Theory) [21, 22].

After this background, we now move towards the thesis problem and its motivation.

1.2 Motivation & Problem

Finite–density systems are all around us — they are not only indispensable for understanding the universe but also deeply fascinating. These systems arise in a wide range of physical contexts, from high-energy physics to condensed matter physics, and even in astrophysics (e.g., neutron stars). Yet many of these systems remain only partially understood, and their dynamics continue to challenge our theories. Here are a few notable examples:

1. **High-energy physics:** The *quark-gluon plasma* (QGP) at finite baryon density, a state of matter relevant for heavy-ion collisions and early-universe cosmology.

2. **Condensed matter physics:** Exotic states of matter, such as *non-Fermi liquids* (Strange metals)[3] and high-temperature superconductors (Cuprates), where finite density plays a crucial role.

In these systems, not only is it difficult to calculate transport coefficients like conductivity and viscosity, but even understanding their responses to external perturbations can be highly non-trivial. This difficulty can be traced to two inter-related features. First,

[3]Non-Fermi liquids deviate from conventional Landau's Fermi liquid theory [23], which assumes Fermi's surface and well-defined quasiparticles to describe metallic behaviour.

the absence of a well-defined *quasiparticle* description [24, 25] means that excitations cannot be treated as weakly interacting particle-like entities, a cornerstone of traditional condensed matter theory. Second, the strong coupling present in these systems prevents the use of conventional perturbative techniques that typically rely on small interaction strengths. Instead, their collective behaviour emerges from highly entangled many-body dynamics that defy standard analytic methods [26–29].

One prominent manifestation of these difficulties is the appearance of strange metallic behaviour where resistivity scales linearly with temperature [30, 31], violating the expectations of Fermi liquid theory, and the breakdown of the Wiedemann-Franz (WF) law[4] [32], which relates electrical and thermal conductivities in conventional metals. These anomalies point to fundamentally new transport mechanisms that remain elusive in standard theoretical frameworks.

Holographic techniques, inspired by the AdS/CFT correspondence, offer a promising lifeline with solvable toy models for addressing these challenges [3, 20]. By mapping strongly coupled boundary dynamics to weakly coupled gravitational problems in higher-dimensional spacetimes, they provide a tractable approach to computing correlation functions, transport coefficients, and response functions via classical gravity calculations. In particular, black hole geometries in the bulk play a central role: they naturally encode thermal physics and can mimic finite-density systems through appropriate gauge field configurations in the bulk.

This powerful connection has enabled significant progress in understanding finite-density, strongly correlated systems using holography, as evidenced by the growing body of work in the AdS/CMT literature [33–41]. As a result, black holes — once regarded primarily as objects in high-energy physics and astrophysics — have emerged as useful tools in the study of condensed matter systems, highlighting the deep and surprising interplay between gravity and quantum many-body physics. Interestingly, black holes have also become valuable tools in the context of open systems, where the dynamics of a subsystem (the *probe*) is coupled to a strongly interacting *bath*.

Building on these insights, recent developments have applied effective field theory (EFT) techniques [42, 43] to study dynamics within these holographic models [44–46]

[4]The WF law states that the ratio of thermal conductivity κ to electrical conductivity σ (scaled by temperature) is a constant. This holds because both charge and heat are transported by the same well-defined quasiparticles.

by analysing the behaviour of probe fields (such as electrons) coupled to a strongly interacting background. This naturally leads to the perspective of *open effective field theories* (open EFTs). Here, the strongly coupled *bath* is modelled holographically, while a separate EFT is constructed for the probe, capturing its essential dynamics. Because holographic baths are strongly interacting and therefore highly dissipative — often described as "maximally forgetful" — they typically produce a local EFT for the probe. In contrast, weakly coupled baths tend to retain long-lived correlations (i.e., "memory"), resulting in non-local EFTs. This distinction highlights the unique value of holography in constructing local open EFTs [47–50].

A particularly illustrative example is the quark-gluon plasma (QGP) at finite density. Modelling the QGP as a holographic bath allows one to systematically extract its influence on a probe (e.g., a quark or an electron). This influence is encoded in the *influence functional* [51], which captures both dissipative and stochastic effects. This functional is typically derived using the *Schwinger-Keldysh/real-time* formalism — a framework especially well-suited for computing real-time correlation functions in out-of-equilibrium scenarios, a topic we will explore in detail in the next chapter.

Taken together, these insights naturally lead to a crucial set of questions:

How does holography work in the Schwinger-Keldysh/real-time formalism? Does real-time holography exist in a rigorous sense?

The study of *real-time holography* itself has a rich history, beginning with the seminal works of Son-Starinets, Skenderis-van Rees, and others [52–56]. In this context, real-time holography refers to methods inspired by the Gibbons-Hawking prescription[5] [57] for computing real-time observables in gravitational systems. However, these earlier approaches did not fully incorporate fluctuations or Hawking radiation in the bulk, which are essential for describing dissipation and noise in the boundary theory.

To address this gap, authors in [58] proposed a gravitational dual to the Schwinger-Keldysh formalism of quantum field theory, known as the *grSK geometry*. Concretely, they conjectured that the real-time gravitational path integral is dominated by a geometry in which two copies of the black hole exterior are glued together along their future

[5]The Gibbons-Hawking prescription relates a thermal QFT partition function to the Euclidean on-shell action of a gravitational spacetime via analytic continuation to Euclidean time and regularity at the horizon.

horizons, as illustrated in figure 1.3. This construction captures both the real-time evolution and the Hawking-like fluctuations necessary to reproduce dissipative dynamics in the dual field theory. We will explain the grSK geometry and discuss its validity in the next chapter.

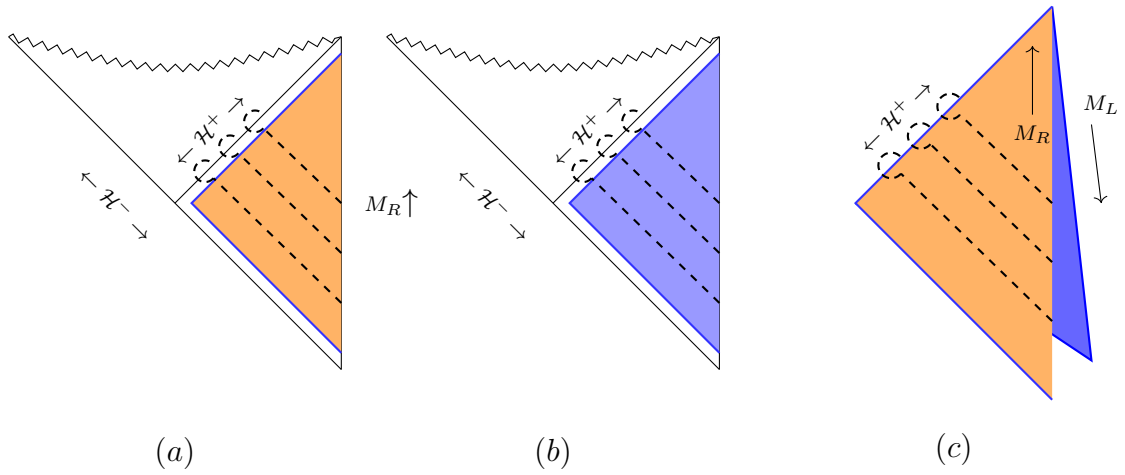

Figure 1.3: Schematic construction of grSK geometry via Penrose diagrams: Figures (a) and (b) show two copies of the AdS black hole, respectively. Figure (c) represents the grSK geometry.

These advances in real-time holography have paved the way for the development of open EFTs in strongly coupled settings [47, 48]. Nevertheless, extending these results to finite-density systems — such as those relevant to the quark-gluon plasma, high-temperature superconductors, and non-Fermi liquids — remained an open challenge until recent years.

From the bulk perspective, the studies of such systems correspond to scattering processes against a black hole background, considering the often overlooked influence of *Hawking radiation* [59]. The grSK geometry captures these thermal fluctuations in a gravitationally consistent way. Its validity has been confirmed across a wide range of contexts [47–50, 60–69], offering a framework that naturally encodes both the thermality and the microscopic unitarity of holographic systems. In [70, 71], it has been recently shown that the grSK results for boundary correlators align with Witten diagrammatics, suggesting an *exterior field theory* for theories without any derivative interactions. It is worth noting that grSK inherently provides an exterior field theory, a presumption made in earlier studies [33, 40, 46].

Since charged black holes provide the gravitational duals of finite-density systems, it is

natural to seek a generalisation of the grSK framework to such backgrounds. However, it is not immediately clear how to extend grSK to include charged black holes. In particular, the presence of multiple horizons raises questions about how the glueing procedure should be modified.

To address this, we propose the *RNSK geometry* — a real-time extension of the Reissner–Nordström black hole geometry adapted to the Schwinger–Keldysh contour [49]. We will present the details of this construction in chapter 3. This prescription provides a gravity dual to the Schwinger–Keldysh formalism at non-zero chemical potential, allowing us to study fluctuation and dissipation phenomena in holographic systems at finite density.

A key question now arises: Can we compute real-time correlation functions purely from an *exterior field theory* — that is, a theory defined entirely outside the black hole horizon — even at finite density? As we will see later, the answer is affirmative, as explicitly demonstrated in [72]. Much like the zero-density case [70], this construction remains valid and continues to encode the essential physics of thermal fluctuations.

The presence of Hawking radiation in finite-density backgrounds prompts a deeper question:

How are these fluctuations related to the dissipative behaviour governed by quasi-normal modes?

Since any thermal system must obey a version of the *fluctuation-dissipation theorem* (FDT), establishing its precise form in this setting could offer new insights into the real-time dynamics of strongly coupled finite-density systems. In what follows, we will highlight the distinction between linear and non-linear versions of the FDT,[6] and examine how they emerge from the holographic perspective.

Linear FDT has been extensively studied in systems ranging from weakly to strongly coupled regimes. A classic example is Brownian motion described by the following Langevin's equation for variable q:

$$\ddot{q} + \gamma\dot{q} = \mathfrak{f}\,\eta(t)\ , \tag{1.5}$$

[6] As the names suggest, the linear and non-linear FDT relate the linear and non-linear fluctuation and dissipation coefficients of a system's dynamical equations, respectively.

with linear FDT given by,

$$\frac{2}{\beta}\gamma = \mathfrak{f} \,, \tag{1.6}$$

where γ is the damping coefficient, β denotes inverse temperature, η denotes noise and $\mathfrak{f}$ measures fluctuation strength. The intuition behind this relation is that random kicks from the environment not only slow down the particle's motion but also generate fluctuations in the form of noise. The FDT then asserts that, on average, the energy injected by these stochastic forces exactly balances the energy dissipated through damping. At a more fundamental level, this relationship is rooted in equilibrium statistical mechanics: the linear FDT follows directly from the two-point Kubo-Martin-Schwinger (KMS) condition [73, 74] (see [75] for detailed derivation of FDT from KMS condition).

However, calculating non-linear FDTs in strongly coupled field theories remains highly challenging and has only been carried out up to a certain order. Recent developments in grSK geometry have enabled the computation of non-linear FDTs at zero density to arbitrary order [47]. As of now, this is the only known method capable of deriving non-linear FDTs at all orders, with higher-order results remaining unverified by any other approach.

Regarding non-linear FDTs at finite density, to the best of our knowledge, they have not yet been explored in the context of strongly coupled field theories, e.g. holographic theories. This naturally raises two key questions:

Do non-linear holographic FDTs exist at finite density? And if they do, how do they differ from their zero-density counterparts?

As we will demonstrate, the answer to the first question is in affirmative [72].

We conclude the introduction with a brief comment on the physical implications of non-linear FDTs at finite-density. FDTs are particularly important for strongly interacting systems at non-zero chemical potential — such as non-Fermi liquids, dense plasmas, and neutron star — where the presence of a finite density can qualitatively alter both correlations and response functions. In such settings, non-linear FDTs become essential because they relate transport coefficients not only to two-point functions but also to higher-order correlations. This is especially relevant in regimes where linear response theory breaks down, for instance near critical points, where fluctuations become large, non-Gaussian, and beyond the reach of mean-field descriptions. In these regimes, the

linear FDT is no longer sufficient, and non-Gaussian corrections play a central role in determining transport, noise, and dissipation. For these reasons, finite-density non-linear FDRs are important both for theoretical analyses and for interpreting experimental data in complex quantum systems.

Outline

In this work, we begin with an introduction in chapter 1, where we outline the background, motivation, and the central problem under investigation.

Chapter 2 reviews the Schwinger–Keldysh (SK) formalism in quantum field theory and describes its gravitational realization within the AdS/CFT correspondence.

In chapter 3, we present our prescription for the gravitational dual of the SK formalism in finite-density systems, which we refer to as the RNSK geometry. We study free fields in this background and explain how to compute real-time boundary correlators. We also perform various consistency checks on the geometry.

In chapter 4, we move beyond the free-field approximation by introducing interactions through a self-interacting complex scalar field. We demonstrate how an effective field theory localised outside the black hole horizon emerges and reproduces the full boundary SK generating functional.

With the generating functional at hand, we turn in chapter 5 to the computation of fluctuation–dissipation relations in our holographic setup. After reviewing the fluctuation–dissipation theorem through the examples of a Brownian particle and a zero-density holographic system, we present our results for holographic fluctuation–dissipation relations at finite density. These are then compared to the corresponding relations at zero density.

Finally, the chapter 6 summarises our findings and outlines possible directions for future work.

Detailed calculations and technical derivations omitted from the main text are provided in the appendices.

Chapter 2

Schwinger-Keldysh formalism in Holography

In this chapter, we will begin with a brief review of the Schwinger-Keldysh formalism in quantum field theory. Along the way, we will establish the notational conventions similar to those given in [76] that will be used throughout the remainder of the discussion. We will then highlight the relevance of this formalism in the study of open quantum systems. Later in the chapter, we will examine the role of the Schwinger-Keldysh framework in holography, focusing on the central question:

What is the gravitational dual of the Schwinger-Keldysh formalism ?

Throughout this chapter, we only focus on the Schwinger-Keldysh formulation for bosonic field theories, though the formalism can be readily extended to fermionic cases. We now proceed to outline the basic structure of the formalism.

2.1 Schwinger-Keldysh formalism

The Schwinger–Keldysh formalism [77, 78] offers a powerful real-time framework for studying non-equilibrium phenomena in quantum field theory.[1] One of its key strengths lies in its ability to systematically incorporate fluctuations, making it indispensable in out-of-equilibrium settings. Unlike conventional approaches that focus on transition amplitudes between initial and final states, the Schwinger–Keldysh formalism is designed to

[1] For textbook-level discussions, see [75, 79–81].

compute expectation values and correlation functions without reference to a final state — hence the name "in-in" formalism, particularly common in cosmological contexts.

The key idea is to evolve both forward and backward in time along a *closed time contour* $\mathcal{C}$ in the complex time plane, as depicted in figure 2.1 below–

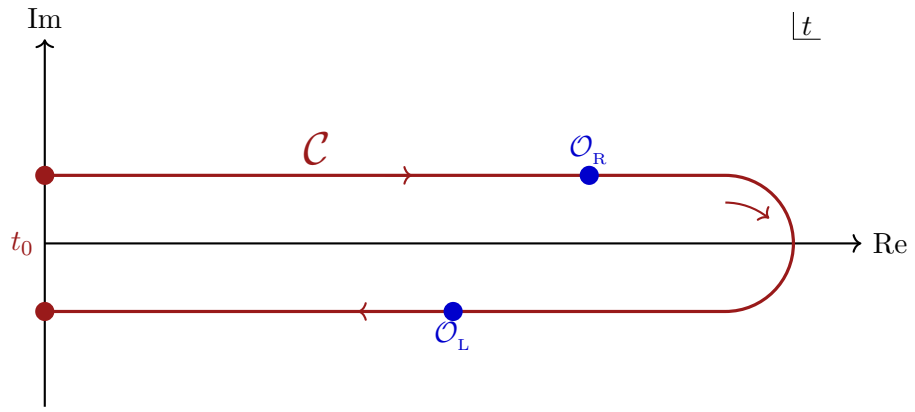

Figure 2.1: Closed time contour $\mathcal{C}$ starting at the initial time t_0, with two operator insertions: $\mathcal{O}_{\rm R}$ on the forward (right) branch and $\mathcal{O}_{\rm L}$ on the backward (left) branch. The end-points are used for the preparartion of initial state.

The contour $\mathcal{C}$ starts out from $t = t_0 + i\epsilon$ and moves horizontally till $t = \infty + i\epsilon$ and then takes a turn in imaginary direction till $t = \infty - i\epsilon$ and starts moving back to $t = t_0 - i\epsilon$.[2] For later importance, note that the end-points of the contour are not identified. The corresponding *contour-ordered* evolution operator $U_{\mathcal{C}}$ is given by,

$$U_{\mathcal{C}} = \mathcal{T}_{\mathcal{C}} \exp\left(-i \oint_{\mathcal{C}} H_{\rm int}(t')\, dt'\right) , \tag{2.1}$$

where $H_{\rm int}$ is the interaction Hamiltonian and the integration parameter t' runs over the contour specified in the above diagram. Here, the symbol $\mathcal{T}_{\mathcal{C}}$ refers to contour time–ordering, which we will explain in a moment. Note that we have suppressed the dependence on spatial direction $\mathbf{x}$ in the Hamiltonian.

Using the contour-ordering, we can now write down the associated Schwinger-Keldysh (SK) two-point Green's functions of a bosonic operator[3] $\mathcal{O}$ as:

$$G_{\mathcal{C}}(t_1, t_2) = -i \langle\Omega|\mathcal{T}_{\mathcal{C}}\{\mathcal{O}(t_1)\mathcal{O}(t_2)\}|\Omega\rangle \ , \qquad \text{where} \quad t_1, t_2 \in \mathcal{C} \ , \tag{2.2}$$

[2]Unless otherwise stated, we assume that the initial time is taken to be far in the past, i.e., $t_0 = -\infty$ throughout this work.

[3]The operator $\mathcal{O}$ could also be composite, i.e. made up of the fundamental fields present in the QFT.

where $|\Omega\rangle$ is the ground state of the full interacting theory. Note that our convention for the Green's function corresponds to the inverse Laplacian operator (rather than minus the inverse Laplacian operator, as is common in literature), as shown below[4]

$$G = \Box^{-1} \ , \qquad \text{where} \quad \Box \equiv \partial^2 = -\partial_t^2 + \nabla^2 \ . \tag{2.3}$$

Note that we are working in a mostly positive signature.

This SK contour $\mathcal{C}$ has *forward* as well as *backward* time-evolving parts and is useful to label them as right R and left L parts, respectively. It is also convenient to think of fields/operators $\mathcal{O}$ and sources J living on this contour, as divided into these two different parts, given as follows:

$$\begin{aligned} \mathcal{O}(t+i\epsilon) &\equiv \mathcal{O}_{\text{R}}(t) \ , & \mathcal{O}(t-i\epsilon) &\equiv \mathcal{O}_{\text{L}}(t) \ , \quad \forall \quad t \in \mathbb{R} \ , \\ J(t+i\epsilon) &\equiv J_{\text{R}}(t) \ , & J(t-i\epsilon) &\equiv J_{\text{L}}(t) \ , \quad \forall \quad t \in \mathbb{R} \ , \end{aligned} \tag{2.4}$$

where t runs over the real axis. Then, the analysis becomes exactly similar to working with a doubled number of fields, and the SK two-point Green's function can be thought of as a 2×2 matrix, given by:

$$G_{\mathcal{C}} = \begin{pmatrix} G_{\text{RR}} & G_{\text{RL}} \\ G_{\text{LR}} & G_{\text{LL}} \end{pmatrix} \ , \tag{2.5}$$

where the subscript denotes the position of operator insertion on the SK contour.

In contour ordering, the *standard time* increases along the arrow on the upper part of the contour and decreases along the arrow on the lower part. Moreover, any point on the lower part is considered to have greater *contour time* than any point on the upper part. Then, it is not hard to check that the following holds:

$$\begin{aligned} G_{\text{RR}}(t_1, t_2) &= -i \, \langle \Omega | \mathcal{T}\{\mathcal{O}(t_1)\mathcal{O}(t_2)\} | \Omega \rangle \equiv G_F \ , \\ G_{\text{RL}}(t_1, t_2) &= -i \, \langle \Omega | \mathcal{O}(t_2)\mathcal{O}(t_1) | \Omega \rangle \equiv G_< \ , \\ G_{\text{LL}}(t_1, t_2) &= -i \, \langle \Omega | \overline{\mathcal{T}}\{\mathcal{O}(t_1)\mathcal{O}(t_2)\} | \Omega \rangle \equiv G_{\bar{F}} \ , \\ G_{\text{LR}}(t_1, t_2) &= -i \, \langle \Omega | \mathcal{O}(t_1)\mathcal{O}(t_2) | \Omega \rangle \equiv G_> \ , \end{aligned} \tag{2.6}$$

[4]Throughout this work, we adopt the mostly positive signature convention for the spacetime metric.

where $\mathcal{T}$ and $\overline{\mathcal{T}}$ represent the time ordering and the anti-time ordering in real-time, respectively. In standard QFT textbooks [82, 83], G_F and $G_{\bar{F}}$ are Feynman and anti-Feynman propagators and $G_{<,>}$ are two different Wightman functions.

These Green's functions are not independent of each other; rather, they are related by the following relation,

$$G_F + G_{\bar{F}} = G_< + G_> \ , \tag{2.7}$$

which can be easily checked using the time-ordering property. For instance, writing the Feynman propagator and the anti-Feynman propagator in terms of Wightman functions as,

$$\begin{aligned} G_F(t_1,t_2) &= \Theta(t_1 > t_2) G_>(t_1,t_2) + \Theta(t_2 > t_1) G_<(t_1,t_2) \ , \\ G_{\bar{F}}(t_1,t_2) &= \Theta(t_2 > t_1) G_>(t_1,t_2) + \Theta(t_1 > t_2) G_<(t_1,t_2) \ , \end{aligned} \tag{2.8}$$

where $\Theta(t > t')$ represents the Heavyside step function.

It is useful to define another basis called the *average-difference* basis,[5] where some of the physical properties (like the relationship given in (2.7)) are manifested. In this basis, the operators/fields/sources are defined as,

$$\begin{aligned} \mathcal{O}_a &\equiv \frac{\mathcal{O}_{\rm R} + \mathcal{O}_{\rm L}}{2} \ , & \mathcal{O}_d &\equiv \ \mathcal{O}_{\rm R} - \mathcal{O}_{\rm L} \ , \\ J_a &\equiv \frac{J_{\rm R} + J_{\rm L}}{2} \ , & J_d &\equiv \ J_{\rm R} - J_{\rm L} \ , \end{aligned} \tag{2.9}$$

give rise to SK two-point Green's functions as:

$$\begin{aligned} G_{dd}(t_1,t_2) &= 0 \ , \\ G_{ad}(t_1,t_2) &= -i\,\Theta(t_2 > t_1)\,\langle\Omega|[\mathcal{O}(t_2),\mathcal{O}(t_1)]|\Omega\rangle \equiv G_{\rm ret} \ , \\ G_{da}(t_1,t_2) &= -i\,\Theta(t_1 > t_2)\,\langle\Omega|[\mathcal{O}(t_1),\mathcal{O}(t_2)]|\Omega\rangle \equiv G_{\rm adv} \ , \\ G_{aa}(t_1,t_2) &= -\frac{i}{2}\,\langle\Omega|\{\mathcal{O}(t_1),\mathcal{O}(t_2)\}|\Omega\rangle \equiv G_{\rm kel} \ , \end{aligned} \tag{2.10}$$

where $\{G_{\rm ret}, G_{\rm adv}, G_{\rm kel}\}$ are the retarded, advanced and Keldysh two-point Green's functions. In the 2×2 matrix notation, we can write the contour-ordered Green's function

[5] In literature [79] the average-difference basis is also referred to as Keldysh basis or Keldysh rotation

as,

$$G_{\mathcal{C}} = \begin{pmatrix} G_{aa} & G_{ad} \\ G_{da} & G_{dd} \end{pmatrix} = \begin{pmatrix} G_{\rm kel} & G_{\rm ret} \\ G_{\rm adv} & 0 \end{pmatrix} \ . \tag{2.11}$$

The retarded (advanced) 2-point Green's function $G_{\rm ret}(G_{\rm adv})$ tells about the causal (acausal) response while Keldysh 2-point correlator $G_{\rm kel}$ contains the statistical information and tells about the fluctuations in field theory. Note the fact that $G_{dd} = 0$ is the direct consequence of Eq. (2.7) when expressed in the average-difference basis. Thus, SK formalism naturally gives out all real-time correlators without getting into any analytical continuation arguments.

Similarly, we can easily write down the higher point functions. An n-point SK Green's function can be obtained by inserting n operators inside the contour ordering, leading to a $2n \times 2n$ matrix. To systematically extract these correlators, it is useful to introduce the SK generating functional, from which all SK correlators can be derived via functional differentiation. Thus, we now turn to the discussion of this generating functional and its properties.

2.1.1 Schwinger-Keldysh generating functional

Before we start writing correlators in any particular state, let us for once write the general SK generating functional for an arbitrary initial density matrix ρ,

$$Z_{\rm SK} = \int \mathcal{D}\mathcal{O}\ \rho\left(\mathcal{O}_{\rm R}(t_0), \mathcal{O}_{\rm L}(t_0)\right) \exp\left[i \oint_{\mathcal{C}} \left(\mathcal{L}[\mathcal{O}] + J\,\mathcal{O}\right)\right] . \tag{2.12}$$

where t_0 is the initial time as shown in figure 2.1. Here $\mathcal{L}$ is the Lagrangian for the field/operator of interest, and J is the source defined along the SK contour, with the contour integral defined as:

$$\oint_{\mathcal{C}} \equiv \int dt_{\mathcal{C}}\ d^{d-1}\mathbf{x}\ , \tag{2.13}$$

where $t_{\mathcal{C}}$ is the contour time. Here, we have suppressed the spacetime dependence in the expression for the SK generating functional. A similar expression can be written down for pure initial states also, see [75, 79–81] for more details.

Let us begin with correlations in the vacuum state. To calculate vacuum SK correla-

tors, the SK generating function $Z_{\rm SK}$ is given by,

$$Z_{\rm SK}[J] = \langle\Omega|\mathcal{T}_{\mathcal{C}} \exp\left(i \oint_{\mathcal{C}} \Big[\mathcal{L}[\mathcal{O}] + J\,\mathcal{O}\Big]\right)|\Omega\rangle \ , \tag{2.14}$$

Now, writing the SK generating functional in the Right-Left (RL) basis as,

$$Z_{\rm SK}[J_{\rm R}, J_{\rm L}] = \langle\Omega|\mathcal{T}_{\mathcal{C}} \exp\left(i \int \Big[\mathcal{L}[\mathcal{O}_{\rm R}] - \mathcal{L}[\mathcal{O}_{\rm L}] + J_{\rm R}\,\mathcal{O}_{\rm R} - J_{\rm L}\,\mathcal{O}_{\rm L}\Big]\right)|\Omega\rangle \ , \tag{2.15}$$

where we have used the following notation,

$$\int \equiv \int d^d x = \int dt\ d^{d-1}\mathbf{x} \ . \tag{2.16}$$

Note that in the expression for the generating functional, the sign difference in the terms associated with the left (L) segment arises from the orientation of the SK contour. The underlying reason behind this orientation is the fact that ket and bra states evolve oppositely in time. The same SK generating functional in the average-difference basis, $Z_{\rm SK}[J_a, J_d]$, is given by–

$$\langle\Omega|\mathcal{T}_{\mathcal{C}} \exp\left(i \int \left\{\mathcal{L}\left[\mathcal{O}_a + \frac{\mathcal{O}_d}{2}\right] - \mathcal{L}\left[\mathcal{O}_a - \frac{\mathcal{O}_d}{2}\right] + J_a\,\mathcal{O}_d + J_d\,\mathcal{O}_a\right\}\right)|\Omega\rangle \ . \tag{2.17}$$

More generally, one should work with density matrices rather than pure states in Hilbert space. Accordingly, the SK generating functional is given by,

$$Z_{\rm SK}[J_{\rm R}, J_{\rm L}] = {\rm Tr}\left[U[J_{\rm R}]\,\hat{\rho}_{\rm initial}\ (U[J_{\rm L}])^\dagger\right] \tag{2.18}$$

where $\hat{\rho}_{\rm initial}$ denotes the initial density matrix of the system. Here, we have expressed the contour evolution in terms of the right-left basis, given by:

$$\begin{aligned} U[J] &= \mathcal{T} \exp\left(-i \int_{t_i}^{t} dt'\ H[J]\right) \ , \\ (U[J])^\dagger &= \bar{\mathcal{T}} \exp\left(i \int_{t_i}^{t} dt'\ H[J]\right) \ , \end{aligned} \tag{2.19}$$

where t_i denotes the time at which the initial state is prepared. For notational simplicity, we have dropped the subscript on the Hamiltonian indicating the interaction picture. We

can then functionally differentiate this generating functional,

$$\frac{1}{Z_{\rm SK}}\prod_{i=1}^{n}\left(\frac{-i\ \delta}{\delta J_{\rm R}(x_i)}\right)\prod_{i=n+1}^{m}\left(\frac{i\ \delta}{\delta J_{\rm L}(x_i)}\right)Z_{\rm SK}\Big|_{J_{\rm R}=J_{\rm L}=0}\ , \tag{2.20}$$

to obtain m-point SK correlators of the following type,

$$\text{Tr}\ \left[\hat{\rho}_{\rm initial}\ \mathcal{T}\Big(\mathcal{O}_1\mathcal{O}_2\ldots\mathcal{O}_n\Big)\ \bar{\mathcal{T}}\Big(\mathcal{O}_{n+1}\mathcal{O}_{n+2}\ldots\mathcal{O}_m\Big)\right]\ , \tag{2.21}$$

where we have denoted $\mathcal{O}_i \equiv \mathcal{O}(x_i)$.

From the above definition of the SK generating functional, we see that the following relation holds:

$$Z_{\rm SK}[J_{\rm R}=J_{\rm L}]=1 \qquad \text{or} \quad Z_{\rm SK}[J_d=0]=1\ , \tag{2.22}$$

where we have used the cyclicity of the trace, the unitarity $U^\dagger U=1$ and the normalization of the density matrix, in that order in Eq. (2.18). This relation is called the Schwinger-Keldysh *collapse* rule: it states that forward and backward evolution cancel each other if the sources are equal on both legs. At the level of two-point functions, this leads directly to Eq. (2.7). For higher-point functions, the collapse rule is most transparent in the average-difference basis, where it implies that any correlator involving only difference operators vanishes, i.e., $G_{dd\ldots d}=0$.[6]

In our discussion, we will be interested in the thermal state as the initial state, and the thermal density matrix is given by $\rho_\beta = e^{-\beta H}$. Such a state amounts to an Euclidean segment of imaginary time evolution with the compact circle of size given by inverse temperature β. Then, adding this Euclidean compact segment to the previous SK contour, the SK contour at finite temperature is given by,

[6]This collapse condition is the *largest time equation*, see section (2.4.2) of [81] for further discussion on it.

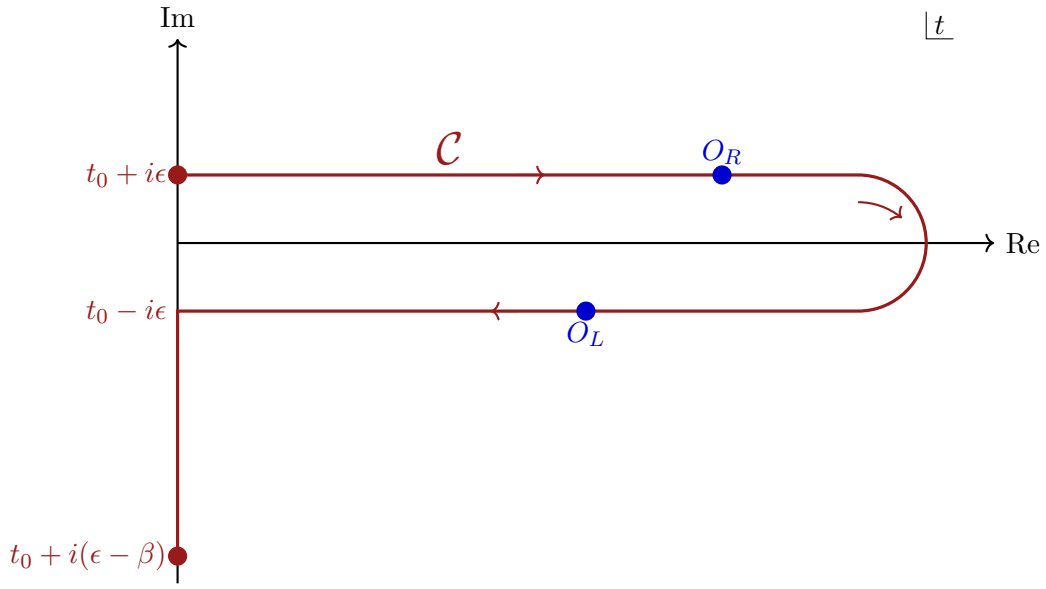

Figure 2.2: The SK contour at finite temperature $T = \frac{1}{\beta}$ where starting and end points of the contour are identified. The direction of the arrow represents the direction of contour time $t_{\mathcal{C}}$, involving both forward (R) and backward (L) time-evolving parts.

Let me begin by clarifying an important point: the $\beta \to 0$ limit of figure 2.2 *does not* reproduce figure 2.1. In fact, the figure 2.1 does not represent the vacuum state. It contains two endpoints, each of which must still be used to assign a state, e.g., a density matrix. In the genuine zero-temperature limit ($\beta \to \infty$), the thermal Euclidean circle S^1_β decompactifies, and the imaginary-time direction becomes non-compact. This reproduces the standard Euclidean definition of the vacuum: vacuum correlation functions are computed from a path integral defined on a non-compact imaginary-time axis, where the limits $t_E \to \pm\infty$ project onto the ground state. Thus, the $\beta \to \infty$ limit of the thermal formalism reduces smoothly to the Euclidean vacuum path integral.

We now conclude this section with a quick review of the path integral formulation of the SK formalism. In this approach, the path integral evolves mixed states using the closed time contour $\mathcal{C}$ introduced before, which consists of forward and backward segments in real time. Such a contour construction enables the direct computation of real-time correlation functions to arbitrary order..

Since we will later focus on holographic scenarios, consider a holographic conformal field theory in d spacetime dimensions (CFT_d), governed by the action S_{CFT}. Let $\mathcal{O}$ be a bosonic operator in this CFT, and J be its source, both living on the SK contour $\mathcal{C}$.

The SK generating functional $Z_{\rm SK}$ of the CFT is then given by the path-integral:

$$Z_{\rm SK}\left[J\right] = \int \mathcal{D}\mathcal{O}\ \exp\left(iS_{\rm CFT} + i\oint \mathrm{d}t_c\, \mathrm{d}^{d-1}\mathbf{x}\ J(x)\mathcal{O}(x)\right) . \tag{2.23}$$

Assuming there are no sources on the imaginary segment of the contour,[7] it remains convenient to treat the fields on the right and left segments separately. We can then write $Z_{\rm SK}$ as

$$Z_{\rm SK}[J_{\rm R}, J_{\rm L}] = \left\langle \exp\left\{ i\int \mathrm{d}^d x\ \left[J_{\rm R}(x)\mathcal{O}_{\rm R}(x) - J_{\rm L}(x)\mathcal{O}_{\rm L}(x)\right]\ \right\}\right\rangle_{\rm CFT} , \tag{2.24}$$

and functional derivatives of $Z_{\rm SK}$ yield the Schwinger-Keldysh correlators of the operators in the CFT. These correlators play a central role in understanding real-time responses and capturing the role of fluctuations in the theory.

Before turning to the gravitational counterpart of the SK formalism, we now briefly highlight the importance of the SK formalism in the study of open quantum systems.

2.1.2 SK formalism & Open systems

Open systems arise in a wide variety of contexts—from something as familiar as a boiling pot to something as complex as an evaporating black hole. While these examples may appear mismatched, they are chosen deliberately to illustrate the broad scope of open-system dynamics, spanning both everyday phenomena and highly theoretical scenarios. Studying such systems is crucial for understanding how they evolve, how they exchange information and energy with their surroundings, and how their behaviour can be modelled, controlled, or exploited in both practical and theoretical frameworks.

Our aim here is not to provide a comprehensive overview of open systems—readers may refer to standard textbooks [84, 85] for that—but rather to highlight the role of the Schwinger-Keldysh formalism in their analysis. As an example, we introduce the concept of the *influence functional*, originally developed by Feynman and Vernon [51] to study the dynamics of open systems. The key idea is to first double the degrees of freedom (d.o.f) for both the system and the environment (or bath), and then integrate out the environmental d.o.f. This yields an *effective field theory* (EFT) that captures the

[7] We omit sources on the imaginary part of the contour to preserve the initial thermal state.

behaviour of the system coupled to its environment.

The resulting EFT describes the system's non-unitary evolution, incorporating the effects of dissipation and decoherence due to environmental interactions. These effects are encoded in what is known as the influence functional, which we now describe in more detail.

The setup we have is the following: consider a single system degree of freedom $\mathfrak{X}$ coupled with many bath degrees of freedom X_i. The total action of the combined unitary theory is,

$$S_{\rm tot}[\mathfrak{X}, X_i] = \; S_{\rm s}[\mathfrak{X}] + S_{\rm b}[X_i] + S_{\text{s-b}}[\mathfrak{X}, X_i] \;, \tag{2.25}$$

where $S_{\rm s}$, $S_{\rm b}$ and $S_{\text{s-b}}$ are parts of the action describing the system, the bath and the interaction between them, respectively. Here, we want readers to note that these actions are not written in SK formalism; rather, they are written as in standard field theory –

$$S[\phi] = \int_{-\infty}^{\infty} dt \int d^{d-1}\mathbf{x}\; \mathcal{L}[\phi] \;, \quad \text{where} \quad \phi \in \{\mathfrak{X}, X_i\} \;. \tag{2.26}$$

Then the path integral required for the evolution of this 'total' setup is given by,

$$\int \mathcal{D}\mathfrak{X}\, \mathcal{D}X_i \, \exp\left(iS_{\rm tot}[\mathfrak{X}, X_i]\right) \;. \tag{2.27}$$

Following the idea of Feynman and Vernon [51], we double the degrees of freedom (d.o.f) of both the system and the bath, and then integrate out the 'doubled' bath d.o.f X_i to obtain the following path integral,

$$\int \mathcal{D}\mathfrak{X}_{\rm R}\, \mathcal{D}\mathfrak{X}_{\rm L} \, \exp\left(iS_{\rm s}[\mathfrak{X}_{\rm R}] - iS_{\rm s}[\mathfrak{X}_{\rm L}] + iS_{\rm IF}[\mathfrak{X}_{\rm R}, \mathfrak{X}_{\rm L}]\right) \;, \tag{2.28}$$

where $\mathfrak{X}_{\rm R}$ and $\mathfrak{X}_{\rm L}$ are two copies of system degrees of freedom and $S_{\rm IF}[\mathfrak{X}_{\rm R}, \mathfrak{X}_{\rm L}]$ is the *influence phase* (or influence functional), containing the influence of the bath on the system. The influence phase describes the non-unitary evolution of the system, arising from its contact with the bath/environment.

The influence phase generates the real-time correlators of the operator $\mathcal{O}(X_i)$ coupled to the system degree of freedom $\mathfrak{X}$.[8] More precisely, $S_{\rm IF}[\mathfrak{X}_{\rm R}, \mathfrak{X}_{\rm L}]$ is the real-time or the *Schwinger-Keldysh* generating functional of the bath.

[8]Here we assume that the interaction action $S_{\rm s-b}$ is given by $S_{\rm s-b} = \int d^d x \; \mathcal{O}\, \mathfrak{X}$.

As discussed in the introduction, we aim to construct an open *Effective Field Theory* (EFT) for a *system* coupled to a holographic *thermal bath*. For that, we are going to use the above-mentioned *Influence functional formalism*. As we just saw that, it amounts to working in the SK or real-time formalism. Since we are interested in holographic systems, we require a real-time formulation of holography that maps boundary QFT dynamics to a gravitational dual.

Real-time holography has a rich development history, beginning with the foundational works of Son and Starinets [52], and Skenderis and van Rees [53, 54]. A central question addressed in these studies is:

What is the gravitational geometry that dominates the gravitational path integral with the SK contour in the boundary limit?

This question is analogous to that answered by the Gibbons-Hawking (GH) prescription [57], which selects the Euclidean cigar geometry as the bulk dual of a thermal state in the boundary theory.

We now turn to this question in detail and review recent developments in the construction of real-time gravitational geometries.

2.2 Gravity Dual of the Schwinger-Keldysh Formalism

An early attempt to construct a gravity dual for the SK formalism involved using the Kruskal extension of black hole geometries [55, 86], where the two asymptotic boundaries were associated with the forward and backward segments of the SK contour. However, this approach was limited in scope — it was only suitable for computing two-point functions and lacked a systematic prescription for higher-point functions or interactions.

In parallel, other proposals were put forward to realize bulk duals of the SK formalism [52–54]. While these offered valuable insights, they also faced important limitations. One among them was the absence of a clear mechanism to incorporate Hawking radiation and its effects on boundary dynamics. This omission posed a challenge for developing a complete description of real-time processes, especially those involving fluctuations.

To address these gaps, the authors [58] proposed a gravitational dual to the SK

formalism called grSK geometry. This is the prescription we will use and discuss in detail now.

2.2.1 grSK geometry

Consider a Conformal Field Theory (CFT) at finite temperature in the SK formalism. Via AdS/CFT correspondence, the thermal states of the CFT correspond to AdS black holes [10]. As we have seen in the §2.1 of this chapter, fields living on SK contour should be thought of as a duplication of fields. This doubling of the CFT fields directly corresponds to the doubling of the AdS black hole geometry as detailed in [53, 54]. Then, the *gravitational Schwinger-Keldysh (grSK) geometry* should be constructed from these two copies of the AdS black hole geometry such that it gives the SK contour in the boundary limit. First prescribed by authors in [58], we will now explicitly construct this grSK geometry.

Consider a black brane[9] in an asymptotically AdS_{d+1} background in the *ingoing Eddington-Finkelstein* (EF) coordinates, given by:

$$\mathrm{d}s^2 = -r^2 f(r)\,\mathrm{d}v^2 + 2\,\mathrm{d}v\,\mathrm{d}r + r^2\,\mathrm{d}\mathbf{x}^2\,, \qquad f(r) = 1 - \left(\frac{r_h}{r}\right)^d\,, \tag{2.29}$$

where r_h is the horizon radius. We first complexify the radial coordinate, resulting in a $(d+2)$–real-dimensional manifold. The grSK geometry is then defined as a codimension-1 slice of this manifold: the radial coordinate in grSK varies along a contour in the complex radial plane as shown in figure 2.3.

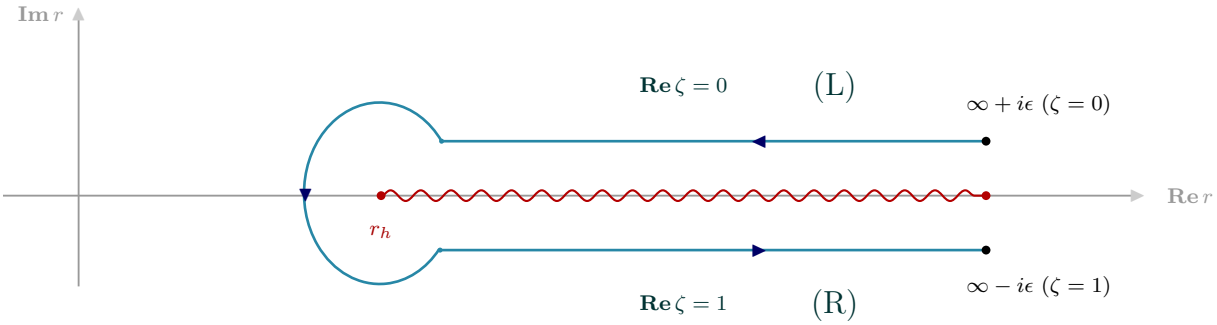

Figure 2.3: **grSK geometry :** The radial contour drawn on the complex r plane at fixed v, parametrized by coordinate ζ.

[9]Black brane is a solution of Einstein field equations similar to that of a black hole but with a planar horizon.

It is convenient to parametrize this radial contour by a complexified *mock tortoise coordinate* ζ defined via

$$\frac{\mathrm{d}\zeta}{\mathrm{d}r} = \frac{2}{i\beta\, r^2 f(r)} \ , \tag{2.30}$$

where $\beta \equiv \frac{4\pi}{dr_h}$ is the inverse Hawking temperature of the black brane. The coordinate ζ has a branch cut along the exterior and is normalised to have a unit monodromy around the horizon branch point $r = r_h$.

To gain a clearer insight into the grSK geometry, it is helpful to use Penrose diagrams. These diagrams provide a clear visualization of how the grSK geometry is constructed from the standard black brane geometry. The grSK geometry is constructed in two steps, illustrated in figure 2.4 below.

1. Take two AdS Schwarzschild black branes in ingoing EF coordinates.

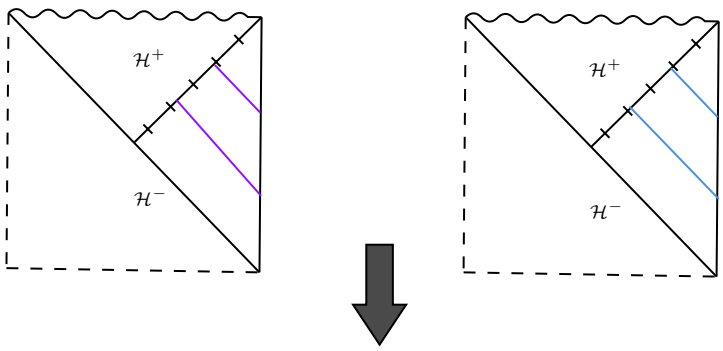

2. Glue them across their future horizons, i.e. $\mathcal{H}^+$.

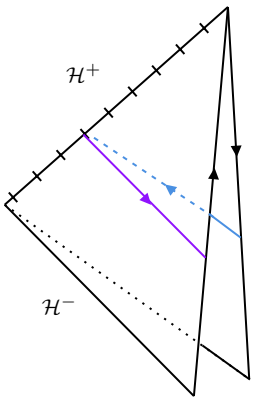

Figure 2.4: Schematic representation of the construction of the grSK geometry via Penrose diagrams.

Here, we first consider the two exteriors of the AdS black brane geometry in ingoing EF coordinates. Next, we glue these two copies of black brane geometries across their future horizons $\mathcal{H}^+$, resulting in the formation of the grSK geometry.

Regarding the diagram in figure (2.4), it is important to note a couple of aspects. Firstly, the diagram does not explicitly depict what happens at the future horizons during the glueing process. Additionally, it lacks a connection to the *cigar* geometry, which represents the initial thermal state in the CFT. Therefore, it is crucial to view this Penrose diagram of the grSK geometry as purely representational. For a more in-depth understanding of the Penrose diagram of the grSK geometry, readers are encouraged to look at [47]. Concluding our discussion of the grSK geometry, it is worth mentioning that this framework has been extended to include charged and rotating black holes, as explored in [49, 87].[10]

Now we take a brief detour to comment on the geometrical aspects of the grSK construction. Locally, the Lorentzian segments of the grSK geometry resemble the AdS–Schwarzschild exterior. Given this similarity, one might naturally wonder whether familiar geometric properties of standard AdS black holes — such as the geodesic structure or geodesic incompleteness – carry over to the grSK setting. However, the grSK geometry is far more subtle. At present, its global geometric properties — particularly the notion of geodesics and geodesic completeness — have not been rigorously characterised. This is not simply because the geometry is complex, but because we currently lack a well-defined framework for analysing geodesic structure in complexified Lorentzian spacetimes. Likewise, a fully non-perturbative prescription for constructing grSK geometries also remains unknown.

It is also natural to ask how much of this structure survives in more general settings. For example, in non-equilibrium steady states one expects substantial modifications: the absence of a thermal state removes the Euclidean cigar and, with it, the KMS periodicity that underlies the standard gluing prescription. To the best of our knowledge, constructing a genuine grSK analogue for such non-equilibrium configurations remains an open problem and an interesting direction for future work. With this detour concluded, we now return to the main theme of the section.

Now that we have described the grSK prescription, the next natural step is to examine its validity. One way to test this prescription is to probe the grSK geometry with a field and evaluate the corresponding on-shell action. This on-shell action yields the boundary Schwinger–Keldysh generating functional, $\mathcal{Z}_{\rm SK}$, which can then be used to compute real-

[10]For the gravitational dual of the deformed SK contour, see [88].

time correlators in the boundary theory, as demonstrated in [47, 60].

This setup allows for consistency checks against known properties of the boundary theory, such as unitarity and thermality. Unitarity can be verified by checking the collapse rules at the level of the generating functional, while thermality follows from the Kubo-Martin-Schwinger (KMS) condition—reflecting the periodicity in imaginary time due to the thermal density matrix.

The grSK prescription has been subjected to a range of such consistency checks and has proven successful in capturing the physics of Hawking radiation across multiple scenarios. These include systems involving Brownian particle [60, 89], scalar fields [47, 50, 67], fermionic fields [48], gauge fields [63, 65], and even linearized gravity [62]. However, much of the progress within the gravitational Schwinger–Keldysh framework has thus far been limited to systems at zero density. Many fundamental questions concerning finite-density systems remain unanswered, e.g.,

What is the gravitational dual of the Schwinger–Keldysh formalism at finite density?

In what follows, we turn our attention to addressing this question.

Chapter 3

Generalization of the grSK prescription to finite density

This chapter is based on [49] written by the author in collaboration with R. Loganayagam, Krishnendu Ray and Akhil Sivakumar.

In the last chapter §2, we reviewed the grSK geometry as the gravitational dual of the SK formalism for thermal equilibrium. Now, in this chapter, we extend this framework to include thermal systems at finite density. The core idea is that the finite-density holographic systems correspond to the charged black holes in the bulk via the AdS/CFT correspondence. Using this fact, we adapt the grSK prescription to charged black holes to account for such systems. This setup describes a boundary CFT at finite temperature and finite density within the SK formalism. Finally, we probe the prescribed geometry with a free massless Dirac field and perform some consistency checks.

3.1 The prescription: RNSK geometry

Consider a d-dimensional holographic boundary CFT_d at finite inverse temperature β and finite chemical potential μ. Its gravitational bulk dual is described by a charged black brane in the asymptotically AdS_{d+1} background. Since we will be interested in studying fluctuations in this field theory, it requires us to work in the SK formalism. To provide the gravitational prescription of SK formalism at finite density, we will follow the steps similar to those of the grSK construction given in section §2.2.1.

Let us start with the Reissner–Nordström (RN) black brane solution in asymptotic

AdS_{d+1} spacetime, written in ingoing Eddington–Finkelstein (EF) coordinates as:

$$\begin{aligned} \mathrm{d}s^2 &= g_{MN}(x)\, dx^M dx^N = -r^2\, f\, \mathrm{d}v^2 + 2\, \mathrm{d}v\, \mathrm{d}r + r^2\, \mathrm{d}\mathbf{x}_{d-1}^2 \ , \\ \mathbb{A} &= \mathcal{A}_M(x)\, \mathrm{d}x^M = -\mu \left(\frac{r_+}{r}\right)^{d-2} \mathrm{d}v \ , \end{aligned} \tag{3.1}$$

where f is the emblackening factor of the RN–AdS black brane, β is its inverse Hawking temperature, r_+ is its outermost horizon radius, and μ is the chemical potential of the dual boundary theory. Note that adding a constant to the 1-form gauge field $\mathbb{A}$ does not affect the solution. Hence, we choose the gauge so that the field vanishes at infinity (i.e., $r \to \infty$), unlike in [33, 41, 46], where it is set to vanish at the horizon. As a result, the chemical potential is determined by the gauge field at the horizon rather than at the boundary, unlike given in standard literature.

The quantities mentioned above can also be given in terms of the mass parameter M and the charge parameter Q of the black brane as,

$$\begin{aligned} f(r) &= 1 + \frac{Q^2}{r^{2d-2}} - \frac{M}{r^d} \ , \\ \frac{1}{\beta} &= \frac{d\, r_+}{4\pi} \left(1 - \frac{(d-2)\, Q^2}{d\, r_+^{2d-2}}\right) \ , \\ \mu &= \frac{g_{_F}\, Q}{r_+^{d-2}} \left[\frac{d-1}{2\,(d-2)}\right]^{\frac{1}{2}} \ , \end{aligned} \tag{3.2}$$

where $g_{_F}$ represents the gauge coupling constant in the Einstein-Maxwell bulk action, given by:

$$\frac{1}{2\kappa^2} \int d^{d+1}x \sqrt{-g} \left[\mathcal{R} + d(d-1) - \frac{1}{g_{_F}^2} \mathcal{F}_{MN} \mathcal{F}^{MN}\right] \ , \tag{3.3}$$

where κ^2 labels Newton's gravitational constant, and we have set the AdS radius to unity ($l_{\mathrm{AdS}} = 1$). Here, $\mathcal{R}$ is the Ricci scalar, and $\mathcal{F}_{MN}$ is the field strength corresponding to the gauge field $\mathcal{A}_M$,

$$\mathcal{F}_{MN} = \nabla_M \mathcal{A}_N - \nabla_N \mathcal{A}_M \ , \tag{3.4}$$

where ∇_M is the covariant derivative.

We can then obtain Einstein's field equations by varying the above action w.r.t the metric g_{MN}, as

$$\mathcal{R}_{MN} - \frac{1}{2} g_{MN} \mathcal{R} - \frac{d(d-1)}{2} g_{MN} = T_{MN} \ , \tag{3.5}$$

where we have used the following relations,

$$\begin{aligned}
\delta\sqrt{-g} &= -\frac{1}{2}\sqrt{-g}\; g_{MN}\delta g^{MN} \ , \\
\delta\mathcal{R} &= \mathcal{R}_{MN}\delta g^{MN} + (\text{ total derivative term}) \ , \\
\delta\left(\mathcal{F}_{MN}\mathcal{F}^{MN}\right) &= 2g^{PQ}\mathcal{F}_{MP}\mathcal{F}_{N}{}^{P}\delta g^{MN} \ , \\
\delta\left(\sqrt{-g}\mathcal{R}\right) &= \sqrt{-g}\left(\mathcal{R}_{MN} - \frac{1}{2}\; g_{MN}\mathcal{R}\right)\delta g^{MN} \ .
\end{aligned} \tag{3.6}$$

Upon ignoring total derivative term, it leads to

$$\begin{aligned}
&\delta\left(\sqrt{-g}\;\mathcal{L}\right) = \\
&\delta\left(\sqrt{-g}\left[\mathcal{R} + d(d-1) - \frac{1}{g_{_F}^2}\mathcal{F}_{MN}\mathcal{F}^{MN}\right]\right) = \\
&\sqrt{-g}\left(\mathcal{R}_{MN} - \frac{1}{2}\; g_{MN}\mathcal{R} - \frac{d(d-1)}{2}g_{MN} + \frac{1}{2g_{_F}^2}g_{MN}\mathcal{F}_{AB}\mathcal{F}^{AB} - \frac{2}{g_{_F}^2}\mathcal{F}_{MP}\mathcal{F}_{N}{}^{P}\right)\delta g^{MN} \ ,
\end{aligned} \tag{3.7}$$

and defining the energy-momentum tensor of the electromagnetic (EM) field

$$T_{MN} = \frac{2}{g_{_F}^2}\left(\mathcal{F}_{MP}\mathcal{F}_{N}{}^{P} - \frac{1}{4}g_{MN}\mathcal{F}_{AB}\mathcal{F}^{AB}\right) \ . \tag{3.8}$$

Then, we can see

$$\begin{aligned}
&\delta\left(\sqrt{-g}\;\mathcal{L}\right) = \\
&\sqrt{-g}\left(\mathcal{R}_{MN} - \frac{1}{2}\; g_{MN}\mathcal{R} - \frac{d(d-1)}{2}g_{MN} - T_{MN}\right)\delta g^{MN} \ ,
\end{aligned} \tag{3.9}$$

leads to Einstein's field equation. Similarly, by varying w.r.t the gauge field $\mathcal{A}_M$, we obtain Maxwell's field equations:

$$\nabla_M\mathcal{F}^{MN} = 0 \ . \tag{3.10}$$

The ADM mass density $\mathcal{M}$ and the charge density $\mathcal{Q}$ are given by,

$$\mathcal{M} = \frac{(d-1)M}{2\kappa^2} \ , \qquad\qquad \mathcal{Q} = \frac{\sqrt{2(d-1)(d-2)}}{g\,\kappa^2}Q \ . \tag{3.11}$$

Now, we define a *mock tortoise coordinate* ζ, as related to the standard radial coordinate

r via the following differential equation,

$$\frac{\mathrm{d}r}{\mathrm{d}\zeta} = \frac{i\beta}{2} r^2 f(r)\,. \tag{3.12}$$

The differential equation above normalizes the new coordinate ζ so that it has a unit jump across the logarithmic branch cut originating from the outermost horizon r_+ and sets $\zeta(r = \infty + i\varepsilon) = 0$ without loss of generality. This condition, along with the above differential equation, then uniquely defines ζ everywhere in the neighbourhood of $r \in [r_+, \infty)$ (see figure 3.1). The real part of ζ starts at 0, remains unchanged as the contour moves toward r_+ above the real axis in the complex r-plane, and gains $+1$ when the contour passes below the real axis, maintaining this value at the other infinity. The imaginary part of ζ has no monodromy and parametrizes both legs of the contour in the complex r-plane identically.

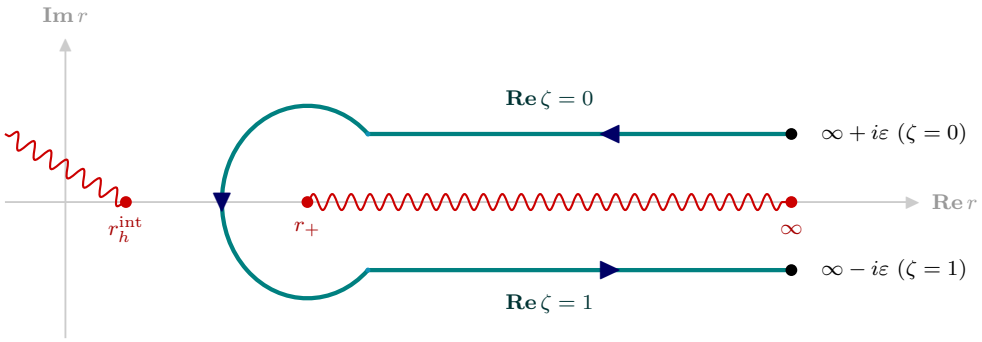

Figure 3.1: The radial contour drawn on the complex r plane, at fixed v. The locations of the two boundaries, the two horizons and the branch cuts have been indicated.

With this new coordinate defined, we define the *Reissner-Nordström Schwinger-Keldysh* (RNSK) geometry as one constructed by taking the RN–AdS exterior and replacing the radial interval extending from the outer horizon to infinity by the doubled contour labelled by ζ, as indicated in figure 3.1. Thus, the metric for the RSNK geometry is given by:

$$\mathrm{d}s^2 = -r^2 f\,\mathrm{d}v^2 + i\,\beta\,r^2 f\,\mathrm{d}v\,\mathrm{d}\zeta + r^2\,\mathrm{d}\mathbf{x}_{d-1}^2\,. \tag{3.13}$$

We then obtain a geometry with two copies of RN–AdS exteriors smoothly stitched together by an 'outer-horizon cap' region. This spacetime requires one further identification — each radially constant slice must meet at the future turning point.

Using sections of the Penrose diagram, the following figure (Fig. 3.2) schematically

describes the construction of RNSK geometry. These diagrams provide a clear visualization of how the RNSK geometry is constructed from the standard RN-AdS black brane geometry. Similar to the construction of the grSK geometry, as illustrated in figure (2.4), the RNSK geometry is also constructed in two steps. First, consider the two exteriors of the RN-AdS black brane geometry as shown in parts (a) and (b) of figure (3.2). Next, we connect these geometries across their outermost future horizons, resulting in the formation of the RNSK geometry, i.e. the part (c) of figure (3.2). Now, it is easy to see that the boundary limit of this geometry is nothing but the boundary SK contour.[1]

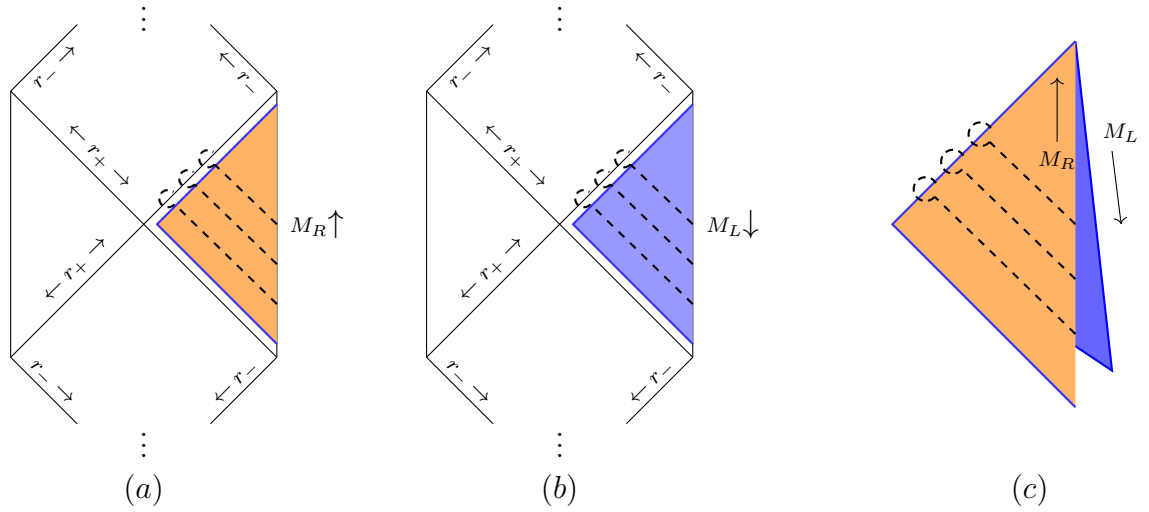

Figure 3.2: Schematic construction of RNSK geometry: Figures (a) and (b) show two copies of RN-AdS with their coloured exterior region, respectively. Figure (c) represents the RNSK geometry with the black dashed lines denoting the fixed v contours shown in figure 3.1.

Instead of working in a coordinate basis, one could equally choose to work in *local orthonormal* frame whose basis 1-forms are E^a and the line element is–

$$\mathrm{d}s^2 = \eta_{ab}\ E^a(x)E^b(x)\ , \tag{3.14}$$

where we note that all spacetime dependency goes to the basis and the coefficients are constants. Note that the choice of basis – whether a coordinate basis or an orthonormal 1-form basis – does not matter. Thus, the metric can be equivalently described by giving a set of orthonormal 1-forms. However, given a metric, orthonormal 1–forms are defined

[1] As in the case of the grSK construction, it is important to emphasize that the Penrose diagram here should be understood as purely representational.

only up to *local Lorentz transformation* (LLT) Λ^a_b, as shown below,

$$\mathrm{d}s^2 = \eta_{ab}\; E^a(x)E^b(x) = \eta_{ab}\; \tilde{E}^a(x)\tilde{E}^b(x) \qquad \text{where} \quad \tilde{E}^a = \Lambda^a_b\, E^b \;, \tag{3.15}$$

where we have used the Lorentz invariance, i.e $\eta = \Lambda^T \eta \Lambda$.

Thus, we can replace the description in terms of the metric with one in terms of a set of orthonormal 1–forms (called vielbeins or tetrads) [48, 90],

$$\begin{aligned} E^{(v)} &= \frac{r}{2}\,\mathrm{d}v - \frac{f}{2}\,r\left(i\beta\,\mathrm{d}\zeta - \mathrm{d}v\right) \;, \\ E^{(\zeta)} &= \frac{r}{2}\,\mathrm{d}v + \frac{f}{2}\,r\left(i\beta\,\mathrm{d}\zeta - \mathrm{d}v\right) \;, \\ E^{(i)} &= r\,\mathrm{d}x^i \;, \end{aligned} \tag{3.16}$$

where the parenthesis in the superscript denotes that the indices are written in the orthonormal (or tangent) frame, whereas indices without parentheses describe spacetime indices. This convention is similar to one present in [48, 49].

The way of writing these vielbeins/tetrads in the above form has a few advantages. Notably, all of their components and their derivatives are well behaved everywhere, e.g. there are no poles or branch points in the radial plane. Thus, we can easily say that the RNSK geometry, even in an orthonormal basis, is smooth at the future horizon where the process of glueing has happened. As we will see later in section §3.3, this equivalent way of writing the metric, i.e. using vielbeins/tetrads, is necessary to describe the spinors in curved spacetime. For a textbook discussion of spinors in curved spacetime, see [91, 92].

3.2 CPT action in RNSK geometry

Now that we have elaborated on the RNSK geometry and its associated notation, let us answer the following question: Given the ingoing modes, how do we construct the outgoing Hawking modes? The idea is to make use of the CPT symmetry of the boundary CFT, which acts as,

$$v \longmapsto -v \,, \qquad \mathbf{x} \longmapsto -\mathbf{x} \,, \tag{3.17}$$

in addition to a charge conjugation. The reader can quickly verify that the transformations as written above do not preserve the RN–AdS (or RNSK) solution given in Eqs. (3.1) and (3.16), respectively. So, how then do we implement this symmetry on the RNSK solution?

The answer to this question lies in the fact that, by the standard rules of AdS/CFT, the boundary symmetries can always be composed with bulk gauge symmetries (since they act trivially on the Hilbert space of states of the boundary theory). In this case, we combine the boundary CPT transformation with bulk diffeomorphisms, local Lorentz transformations and gauge transformations. In fact, the reader can check that the following transformations preserve the RN–AdS solution: we combine a charge conjugation

$$\mathcal{A}_M \mapsto -\mathcal{A}_M \ , \tag{3.18}$$

a diffeomorphism,

$$v \longmapsto i\beta\zeta - v \, , \qquad \mathbf{x} \longmapsto -\mathbf{x} \, , \tag{3.19}$$

a gauge transformation with the following parameter,

$$\mathbb{\Lambda} \equiv \ -i\beta \int_0^\zeta \mathrm{d}\zeta' \ \mathcal{A}_v(\zeta') \, , \tag{3.20}$$

and a non-orthochronous local Lorentz transformation,

$$\mathcal{T}^a{}_b \equiv \begin{pmatrix} -1 & 0 & 0 \\ 0 & 1 & 0 \\ 0 & 0 & -\mathbb{1}_{d-1} \end{pmatrix} \begin{pmatrix} \cosh\vartheta & \sinh\vartheta & 0 \\ \sinh\vartheta & \cosh\vartheta & 0 \\ 0 & 0 & \mathbb{1}_{d-1} \end{pmatrix} \ , \quad \text{where} \quad \vartheta \equiv \log f. \tag{3.21}$$

The linear transformation $\mathcal{T}$ is an idempotent local Lorentz transformation (LLT) composed of a boost along ζ with rapidity ϑ followed by a reflection of the v and $\mathbf{x}$ axes.

To check the invariance of the geometry, we will write the diffeomorphism in Eq. (3.19)

in the form $X^A \mapsto X^B \, \mathcal{J}_B{}^A$ where,

$$\mathcal{J}_A{}^B \equiv \begin{pmatrix} -1 & 0 & 0 \\ i\beta & 1 & 0 \\ 0 & 0 & -\mathbb{1} \end{pmatrix} . \tag{3.22}$$

The invariance is then the statement that

$$\mathcal{T}^a{}_b \, \mathcal{J}_A{}^B \, E^b_B = E^a_A \ , \qquad\qquad -\left(\mathcal{J}_N{}^M \, \mathcal{A}_M + \partial_N \mathbb{\Lambda}\right) = \mathcal{A}_N \ , \tag{3.23}$$

as can be readily checked.

It is instructive to unify these transformations by imagining the gauge field as descending from a Kaluza–Klein (KK) reduction over a circle. Say there was an extra circle direction denoted by φ, along which we have a 1–form, $\mathrm{d}\varphi + \mathcal{A}_N \, \mathrm{d}X^N$, that is orthonormal to the set of 1–forms, $E^a_M \, \mathrm{d}X^M$. The action of charge conjugation and gauge transformation in this picture can then be thought of as the KK diffeomorphism $\varphi \mapsto \mathbb{\Lambda} - \varphi$ (which extends $\mathcal{J}_A{}^B$ to the φ direction) along with a KK LLT that acts as a reflection along the φ axis (which extends $\mathcal{T}^a{}_b$ to the φ direction). The mathematically inclined reader would recognise that we have essentially described the boundary CPT transformation as an automorphism of the RN–AdS principle bundle.

Having implemented the boundary CPT in the bulk, we will now use this symmetry to generate new solutions to the bulk field equations linearised about the RN–AdS background. To see how this is done, let us begin with the simplest example of a complex scalar field with charge q probing the RN–AdS black brane. In the Fourier domain, we can expand a field configuration in terms of planar waves:

$$\int \frac{\mathrm{d}k^0 \ \mathrm{d}^{d-1}\mathbf{k}}{(2\pi)^d} \ \Phi(q, k^0, \zeta, \mathbf{k}) \, e^{-ik^0 v + i\mathbf{k}\cdot\mathbf{x}} \, . \tag{3.24}$$

Say this configuration solves the diffeomorphism/gauge covariant linear PDE in the bulk. How do we use the $\mathbb{Z}_2$ invariance we constructed above to get new solutions? The quickest way to answer this is to use the KK (or the principal bundle) picture described above. To this end, we think of the above field as drawn from a KK decomposition of a higher-

dimensional scalar field of the form,

$$\sum_{q\in\mathbb{Z}} e^{iq\varphi} \int \frac{\mathrm{d}k^0\ \mathrm{d}^{d-1}\mathbf{k}}{(2\pi)^d}\ \Phi(q,k^0,\zeta,\mathbf{k})\, e^{-ik^0 v+i\mathbf{k}\cdot\mathbf{x}}\,. \tag{3.25}$$

The diffeomorphism/gauge covariant linear PDE can then be lifted to a PDE covariant under higher-dimensional diffeomorphisms. We perform a higher dimensional diffeomorphism $\{v \mapsto i\beta\zeta - v\ , \mathbf{x} \mapsto -\mathbf{x}\ , \varphi \mapsto \mathbb{\Lambda} - \varphi\}$ on the Fourier domain expression given above. After relabelling the sum/integrals, we obtain,

$$\sum_{q\in\mathbb{Z}} e^{iq\varphi} \int \frac{\mathrm{d}k^0\ \mathrm{d}^{d-1}\mathbf{k}}{(2\pi)^d}\ e^{-\beta k^0\zeta - iq\mathbb{\Lambda}}\ \Phi(-q,-k^0,\zeta,-\mathbf{k})\, e^{-i\omega v+i\mathbf{k}\cdot\mathbf{x}}\,. \tag{3.26}$$

The higher-dimensional diffeomorphism covariance of the linear PDE then guarantees that the map

$$\Phi(q,k^0,\zeta,\mathbf{k}) \longmapsto e^{-\beta k^0\zeta - iq\mathbb{\Lambda}}\ \Phi(-q,-k^0,\zeta,-\mathbf{k}) \tag{3.27}$$

generates new solutions. In fact, the pre–factor in the exponent shows that this map takes ingoing solutions that are analytic in r to outgoing solutions which exhibit branch cut. To see the branch cut in Eq. (3.27), recall that the coordinate ζ itself possesses a branch cut, as illustrated in figure (3.1). Because the prefactor in Eq. (3.27) contains ζ, it inherits the same branch structure — namely, a cut extending from the outer horizon out to infinity. We can thus generate the Hawking modes from quasi–normal modes via the map, given by–

$$\Phi^{\rm in}_{\rm q}(\zeta,k) \longmapsto e^{-\beta k^0\zeta} e^{\beta\mu_q\, \mathfrak{O}}\ \Phi^{\rm in}_{-\rm q}(\zeta,-k) \equiv \Phi^{\rm out}_{\rm q}(\zeta,k)\ , \tag{3.28}$$

where k denotes the pair $\{k^0,\mathbf{k}\}$ and we have defined

$$\mu_q \equiv\ \mu\, q\ , \qquad\qquad \mathfrak{O}(\zeta) \equiv\ \frac{\mathbb{\Lambda}(\zeta)}{i\beta\mu} = \int_0^\zeta \mathrm{d}\zeta' \left(\frac{r_+}{r}\right)^{d-2}\ . \tag{3.29}$$

Note that we have chosen to indicate the charge q as a subscript on the field, and we will continue to follow this convention throughout the text.

The extension to other fields is straightforward. As a pertinent example, let us consider how this works for charged Dirac spinors. The main novelty in this case is the additional action of LLTs on spinor indices. The complex boost given in Eq. (3.21) acts

on spinor indices via

$$\mathfrak{T} \equiv \Gamma^{(\zeta)} \cdot \exp\Big(\frac{\vartheta}{2}\,\Gamma^{(\zeta)}\,\Gamma^{(v)}\Big) = \sqrt{f}\;\mathbb{\Gamma} + \frac{1}{\sqrt{f}}\,\mathbb{\Gamma}^{\dagger}\,, \tag{3.30}$$

where we have defined,

$$\mathbb{\Gamma} \equiv \frac{1}{2}\left(\Gamma^{(v)} + \Gamma^{(\zeta)}\right). \tag{3.31}$$

The Gamma matrix notation here is standard and our convention for the Clifford algebra is $\left\{\Gamma^a, \Gamma^b\right\} = 2\,\eta^{ab}\,\mathbb{1}$, with a mostly positive signature η^{ab}. The explicit construction of Gamma matrices and Clifford algebra is explained in much more detail in appendix A. The map from ingoing to outgoing solutions, in this case, is given by,

$$\Psi^{\rm in}_{\rm q}(\zeta,k) \longmapsto e^{-\beta k^0\zeta+\beta\mu_q\,\mathbb{\Theta}}\;\mathfrak{T}\cdot\Psi^{\rm in}_{-\rm q}(\zeta,-k) \;\equiv\; \Psi^{\rm out}_{\rm q}(\zeta,k)\,. \tag{3.32}$$

In order to streamline the analysis that is to follow, we end this section with a discussion of how the quantities that we have introduced behave as they traverse the horizon cap. As noted before, the mock tortoise coordinate has a unit jump when it encircles $r = r_+$. Noting that the gauge field $\mathcal{A}_v$ has the value $-\mu$ at the horizon, we see that the scale factor in $e^{\beta\mu_q\,\mathbb{\Theta}}$ is the fugacity z of the boundary theory. To see, recall that there is no $\sqrt{-g}$ in the integrand in the expression for $\mathbb{\Theta}$ (See Eq. (3.29)). So, $\mathbb{\Theta}$ suffers a discontinuity of unity around the horizon despite $\mathcal{A}_v$ being analytic on the full RNSK contour. Thus, the fugacity can be seen by evaluating different boundary limits as shown below

$$\lim_{\zeta\to 0} e^{\beta\mu_q\,\mathbb{\Theta}} = 1\;, \qquad \lim_{\zeta\to 1} e^{\beta\mu_q\,\mathbb{\Theta}} = e^{\beta\mu_q} \equiv z\;. \tag{3.33}$$

The rapidity parameter ϑ, on the other hand, has a jump of $2\pi i$ when it encircles the outer horizon — this can be traced to the phase $e^{2\pi i}$ that the function f picks up around the same path. As a result, every spinor index receives an additional 'fermionic' minus sign as it crosses the horizon cap. For example, the factor $\sqrt{f}$ appearing in $\mathfrak{T}$ contributes an extra sign when we cross the horizon, while preserving the same branch-cut structure. For a field of spin s, one gains the statistical factor $(-1)^{2s}e^{-\beta(k^0-\mu_q)}$ which is identical to the factor gained in Euclidean path integrals as we traverse the thermal circle. As we

will argue below, this factor is crucial to how the RNSK geometry gets the physics of Hawking radiation right.

3.3 Probing RNSK geometry by free fermions

We will now apply the preceding slightly abstract discussion to the explicit example of a free Dirac spinor in the RNSK background. The action for a bulk Dirac spinor Ψ of charge q and mass m living on the RNSK geometry is given by,

$$\mathbb{S}_{\Psi} = \oint \mathrm{d}\zeta \int \mathrm{d}^d x \, \sqrt{-g} \, i \, \overline{\Psi} \left(\Gamma^M \, \mathbb{D}_M - m \right) \Psi + \int \mathrm{d}^d x \, i \, \overline{\Psi} \, \mathcal{P}_- \, \Psi \Big|_{\zeta=0}^{\zeta=1} . \tag{3.34}$$

Let us explain each of the above terms one by one. The first is the standard bulk Dirac action, which fixes the equations of motion to be the Dirac equation in this curved spacetime. Here, we have introduced the following covariant Dirac derivative,

$$\mathbb{D}_M \equiv \partial_M - iq\mathcal{A}_M + \frac{1}{4}\omega_{ab\,M}\Gamma^a\Gamma^b \, , \tag{3.35}$$

where $\mathcal{A}_M$ is the background gauge potential and $\omega_{ab\,M}$ are the spin–connection 1–forms derived from the tetrads given in Eq. (3.16). The explicit expression for these spin connections is given as follows:

$$\begin{aligned} \omega_{(v)(\zeta)} &= \left(rf - \frac{1}{i\beta f}\frac{\mathrm{d}f}{\mathrm{d}\zeta} \right) \mathrm{d}v - \frac{i\beta}{2} \, rf \, \mathrm{d}\zeta, \\ \omega_{(i)(v)} &= -\frac{1-f}{2} \, r \, \mathrm{d}x^i \, , \\ \omega_{(i)(\zeta)} &= \frac{1+f}{2} \, r \, \mathrm{d}x^i \, , \end{aligned} \tag{3.36}$$

with all other components, not related by symmetry, vanishing.[2]

The second term is a variational boundary term, added to ensure that this action admits a well–posed variational principle when the spinors satisfy semi–Dirichlet boundary conditions [93–96]. When the above action is evaluated on–shell, the bulk term vanishes, and only the boundary term contributes to the final answer. Notice that the boundary term receives contributions from both the left and right boundaries of the RNSK saddle. The operator $\mathcal{P}_-$ involved in the definition of this term is one of two projection operators,

[2]Here, the label i runs over the boundary spatial directions.

defined as,

$$\mathcal{P}_{\pm} \equiv \frac{1}{2}\left(\mathbb{1} \pm \Gamma^{(\zeta)}\right) \ . \tag{3.37}$$

Varying the action in Eq. (3.34), we obtain the Dirac equation:

$$\left(\Gamma^{M}\,\mathbb{D}_{M} - m\right)\Psi = 0 \ . \tag{3.38}$$

When expressed in momentum (Fourier) space, this equation takes the form:

$$\left\{\mathbb{\Gamma}\left(\partial_{\zeta} + \beta k^{0} + \beta q\mathcal{A}_{v} + \frac{1}{2}\partial_{\zeta}\ln f\right) + \frac{\mathbb{\Gamma}^{\dagger}}{f}\partial_{\zeta} - \frac{\beta}{2}\left(\Gamma^{(i)}k_{i} + imr\right)\right\}\left(r^{\frac{d}{2}}\Psi\right) = 0 \ . \tag{3.39}$$

It can be explicitly checked that if $\Psi_{\rm q}(\zeta,k)$ solves this equation, applying the transformation described in Eq. (3.32) to it generates another solution of the same equation.

The relevant AdS/CFT boundary conditions are,

$$\begin{aligned}
&\lim_{\zeta\to 0} r^{\frac{d}{2}-m}\,\mathcal{P}_{+}\,\Psi = \mathcal{P}_{+}S_{0}\,\psi_{\rm L} \ , \\
&\lim_{\zeta\to 1} r^{\frac{d}{2}-m}\,\mathcal{P}_{+}\,\Psi = \mathcal{P}_{+}S_{0}\,\psi_{\rm R} \ .
\end{aligned} \tag{3.40}$$

Here S_0 is a constant boundary–to–bulk matrix defined in [48]. It is defined in terms of the ingoing boundary-to-bulk propagator $S^{\rm in}(\zeta,k)$ as,

$$S_{0} \equiv \lim_{\zeta\to 0} r^{\frac{d}{2}-m}\ S^{\rm in}(\zeta,k) = \lim_{\zeta\to 1} r^{\frac{d}{2}-m}\ S^{\rm in}(\zeta,k) \ . \tag{3.41}$$

The above boundary conditions are a 'doubled' version of the standard semi–Dirichlet conditions in AdS/CFT. These boundary conditions uniquely determine the solution on the RNSK geometry.

To see this, we begin with the most general combination of ingoing and outgoing solutions:

$$\begin{aligned}
\Psi_{\rm q}(\zeta,k) &= -S^{\rm in}_{\rm q}(\zeta,k)\,\psi_{\bar{F}}(k) - S^{\rm out}_{\rm q}(\zeta,k)\,\psi_{\bar{P}}(k)\,e^{\beta\left(k^{0}-\mu_{q}\right)} \ , \\
&= -S^{\rm in}_{\rm q}(\zeta,k)\,\psi_{\bar{F}}(k) - S^{\rm rev}_{\rm q}(\zeta,k)\,\psi_{\bar{P}}(k)\,e^{\beta k^{0}(1-\zeta)-\beta\mu_{q}(1-\mathbb{0})} \ .
\end{aligned} \tag{3.42}$$

Here, we have defined,

$$S^{\rm rev}_{\rm q}(\zeta,k) \equiv S^{\rm in}_{-\rm q}(\zeta,-k) \ , \tag{3.43}$$

and we have used the $\mathbb{Z}_2$ action detailed in the last section to get the outgoing Hawking solution.

The boundary conditions described above fix

$$\psi_{\bar{F}} \equiv n_{\rm FD}\left(\psi_{\rm R} - \psi_{\rm L}\right) - \psi_{\rm R} \ , \qquad \psi_{\bar{P}} \equiv n_{\rm FD}\left(\psi_{\rm R} - \psi_{\rm L}\right) \ , \tag{3.44}$$

with

$$n_{\rm FD} \equiv \frac{1}{e^{\beta(k^0-\mu_q)}+1} \ , \tag{3.45}$$

being the familiar Fermi–Dirac factor at finite chemical potential. We recognise $\psi_{\bar{P}}$ and $\psi_{\bar{F}}$ here, are the *Past-Future* (PF) basis for the boundary spinor sources [97, 98]. Thus, when written in the PF basis, the two combinations of sources precisely multiply the ingoing/quasi-normal bulk–to–boundary propagator and the outgoing bulk–to–boundary propagator, respectively. This is analogous to the corresponding statements at zero chemical potential [47, 48, 56, 60].

As pointed out in [48], the above fact can be used to argue why the generating function of correlations computed using our holographic prescription satisfy both the Schwinger–Keldysh *collapse rules*, as well as the KMS conditions, i.e., the generating function, cannot contain terms with only $\psi_{\bar{P}}$ or terms with only $\psi_{\bar{F}}$. Exactly the same argument is valid for the case of finite chemical potential presented here. We direct the reader to [48] for more details.

Finally, in the *Keldysh–rotated* or *average–difference* basis,

$$\psi_a \equiv \frac{1}{2}\left(\psi_{\rm R} + \psi_{\rm L}\right) \ , \qquad \psi_d \equiv \left(\psi_{\rm R} - \psi_{\rm L}\right) \ , \tag{3.46}$$

one gets,

$$\Psi = S^{\rm in}\,\psi_a - \left\{\left(n_{\rm FD} - \frac{1}{2}\right) S^{\rm in} + n_{\rm FD}\; e^{\beta k^0(1-\zeta)-\beta\mu_q(1-\Theta)}\; \mathfrak{T}\cdot S^{\rm rev}\right\}\psi_d \, . \tag{3.47}$$

where we have suppressed the dependence of charge q and coordinates (ζ, k).

This basis makes the Schwinger–Keldysh collapse rules manifest, i.e., there are no terms in the generating function for boundary correlators that have only ψ_a terms. Equivalently, correlation functions composed of only the *difference* operator $\mathcal{O}_d$ vanish. This is

consistent with our earlier discussion of the SK formalism in chapter 2. As we will see in §3.3.1, the influence phase that we derive for the open EFT also satisfies this property.

3.3.1 Gradient expansion

In this subsection, we will find the solution to the Dirac equation in gradient expansion, generalising the work of [48] to *charged* black branes. We only consider the case of a massless spinor field for simplicity. However, we expect the analysis to go through for a massive case also.

We begin by writing the Dirac field in the spacetime domain $\Psi \equiv \Psi(v, \zeta, \mathbf{x})$. We then write the most general solution Ψ in a gradient expansion, compatible with rotational invariance as,

$$\Psi = \frac{1}{r^{d/2}}\Big\{\mathbb{1} + C_a^{(1)} M^a \partial_v + D_a^{(1)} M^a \Gamma^{(i)} \partial_i + C_a^{(2)} M^a \partial_v^2 + D_a^{(2)} M^a \partial_i^2 + \dots \Big\} S_0\, \psi \tag{3.48}$$

where $\psi \equiv \psi(v, \mathbf{x})$ is the boundary spinor acting as a source at the boundary and the factor $r^{-d/2}$ has been taken out to satisfy boundary conditions, given in Eq. (3.40). The functions $\{C^{(\mathrm{i})}, D^{(\mathrm{j})}, \dots\}$ are some unknown functions of the radial coordinate ζ. The matrices M^a that appear in the above equation belong to the set $\{\mathbb{1}, \Gamma^{(\zeta)}\}$ and in order to satisfy the Dirac equation (3.39) at zero derivative order, we will fix S_0 to be a constant matrix annihilated by $\mathbb{\Gamma}$, i.e., $\mathbb{\Gamma}\, S_0 = 0$.

The bulk–to–boundary Green's function satisfying ingoing boundary conditions can be computed by substituting the above ansatz into the Dirac equation and solving it order by order in derivative expansion. In the Fourier domain, we get an expression of the form,

$$\begin{aligned} S^{\text{in}} = \frac{1}{r^{d/2}}\Bigg\{ 1 + \frac{\beta}{2}\Big(H\,\Gamma^{(\zeta)} - H_{(0)}\Big)\Gamma^{(i)}\, k_i - \frac{\beta^2\, k^0}{2}\Big(\widetilde{H}\,\Gamma^{(\zeta)} - \widetilde{H}_{(0)}\Big)\Gamma^{(i)}\, k_i \\ - \frac{\beta^2\, \mathbf{k}^2}{8}\Big(f\, G^2 - f_{(0)}\, G^2_{(0)}\Big) - \frac{\beta^2\, \mathbf{k}^2\, H_c}{4}\Big(H\,\Gamma^{(\zeta)} - H_{(0)}\Big) + \dots \Bigg\} S_0 \,. \end{aligned} \tag{3.49}$$

where $\mathbf{k}^2 = k_i k^i$ and the subscript '(0)' denotes the value of the functions at the conformal boundary, i.e. $\zeta = 0$. Here, we have written the results only up to the second order in the gradient expansion. However, we can write down the solution up to arbitrary order

in a similar fashion.

The unknown functions H, $\widetilde{H}$, and G must satisfy the following radial differential equations:

$$\begin{aligned}
\frac{d}{d\zeta}\left(e^{iq\mathbb{\Lambda}}\sqrt{f}\,H\right) &= e^{iq\mathbb{\Lambda}}\sqrt{f}\ , \\
\frac{d}{d\zeta}\left(e^{iq\mathbb{\Lambda}}\sqrt{f}\,\widetilde{H}\right) &= e^{iq\mathbb{\Lambda}}\sqrt{f}\ H\ , \\
\frac{d}{d\zeta}\left(\sqrt{f}\,G\right) &= \sqrt{f}\ .
\end{aligned} \tag{3.50}$$

Since we want an ingoing solution, we take H, $\widetilde{H}$, and G to be analytic at the outer horizon which then implies that the functions $\sqrt{f}H, \sqrt{f}\widetilde{H}$ and $\sqrt{f}G$ should vanish at the outer horizon. With this boundary condition specified, the above ODEs have a unique solution for these functions and, hence, the ingoing solution S^{in}.

Now that we have the ingoing solution, we can use CPT isometry to find the outgoing solution for the Dirac field in the RNSK geometry. Using Eq. (3.47), the full solution can be easily written in the gradient expansion. Next, we will use this solution to derive the on-shell action (SK generating functional). Later, we will perform some consistency checks on this on-shell action or influence phase from an open effective field theory context.

3.4 On-shell action or Influence phase

In this section, we will first derive the on-shell action in *average-difference* basis. We will write the on-shell action only up to second order in the gradient expansion.

Let us write the on-shell action $\mathbb{S}_{\text{os}}$ for massless Dirac field in the RNSK geometry

$$\begin{aligned}
\mathbb{S}_{\text{os}} &= \oint \mathrm{d}\zeta \int \mathrm{d}^d x\ \sqrt{-g}\ i\,\overline{\Psi}\Gamma^M \cancel{\mathbb{D}_M \Psi} + \int \mathrm{d}^d x\ i\,\overline{\Psi}\,\mathcal{P}_-\,\Psi\ \Big|_{\zeta=0}^{\zeta=1}\ , \\
&= \int \mathrm{d}^d x\ i\,\overline{\Psi}\,\mathcal{P}_-\,\Psi\ \Big|_{\zeta=0}^{\zeta=1}\ .
\end{aligned} \tag{3.51}$$

Via the AdS/CFT dictionary, the on-shell action in the bulk maps to the generating functional of the boundary. As we discussed in section §2.1.2, the SK generating functional is equivalent influence functional. Thus, the boundary influence functional $\mathbb{S}_{\text{IF}}$ can be obtained by evaluating the bulk on-shell action in the SK formalism.

Inserting the solution Ψ and conjugate solution $\overline{\Psi}$ in average-difference basis, given in Eq. (3.47), we obtain the influence phase as

$$\mathbb{S}_{\rm IF}[\psi_a,\psi_d] = \int \mathrm{d}^d x\, i\Big\{\overline{\psi}_a\,\mathcal{S}^{da}\,\psi_d + \overline{\psi}_d\,\mathcal{S}^{ad}\,\psi_a + \overline{\psi}_d\,\mathcal{S}^{aa}\,\psi_d\Big\}\ , \tag{3.52}$$

where $\mathcal{S}^{ad}$, $\mathcal{S}^{da}$, and $\mathcal{S}^{aa}$ are the retarded, advanced and Keldysh Green's functions, respectively. When the dimension of the boundary theory, d, is odd, their explicit forms are given by,

$$\begin{aligned}
\mathcal{S}^{ad} &= \gamma^{(v)} - \beta H_{(0)}\,\gamma^{(i)}k_i + \beta^2 k^0\,\gamma^{(i)}k_i\widetilde{H}_{(0)} + \frac{\beta^2\mathbf{k}^2(H_{(0)})^2}{2}\gamma^{(v)} + \dots \\
\mathcal{S}^{da} &= -\left(\gamma^{(v)} + \beta H^{\star}_{(0)}\,\gamma^{(i)}k_i + \beta^2 k^0,\gamma^{(i)}k_i\widetilde{H}^{\star}_{(0)} + \frac{\beta^2\mathbf{k}^2(H^{\star}_{(0)})^2}{2}\gamma^{(v)} + \dots\right) \\
\mathcal{S}^{aa} &= \mathfrak{e}\,\gamma^{(v)} + \frac{\beta k^0\,(1-\mathfrak{e}^2)}{2}\,\gamma^{(v)} - \frac{\beta^2(k^0)^2\left[\mathfrak{e}\,(1-\mathfrak{e}^2)\right]}{4}\gamma^{(v)} \\
&\quad + \frac{\mathfrak{e}\,\beta\,(H^{\star}_{(0)} - H_{(0)})}{2}\,\gamma^{(i)}k_i + \frac{\mathfrak{e}\,\beta^2\mathbf{k}^2\,\left[(H^{\star}_{(0)})^2 + H^2_{(0)}\right]}{4}\,\gamma^{(v)} \\
&\quad + \frac{\beta^2 k^0}{4}\gamma^{(i)}\,k_i\left((1-\mathfrak{e}^2)\big(H^{\star}_{(0)} - H_{(0)}\big) + 2\,\mathfrak{e}\,(\widetilde{H}^{\star}_{(0)} + \widetilde{H}_{(0)})\right) + \dots
\end{aligned} \tag{3.53}$$

where we have expanded the Fermi–Dirac factors in powers of k^0 and the superscript '$\star$' denotes the replacement $q \to -q$ in the arguments of the functions. We use the letter $\mathfrak{e}$ to denote the ground state (with $k^0 = 0$) charge

$$\mathfrak{e} \equiv \frac{1}{1+e^{-\beta\mu_q}} - \frac{1}{1+e^{\beta\mu_q}}\ , \tag{3.54}$$

which is the difference between the ground–state occupation of fermionic particles and anti–particles. A similar set of expressions can be obtained d is even, by following the analysis similar to [48].

3.4.1 Holographic KMS relations at finite density

Let us note a few things about the influence phase we obtained above.

1. **SK collapse rule:** Note that no term in the influence phase involves only average sources, i.e. $\mathcal{S}^{dd} = 0$. This is a general feature that arises from microscopic unitarity.

In other words, we can write the SK generating functional $\mathcal{Z}_{\rm SK}$,

$$\mathcal{Z}_{\rm SK}[\psi_a, \psi_d] = 0 = \mathcal{Z}_{\rm SK}[\psi_{\rm R} = \psi_{\rm L}] \ . \tag{3.55}$$

Now, recall that the SK generating functional can be interpreted as coming from the evolution operator on the closed time contour. Then, the above equation simply says that forward evolution exactly cancels the backward evolution if the sources are equal on both legs, as discussed previously in section §2.1.1. This is nothing but the fact that the evolution operator is unitary.

2. **KMS relation:** The coefficients of influence phase are not independent but related by the following two-point KMS relation,

$$\begin{aligned} \mathcal{S}^{aa} &= \frac{1}{2}\frac{e^{\beta k^0} - z}{e^{\beta k^0} + z}\left(\mathcal{S}^{ad} - \mathcal{S}^{da}\right) \\ &= \frac{1}{2}\tanh\left(\frac{\beta(k^0 - \mu_q)}{2}\right)\left(\mathcal{S}^{ad} - \mathcal{S}^{da}\right) \end{aligned} \ . \tag{3.56}$$

where z is the fugacity of the boundary theory. This relation originates from the thermality of the boundary theory at finite density.

3. In the limit $k \to 0$, the influence phase has a very simple form,

$$\mathbb{S}_{\rm IF} = \int \mathrm{d}^d x \ i\Big(\psi_a^\dagger \psi_d - \psi_d^\dagger \psi_a - \mathfrak{e}\, \psi_d^\dagger \psi_d\Big). \tag{3.57}$$

Finally, in the limit of uncharged black branes or vanishing chemical potential ($q,\ \mu \to 0$), all these Green's functions and the influence phase match with the results derived in [48].

Discussion

In this chapter, we extended the prescription for gravitational Schwinger–Keldysh saddles to the case of charged black branes. The resulting geometry is dual to the real–time evolution of a conformal field theory (CFT) at finite temperature and chemical potential. Our construction is a direct generalization of the original grSK prescription [47, 48, 58, 60]. Within this geometry, we demonstrated how outgoing (Hawking) modes arise from CPT–transformed ingoing quasi–normal modes.

To test this proposal, we probed the RN–AdS black brane with free Dirac fermions charged under the bulk gauge field. Using this setup, we derived the influence phase (or on-shell action of the Dirac field) for a probe fermion interacting with the holographic CFT, following the formalism of [48]. We showed that the resulting correlators satisfy the KMS condition, now dressed with the appropriate Fermi—Dirac statistical factors. This constitutes our central result and provides a natural extension of [48] to include the effects of finite chemical potential. Additionally, for massless fermions, we computed the quasi–normal mode solutions up to second order in the boundary derivative expansion. Recently, this geometry has also been used to describe charge diffusion and energy transport in a charged plasma [64, 66].

A natural follow-up for further investigation is the near–extremal limit, where the outer and inner horizons approach each other. This limit introduces subtleties, such as a potential pinching of the holographic radial contour, which may require a refined treatment. It would be interesting to clarify how such effects modify the gravitational SK prescription and whether they connect with the near–extremal derivative expansion discussed in [99].

Finally, an important next step is to move beyond free-field dynamics and study how interactions behave in this background. This is precisely the question we turn to next.

Chapter 4

Interactions in RNSK geometry

This chapter and the next are based on [72], which was written by the author.

In the previous chapter (§3), we described the RNSK geometry and analyzed the behaviour of free fields (e.g. a free Dirac spinor) in this background. Naturally, the next step is to understand how interacting fields behave in this setting. Since the RNSK (or even grSK) geometry is considerably more complex, we do not know *a priori* how the monodromy condition around the horizon affects interacting fields.

In the bulk, this also amounts to studying scattering processes against black holes in the presence of Hawking radiation. Recently, this question — understanding interacting fields in the grSK geometry — has been investigated for both bosons [70] and fermions [71]. In these studies, the authors developed a field-theoretic framework to analyze scattering processes around neutral black holes. By *field-theoretic*, we refer to a diagrammatic approach using Feynman rules to compute on-shell action. It was shown that the dynamics of interacting fields can be treated perturbatively, using Green's function techniques. The basic idea is to compute the boundary-to-bulk and bulk-to-bulk Green's functions and then construct the on-shell action, which corresponds to the boundary generating functional. Interestingly, interactions in the grSK geometry can be effectively described in terms of an exterior field theory living outside the horizon [70, 71].

Here, we do not delve into the technical details of these studies. Instead, we highlight several key features exhibited by the *exterior field theory*:

- *Dissipation*: The theory captures the dissipative effects due to particles falling into the black hole.

- *Fluctuations*: It incorporates thermal fluctuations arising from Hawking radiation.
- *Exterior localization*: All relevant dynamical degrees of freedom and interactions are confined to the region outside the black hole horizon.
- *Microscopic unitarity and causality*: The theory respects unitarity and causality within the exterior region, ensuring physically consistent evolution.
- *Thermal structure of interactions*: Interaction vertices are dressed with appropriate thermal statistical factors — such as Bose-Einstein or Fermi-Dirac distributions — consistent with the expectations from thermal field theory.

The absence of contributions from the black hole horizon — leading to the notion of an exterior field theory — is not immediately obvious. Indeed, it is unclear how the process of glueing at the horizon, which is part of the construction of the grSK geometry, might affect the fields living in this background. Naively, this arrangement appears to obey a principle reminiscent of the *central dogma* [100].[1] However, there are cases where an exterior field theory does not fully capture the dynamics — for example, in theories with derivative interactions, where additional terms localized at the horizon contribute to the field dynamics. This raises important questions about the general existence and applicability of exterior field theories.

To gather more evidence for the validity of the exterior field theory framework, it is necessary to study how interactions behave in more general spacetime backgrounds — for example, around charged black holes, particularly in the RNSK geometry. Such investigations would also help address the following question:

Do exterior field theories exist in the case of charged black holes? If so, how can one be formulated?

In this chapter, we will address this question by considering a simple example: a self-interacting complex scalar field. We will explain how this example leads naturally to an exterior field theory living outside a charged black hole.

[1] This dogma asserts that, for an outside observer, a black hole behaves as a unitary quantum system with a finite number of degrees of freedom, which rapidly scrambles information.

4.1 Our setup & the corresponding dynamics

Let us consider an interacting charged scalar field Φ in a charged black hole background. In particular, we consider this field in the RNSK background as given in Eq. (3.1), which we quote again here,

$$\begin{aligned} \mathrm{d}s^2 &= -r^2\, f\, \mathrm{d}v^2 + 2\,\mathrm{d}v\,\mathrm{d}r + r^2\,\mathrm{d}\mathbf{x}_{d-1}^2 \ , \\ \mathbb{A} &= \mathcal{A}_M(x)\,\mathrm{d}x^M = -\mu\left(\frac{r_+}{r}\right)^{d-2}\,\mathrm{d}v \ . \end{aligned} \tag{4.1}$$

As an illustrative example, we will only consider a massless complex scalar field interacting via a quartic term[2]

$$S = -\oint d\zeta\, d^dx\sqrt{-g}\left[|D_M\Phi|^2 + \frac{\lambda}{2!\,2!}|\Phi|^4\right] \ , \tag{4.2}$$

with the covariant derivative D_M, given by,

$$D_M \equiv \nabla_M - iq\mathcal{A}_M \ , \tag{4.3}$$

where q and λ are the charge and the interaction parameter of the field, respectively. Varying the above action (4.2) w.r.t the field, we obtain the following field equation (non-linear Klein-Gordon equation) for Φ:

$$D_M D^M\Phi = \frac{\lambda}{2!}\Phi|\Phi|^2 \ . \tag{4.4}$$

Before delving into the full dynamics of the field and its implications, we will begin by examining the free part only. Specifically, we will first describe the propagation of the scalar field Φ in the RNSK geometry, excluding interaction terms. This approach will also allow us to establish the necessary notation for subsequent sections. Later in this section, and the following one, we will use this established notation to discuss interactions.

[2]This is chosen for simplicity; however, the whole analysis can be easily generalised to the $|\Phi|^n$ interaction.

4.1.1 Free complex scalar in RNSK geometry

Let us start with the linear part of the EOM (free Klein-Gordon equation) and solve it first. Later, we will correct this by adding non-linear terms in the Klein-Gordon (KG) equation and solve it by using the Green's function.

The field equation for a free complex scalar field Φ is given by,

$$D_M D^M \Phi = 0 \ . \tag{4.5}$$

After the free field equation (4.5), we now turn to the solutions of this equation. As far as solutions are concerned, we will find it convenient to work in momentum space. Thus, passing into the momentum space,

$$\Phi(\zeta, v, \mathbf{x}) = \int \frac{d^d k}{(2\pi)^d} \Phi(\zeta, k) e^{-ik^0 v + i\mathbf{k}.\mathbf{x}} \ , \tag{4.6}$$

where k represents the Fourier transformed tuple $\{k^0, \mathbf{k}\}$ corresponding to the variables $\{v, \mathbf{x}\}$. In the momentum domain, we find that the free field equation given in Eq. (4.5), can be explicitly written as–

$$\begin{aligned} &\frac{d}{d\zeta}\left[r^{d-1}\frac{d\Phi}{d\zeta}\right] + \frac{\beta k^0}{2}\left[r^{d-1}\frac{d\Phi}{d\zeta} + \frac{d}{d\zeta}\left(r^{d-1}\Phi\right)\right] + r^{d-1} f \left(\frac{\beta \mathbf{k}}{2}\right)^2 \Phi \\ &\qquad + \frac{\beta q}{2}\left[r^{d-1}\mathcal{A}_v \frac{d\Phi}{d\zeta} + \frac{d}{d\zeta}\left(r^{d-1}\mathcal{A}_v \Phi\right)\right] = 0 \ . \end{aligned} \tag{4.7}$$

Since the equation of motion is a second-order ODE, the general solution is determined by two linearly independent solutions. We represent the solution using the ingoing and the outgoing solution, which are related by the CPT (Charge-Parity-Time reversal) isometry, given in Eq. (3.28). Thus, the free solution in terms of ingoing G^{in} and outgoing G^{out} boundary-to-bulk Green's function,[3] is given as,

$$\Phi(\zeta, k) = \ -G^{\text{in}}(\zeta, k) J_{\bar{F}}(k) + e^{\beta(k^0 - \mu_q)} G^{\text{out}}(\zeta, k) J_{\bar{F}}(k) \ , \tag{4.8}$$

[3]The approach involving ingoing and outgoing Green's functions can be seen in [56] and subsequently elaborated upon for the grSK geometry in [47, 60].

with the following ingoing and outgoing Green's function relationship,

$$G_{\rm q}^{\rm out}(\zeta,k) = e^{-\beta k^0\zeta} e^{\beta\mu_q \mathfrak{Q}} G_{-\rm q}^{\rm in}(\zeta,-k) \ , \tag{4.9}$$

where we have written the boundary sources in *Future-Past* (FP) basis, defined as,

$$J_{\bar{F}} = -\left[1+n_k\right] J_{\rm R} + n_k\, J_{\rm L} \ , \qquad J_{\bar{P}} = -n_k\left[J_{\rm R} - J_{\rm L}\right] \ , \tag{4.10}$$

with n_k is the Bose-Einstein factor at finite chemical potential, given by,

$$n_k = \frac{1}{e^{\beta(k^0-\mu_q)}-1} \ . \tag{4.11}$$

From the relation in Eq. (4.9), it is clear that the ingoing solution is sufficient to construct the general solution. To solve for the ingoing Green's function, two boundary conditions must be supplied:

1. It must be regular on the horizon, explicitly written as:

$$\left.\frac{dG^{\rm in}}{d\zeta}\right|_{r_+} = 0 \ . \tag{4.12}$$

2. It is normalized to unity at the boundary.

$$\lim_{r\to\infty} G^{\rm in} = 1 \ . \tag{4.13}$$

We will later find it convenient to write the above solution in the *right-left* (RL) basis of the sources as,

$$\Phi(\zeta,k) \equiv \ g_{\rm R}(\zeta,k)\, J_{\rm R}(k) - g_{\rm L}(\zeta,k)\, J_{\rm L}(k) \ , \tag{4.14}$$

where $J_{\rm R}$ and $J_{\rm L}$ denote the right and left boundary sources, respectively. Also, the symbols $g_{\rm R,L}$ denote the boundary-to-bulk Green's functions from the right and left AdS boundaries respectively, which in terms of the ingoing and the outgoing Green's functions

take the form:

$$\begin{aligned} g_{\rm R}(\zeta,k) &\equiv \ (1+n_k)\left[G^{\rm in}(\zeta,k) - G^{\rm out}(\zeta,k)\right] \ , \\ g_{\rm L}(\zeta,k) &\equiv \ n_k\left[G^{\rm in}(\zeta,k) - e^{\beta(k^0-\mu_q)}G^{\rm out}(\zeta,k)\right] \ . \end{aligned} \tag{4.15}$$

As it is clear from the name, the boundary conditions for these Green's functions are:

$$\lim_{\zeta\to 0} g_{\rm R}(\zeta,k) = 0 \ , \qquad \lim_{\zeta\to 0} g_{\rm L}(\zeta,k) = -1 \ , \tag{4.16}$$

and,

$$\lim_{\zeta\to 1} g_{\rm R}(\zeta,k) = 1 \ , \qquad \lim_{\zeta\to 1} g(\zeta,k) = 0 \ . \tag{4.17}$$

Combining the solution with these boundary conditions, we see that in the RL basis, the bulk field Φ satisfies,

$$\lim_{\zeta\to 0} \Phi(\zeta,k) = J_{\rm L}(k) \ , \qquad \lim_{\zeta\to 1} \Phi(\zeta,k) = J_{\rm R}(k) \ . \tag{4.18}$$

To conclude the free Klein-Gordon equation discussion, we also provide the general solution for the free conjugate field $\bar{\Phi}$. Since the analysis for the conjugate field closely mirrors that of the field itself, we will not repeat the steps but directly present the results and move to the interactions.

Before proceeding further, please note that a bar on top of a field, Green's function, or boundary source indicates that it is the conjugate version of the corresponding object. The free solution for the complex-conjugate scalar field is

$$\bar{\Phi}(\zeta,k) = \ -\bar{G}^{\rm in}(\zeta,k)\bar{J}_{\bar{F}}(k) + e^{\beta(k^0+\mu_q)}\bar{G}^{\rm out}(\zeta,k)\bar{J}_{\bar{F}}(k) \ , \tag{4.19}$$

with the CPT isometry relates these two Green's functions in the following manner

$$\bar{G}^{\rm out}_{\rm q}(\zeta,k) = e^{-\beta k^0\zeta}e^{-\beta\mu_q\Theta}\bar{G}^{\rm in}_{-\rm q}(\zeta,-k) \ , \tag{4.20}$$

where we have defined the Future-Past conjugate sources as,

$$\bar{J}_{\bar{F}} = -\left[1+\bar{n}_k\right]\bar{J}_{\rm R} + \bar{n}_k\bar{J}_{\rm L} \ , \qquad \bar{J}_{\bar{P}} = -\bar{n}_k\left[\bar{J}_{\rm R} - \bar{J}_{\rm L}\right] \ , \tag{4.21}$$

where $\bar{n}_k$ is the Bose-Einstein factor at finite chemical potential (with sign of q reversed) given by,

$$\bar{n}_k = \frac{1}{e^{\beta(k^0+\mu_q)} - 1} \ . \tag{4.22}$$

In the right-left basis of the conjugate sources

$$\bar{\Phi}(\zeta, k) \equiv \ \bar{g}_{\rm R}(\zeta, k)\, \bar{J}_{\rm R}(k) - \bar{g}_{\rm L}(\zeta, k)\, \bar{J}_{\rm L}(k) \ , \tag{4.23}$$

where $\bar{g}_{\rm R,L}$ denote the boundary-to-bulk conjugate Green's functions from the right and left AdS boundaries for the complex field, which in terms of the ingoing and the outgoing conjugate Green's functions take the form

$$\begin{aligned} \bar{g}_{\rm R}(\zeta, k) &\equiv (1 + \bar{n}_k) \left[\bar{G}^{\rm in}(\zeta, k) - \bar{G}^{\rm out}(\zeta, k)\right] \ , \\ \bar{g}_{\rm L}(\zeta, k) &\equiv \bar{n}_k \left[\bar{G}^{\rm in}(\zeta, k) - e^{\beta(k^0+\mu_q)} \bar{G}^{\rm out}(\zeta, k)\right] \ . \end{aligned} \tag{4.24}$$

Again, the boundary conditions for these conjugate Green's functions are

$$\lim_{\zeta \to 0} \bar{g}_{\rm R}(\zeta, k) = 0 \ , \qquad \lim_{\zeta \to 0} \bar{g}_{\rm L}(\zeta, k) = -1 \ , \tag{4.25}$$

and

$$\lim_{\zeta \to 1} \bar{g}_{\rm R}(\zeta, k) = 1 \ , \qquad \lim_{\zeta \to 1} \bar{g}(\zeta, k) = 0 \ . \tag{4.26}$$

Thus, it is easy that the following boundary limits holds:

$$\lim_{\zeta \to 0} \bar{\Phi}(\zeta, k) = \bar{J}_{\rm L}(k) \ , \qquad \lim_{\zeta \to 1} \bar{\Phi}(\zeta, k) = \bar{J}_{\rm R}(k) \ . \tag{4.27}$$

Here, we should note that the analysis of conjugate field (i.e. field equation, solution, etc), is exactly similar to that of the field itself. The only difference we can spot is the change in the sign of charge, i.e. $q \mapsto -q$.

4.1.2 Interacting complex scalar

Now that we have worked through the free Klein-Gordon equation and its solutions, we can move on to interactions. In this part, we will consider the full quartic theory and use the method of Green's function in the bulk to determine the interactive portion of the

solution.

For completeness, we once again write the full Klein-Gordon field equation as,

$$D_M D^M \Phi = \frac{\lambda}{2!}\Phi|\Phi|^2 \ . \tag{4.28}$$

We will solve this field equation perturbatively in the coupling constant λ by expanding the field Φ as,

$$\Phi = \sum_{i=0}^{\infty} \lambda^i \Phi_{(i)} = \Phi_{(0)} + \lambda\Phi_{(1)} + \lambda^2\Phi_{(2)} \dots \ , \tag{4.29}$$

under the double-Dirichlet boundary conditions (same as for free theory), given by:

$$\lim_{\zeta\to 0,1} \Phi_{(0)} = J_{\text{L,R}} \ , \qquad \lim_{\zeta\to 0,1} \Phi_{(i)} = 0 \quad \forall \quad i > 1 \ , \tag{4.30}$$

where J_{L} and J_{R} are the left and the right boundary sources, respectively. These boundary conditions are *doubled* versions of the standard conditions in AdS/CFT, modified specifically to fit the Schwinger-Keldysh formalism. The leading-order solution $\Phi_{(0)}$ is just the free solution that we have already obtained in Eq. (4.8). Regarding the boundary conditions, $\Phi_{(0)}$ satisfies the GKPW conditions, while all higher-order corrections should vanish at both boundaries, consistent with Eq. (4.30).

To find the higher-order solutions, we use the *bulk-to-bulk* Green's function. This function should vanish at both boundaries and is therefore termed *binormalisable*. The binormalisable bulk-to-bulk Green's function[4] $\mathbb{G}$ satisfies:

$$D_M D^M \mathbb{G}(\zeta|\zeta', k) = \frac{\delta(\zeta - \zeta')}{\sqrt{-g}} \ , \tag{4.31}$$

where $\delta(\zeta - \zeta')$ is the radial delta function on the RNSK contour. The above differential equation should be solved with the following boundary conditions,

$$\lim_{\zeta\to 0} \mathbb{G}(\zeta|\zeta', k) = \lim_{\zeta\to 1} \mathbb{G}(\zeta|\zeta', k) = 0 \ . \tag{4.32}$$

The explicit calculation for the computation of binormalisable bulk-to-bulk Green's func-

[4]Here, we adopt the same notation as in [70], but the convention for the bulk-to-bulk Green's function $\mathbb{G}$ used here differs by an overall sign.

tion is given in the Appendix B and given in Eq. (B.16) by,[5]

$$\mathbb{G}(\zeta|\zeta',k)=\frac{e^{\beta k^0\zeta'-\beta\mu_q\mathbb{Q}(\zeta')}}{(1+n_k)}\left(\frac{\Theta(\zeta>\zeta')g_{\rm L}(\zeta,k)g_{\rm R}(\zeta',k)+\Theta(\zeta<\zeta')g_{\rm R}(\zeta,k)g_{\rm L}(\zeta',k)}{\left[K^{\rm in}_{\rm q}(k)-K^{\rm in}_{-\rm q}(-k)\right]}\right)\ , \tag{4.33}$$

where Θ is the radial Heavyside step function on the RNSK contour. Note that $K^{\rm in}$ is the retarded two-point boundary correlator in the above equation. Additionally, we point out that later (in section §4.3) we will also use the *retarded* $\mathbb{G}_{\rm ret}$ and the *advanced* $\mathbb{G}_{\rm adv}$ bulk-to-bulk Green's functions. These two Green's functions are also derived in Appendix B.1, along with their relationship with each other (B.22) and with binormalisable Green's function (B.21). We reiterate that all Green's functions introduced here are defined with a convention that differs by an overall sign from that used in [70].

With the help of the binormalisable bulk-to-bulk Green's function, the remaining higher-order terms can be written as:

$$\Phi_{(i)}(\zeta,k)=\oint_{\zeta'}\mathbb{G}(\zeta|\zeta',k)\mathbb{J}_{(i)}(\zeta',k)\ ,\qquad\text{with}\quad\oint_{\zeta}\equiv\oint d\zeta\sqrt{-g}\ , \tag{4.34}$$

where $\mathbb{J}_{(i)}$ are bulk sources for i-th order term in the solution. The first two terms of these bulk sources are as follows:

$$\begin{aligned}
\mathbb{J}_{(1)}(\zeta,k)&=\int\prod_{i=1}^{3}\left(\frac{d^dp_i}{(2\pi)^d}\right)(2\pi)^d\delta^d\left(\sum_i^3p_i-k\right)\frac{1}{2!}\Phi_{(0)}(\zeta,p_1)\bar{\Phi}_{(0)}(\zeta,p_2)\Phi_{(0)}(\zeta,p_3)\ ,\\
\mathbb{J}_{(2)}(\zeta,k)&=\int\prod_{i=1}^{3}\left(\frac{d^dp_i}{(2\pi)^d}\right)(2\pi)^d\delta^d\left(\sum_i^3p_i-k\right)\\
&\quad\times\left[\Phi_{(1)}(\zeta,p_1)\bar{\Phi}_{(0)}(\zeta,p_2)\Phi_{(0)}(\zeta,p_3)+\frac{1}{2!}\Phi_{(0)}(\zeta,p_1)\bar{\Phi}_{(1)}(\zeta,p_2)\Phi_{(0)}(\zeta,p_3)\right]\ .
\end{aligned} \tag{4.35}$$

Now that we have expressed the solution in formal form, our next task is to construct the on-shell action for the $|\Phi|^4$ theory in the RNSK background. Once the on-shell action is obtained, boundary correlators can be computed by taking functional derivatives with respect to the boundary sources.

4.2 Exterior field theory for charged black branes

Previously, in section §4.1, we explained the method for solving the bulk field equations to arbitrary orders in the coupling constant λ. By substituting these solutions into the

[5]Here, we want to the point out the relationship between $\mathbb{Q}$ and $\mathbb{A}$, i.e. $\mathbb{Q}=\frac{\mathbb{A}}{i\beta\mu}$.

action, we can compute the on-shell action to any desired order in λ.[6] Our approach, also used in [71], circumvents the need to evaluate the boundary terms in the on-shell action explicitly. It leverages the fact that the boundary value of the higher-order solution vanishes, thereby simplifying the computation.

We start with the bare action $S_{\rm bare}$ as given by,

$$S_{\rm bare} = -\oint_{\mathcal{M}} \left(|D_M \Phi|^2 + \frac{\lambda}{2!\,2!} |\Phi|^4 \right) , \qquad \text{where} \quad \oint_{\mathcal{M}} \equiv \oint d\zeta \, d^d x \sqrt{-g} \, , \tag{4.36}$$

where $\mathcal{M}$ denotes the RNSK background. Inserting the perturbative solution into the bare action yields the *on-shell action* $S_{\rm os}$ in the following form:

$$S_{\rm os} = -\int_{\partial\mathcal{M}} \Phi_{(0)} \overline{\left(D_A \Phi_{(0)}\right)} + \lambda \oint_{\mathcal{M}} \left[\frac{1}{2!} \left(\bar{\Phi} - \bar{\Phi}_{(0)} \right) \Phi |\Phi|^2 - \frac{1}{2!2!} |\Phi|^4 \right] , \tag{4.37}$$

where $\partial\mathcal{M}$ denotes the boundary of $\mathcal{M}$. Note that in deriving Eq. (4.37), we have used the field equation for Φ and imposed the appropriate boundary conditions to significantly simplify the expression for the on-shell action.

The on-shell action $S_{\rm os}$, expanded in powers of λ , is expressed as:

$$S_{\rm os} = S_{(2)} + S_{(4)} + S_{(6)} + \dots \, , \tag{4.38}$$

where the subscript indicates the number of boundary sources in each term. For example, the quadratic term $S_{(2)}$, the quartic term $S_{(4)}$ and the term with six sources $S_{(6)}$ are given by:

$$\begin{aligned} S_{(2)} &= -\int_{\partial\mathcal{M}} \Phi_{(0)} \overline{\left(D_A \Phi_{(0)}\right)} \, , \\ S_{(4)} &= -\frac{\lambda}{2!\,2!} \oint_{\mathcal{M}} \left(\bar{\Phi}_{(0)} \Phi_{(0)} \right)^2 \, , \\ S_{(6)} &= -\frac{\lambda^2}{2} \oint_{\mathcal{M}} \bar{\Phi}_{(0)} \Phi_{(1)} \bar{\Phi}_{(0)} \Phi_{(0)} \, . \end{aligned} \tag{4.39}$$

As we will see soon, the terms above correspond to the free, contact, and single-exchange contributions at the tree level in Feynman diagrams. Within the framework of open effective field theory [47, 50], $S_{(n)}$ represents the n-point influence phase of the boundary

[6] Since our analysis is limited to tree-level diagrams, we use on-shell action and tree-level influence phase interchangeably.

theory.

We find it useful to express the on-shell action in the *Past-Future* (PF) basis, as shown in Eqs. (4.10) and (4.21). In this basis, the Schwinger-Keldysh collapse (unitarity) and the Kubo-Martin-Schwinger conditions (thermality) manifest as the vanishing of coefficients for terms involving all Future and all Past sources, respectively. Furthermore, this basis exclusively incorporates ingoing/outgoing boundary-to-bulk and retarded/advanced bulk-to-bulk propagators in the boundary correlators, ensuring the description of causal scattering processes.

The explicit computation of the on-shell action requires evaluating monodromy integrals on the RNSK contour. This involves a contour integral over the complexified radial coordinate, as illustrated in figure 3.1. The integral simplifies into a single exterior radial integral, with discontinuities arising at the horizon cap. The origin and evaluation of these discontinuities are detailed in Appendix C. Using the discontinuity formulas listed in the appendix (see Eqs. (C.1) and (C.4)), the on-shell action can be expressed in terms of a single exterior radial integral, as shown in Appendix D.

To declutter the expressions, we write the different terms in the on-shell action in the following way:

$$S_{(2n)} = \int_{k_{1,2,\ldots,2n}} \sum_{r,s=0}^{n} \mathcal{I}_{r,s}^{(2n)}(k_1,..,k_{2n}) \prod_{i=1}^{r} \bar{J}_{\bar{F}}(k_i) \prod_{j=1}^{s} J_{\bar{F}}(k_j) \prod_{l=r+1}^{n} \bar{J}_{\bar{F}}(k_l) \prod_{m=s+1}^{n} J_{\bar{F}}(k_m) \ , \quad (4.40)$$

where we have used the following notation,

$$\int_{k_{1,2,\ldots,m}} \equiv \int \frac{d^d k_1}{(2\pi)^d} \int \frac{d^d k_2}{(2\pi)^d} \cdots \int \frac{d^d k_m}{(2\pi)^d} \, \delta^{(d)}\left(k_1 + k_2 + \ldots + k_m\right) \ . \quad (4.41)$$

From this point onward, we will only present the expressions for $\mathcal{I}_{r,s}$ derived from RNSK geometry. The physical interpretation of $\mathcal{I}_{r,s}^{(2n)}$ corresponds to a scattering process, where r and s ingoing modes with charges $-$ and $+$, respectively, scatter into $(n-r)$ and $(n-s)$ outgoing modes with charges $+$ and $-$, respectively. Although the results for $\mathcal{I}_{r,s}^{(2n)}$ themselves are intricate, there is a particularly insightful way (i.e., Feynman diagrammatic way given in section §4.3) to summarise them that highlights their physical significance. We find that our findings can be concisely represented by a diagrammatic expansion governed by the Feynman rules.

As discussed earlier, the explicit computation of the on-shell action in the bulk naturally gives rise to an *exterior field theory*. This theory exists outside the outermost

horizon of the RN-AdS black brane. Next, we will demonstrate how this exterior field theory can be utilized to compute boundary correlation functions. The key idea is to define Feynman diagrammatic rules for the exterior theory and then apply these rules to compute the on-shell action (or boundary generating functional).

Below, we outline the diagrammatic rules for computing the tree-level influence phase (on-shell action).

4.3 Feynman diagrammatics

The conventions for momentum k flow are as follows: In boundary-to-bulk propagators, momentum flows from the boundary to the bulk, while in bulk-to-bulk propagators, it flows from left to right. Here, it is important to highlight that we will only present the Feynman rules/diagrammatics in the PF basis. However, one could also do the same in other basis, but the rules and diagrams might look different in other basis.

The *boundary-to-bulk propagators*(along with their corresponding source) for complex scalar are:

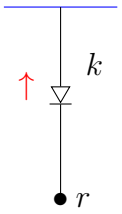

$$\equiv \frac{G^{\rm in}(r,k)}{1+n_k}\; J_{\bar{F}}(k)\;, \qquad \equiv G^{\rm out}(r,k)\; J_{\bar{F}}(k)\;, \tag{4.42}$$

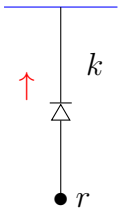

where r denotes the bulk point, and k denotes the momentum carried along the propagator. The red-colored arrow indicates the direction of charge flow. Additionally, note that the orientation of the 'diode' symbol (or triangle) distinguishes whether the propagator is ingoing or outgoing.

The corresponding *boundary-to-bulk propagators* for the conjugate field are:

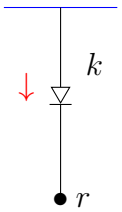

$$\equiv \frac{\bar{G}^{\rm in}(r,k)}{1+\bar{n}_k}\; \bar{J}_{\bar{F}}(k)\;, \qquad \equiv \bar{G}^{\rm out}(r,k)\; \bar{J}_{\bar{F}}(k)\;, \tag{4.43}$$

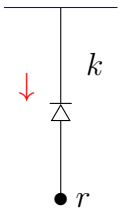

and the retarded and advanced *bulk-to-bulk propagators* are:

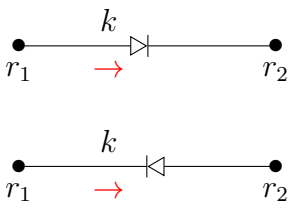

$$\equiv i\,\mathbb{G}_{\rm ret}(r_2|r_1,k)\ , \qquad \equiv i\,\mathbb{G}_{\rm adv}(r_2|r_1,k)\ . \tag{4.44}$$

where r_1 and r_2 are two bulk points connected by these propagators. The explicit expressions for retarded $\mathbb{G}_{\rm ret}$ and advanced $\mathbb{G}_{\rm adv}$ bulk-to-bulk Green's function are given in Eqs. (B.18) and (B.19), respectively. Note that the bulk-to-bulk propagators in our case are given by $i\mathbb{G}$, rather than $-i\mathbb{G}$ as used in [70]. This discrepancy arises because our convention for the Green's function differs from that of [70]: specifically, we define the Green's function as the inverse of the Laplacian, rather than the negative of it (See Eqs. (2.3) and (4.31)).

It is important to note that all these propagators are expressed in a basis that explicitly reveals their causal properties. As a result, the causal structure of Witten diagrams[7] will naturally emerge during their construction, thereby simplifying the understanding of scattering processes against black holes.

The final ingredient needed to construct the Witten diagrams is the set of bulk vertices. Before specifying the vertices in this exterior field theory, it is useful first to define,

$$n_{k,\alpha} \equiv \frac{1}{e^{\beta(k^0-\alpha\,\mu_q)}-1}\ , \qquad \text{and} \quad k_{12\ldots m} \equiv k_1+k_2+\ldots k_m\ , \tag{4.45}$$

where we note $n_{k,1}=n_k$ and $n_{k,-1}=\bar{n}_k$ and we will use these two relations interchangeably later.

Before we write down the bulk vertices, we would like the reader to note that we will exclusively use the $n_{k,\alpha}$ notation in describing vertices. Now, let us come to the *vertices*

[7] Witten diagrams are the AdS/CFT analogues of Feynman diagrams, with the key distinction that their external legs are anchored on the AdS boundary.

in this exterior field theory, given as follows:

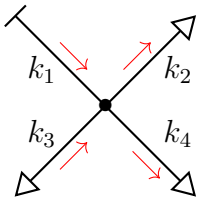

$$= i\lambda \frac{n_{-k_1,-1}}{n_{k_{234},1}} \ , \qquad$$

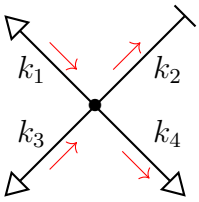

$$= i\lambda \frac{n_{-k_2,1}}{n_{k_{134},-1}} \ , \tag{4.46}$$

and

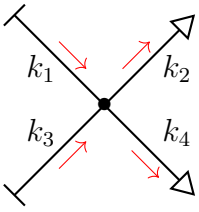

$$= i\lambda \frac{n_{-k_1,-1}n_{-k_3,-1}}{n_{k_{24},2}} \ , \qquad$$

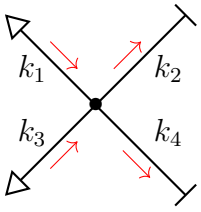

$$= i\lambda \frac{n_{-k_2,1}n_{-k_4,1}}{n_{k_{13},-2}} \ , \tag{4.47}$$

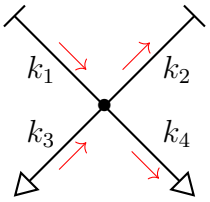

$$= i\lambda \frac{n_{-k_1,-1}n_{-k_2,1}}{n_{k_{34},0}} \ , \tag{4.48}$$

and

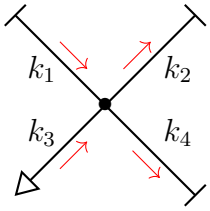

$$= i\lambda \frac{n_{-k_1,-1}n_{-k_2,1}n_{-k_4,1}}{n_{k_3,-1}} \ , \qquad$$

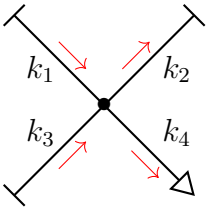

$$= i\lambda \frac{n_{-k_1,-1}n_{-k_2,1}n_{-k_3,-1}}{n_{k_4,1}} \ , \tag{4.49}$$

where one can easily see the charge conservation at the bulk vertex. For each of the vertices above, we have chosen the convention that all momenta flow into the vertex. Only these vertices contribute to non-zero terms, while the rest vanish. More precisely, vertices with the same legs result in no contribution, as shown below:

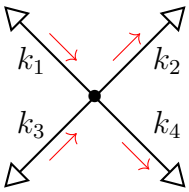

$$= \quad 0 \quad =$$

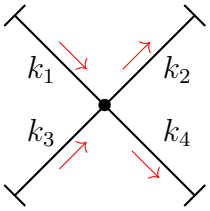

(4.50)

The fact that vertices with only 'triangle' legs or only 'bar' legs vanish follows from the collapse rule and the KMS condition, respectively. Notably, these vertices closely resemble those found in thermal field theory [81]. Here, one can interpret the legs with triangles as a single effective leg carrying the combined momentum and charge, which explains why some scattering processes seem to involve particles with zero or double the charge. This feature is quite general and holds for fermions as well, with the additional observation that two fermions with opposite quantum numbers behave like a boson [71].

Along with the above Feynman rules for propagators and vertices, to obtain the *boundary Schwinger-Keldysh generating functional* (on-shell action), we must further supply with following rules:

1. Multiply every diagram by $-i$.

2. The vertices are integrated over the exterior of the black brane, with the following radial exterior integral
$$\int_{\text{ext}} = \int_{r_+}^{r_c} dr\, r^{d-1} \,, \tag{4.51}$$
where r_c is the radial cut-off required for holographic renormalisation [53].

3. Impose momentum conservation at each vertex and integrate over all momenta.

4. Divide by the symmetry factor of the diagram.

Using these Feynman rules for Witten diagrams outlined above, we can calculate the boundary SK generating functional to any desired order in λ. In this thesis, we only present the result up to quadratic order in λ, incorporating contributions from contact and single-exchange diagrams.

4.3.1 Contact & Exchange terms

We begin with the contact diagrams contributing to the four-point influence phase $S_{(4)}$. The corresponding four-point contact term in the on-shell action is given by:

$$S_{(4)} = -\frac{\lambda}{2!\,2!}\int_{k_{1,2,3,4}} \oint_{\zeta} \prod_{i=1}^{2} \bar{\Phi}_{(0)}(\zeta, k_i) \prod_{j=1}^{2} \Phi_{(0)}(\zeta, k_j) \tag{4.52}$$

where we have taken $S_{(4)}$ from the Eq. (4.39) and written in the momentum space.

Using the solutions of the Klein-Gordon equation and performing the RNSK radial contour integral, as explained in the previous section §4.2. We obtain the on-shell action at linear order in coupling constant $S_{(4)}$, and read off coefficients $\mathcal{I}^{(4)}_{r,s}(k_1, k_2, k_3, k_4)$ as explained in the Appendix D.[8] All the diagrams contributing to the $S_{(4)}$ are:

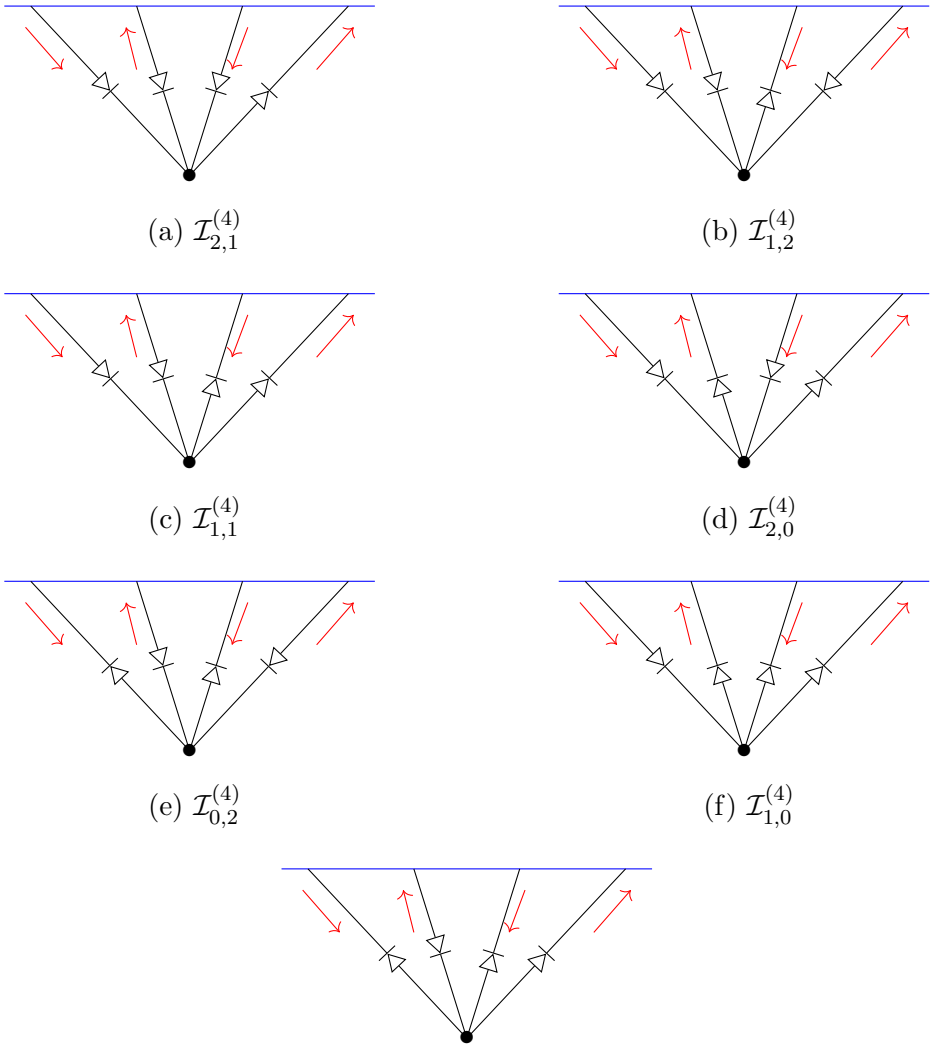

(a) $\mathcal{I}^{(4)}_{2,1}$ (b) $\mathcal{I}^{(4)}_{1,2}$

(c) $\mathcal{I}^{(4)}_{1,1}$ (d) $\mathcal{I}^{(4)}_{2,0}$

(e) $\mathcal{I}^{(4)}_{0,2}$ (f) $\mathcal{I}^{(4)}_{1,0}$

(g) $\mathcal{I}^{(4)}_{0,1}$

Figure 4.1: Witten diagrams contributing to the four-point influence phase $S_{(4)}$. Each sub-figure corresponds to a distinct interaction vertex and its associated term in the influence phase.

Note that these are the only non-zero contributions to the quartic influence phase $S_{(4)}$ at linear order in the coupling λ. The terms corresponding to these diagrams (recall the

[8] Recall that symbol $\mathcal{I}^{(4)}_{r,s}$ labels the coefficients of quartic influence phase, defined in Eq.(4.40).

definition in Eq. (4.40)), listed in the same order, are given as follows:

$$
\begin{aligned}
\mathcal{I}^{(4)}_{2,1} &= -\frac{\lambda}{2}\frac{1}{n_{k_4}}\int_{\text{ext}} \bar{G}^{\text{in}}(r,k_1)G^{\text{in}}(r,k_2)\bar{G}^{\text{in}}(r,k_3)G^{\text{out}}(r,k_4)\ , \\
\mathcal{I}^{(4)}_{1,2} &= -\frac{\lambda}{2}\frac{1}{\bar{n}_{k_3}}\int_{\text{ext}} \bar{G}^{\text{in}}(r,k_1)G^{\text{in}}(r,k_2)\bar{G}^{\text{out}}(r,k_3)G^{\text{in}}(r,k_4)\ , \\
\mathcal{I}^{(4)}_{1,1} &= \lambda\frac{1}{n_{k_{34},0}}\int_{\text{ext}} \bar{G}^{\text{in}}(r,k_1)G^{\text{in}}(r,k_2)\bar{G}^{\text{out}}(r,k_3)G^{\text{out}}(r,k_4)\ , \\
\mathcal{I}^{(4)}_{2,0} &= \lambda\frac{1}{n_{k_{24},2}}\int_{\text{ext}} \bar{G}^{\text{in}}(r,k_1)G^{\text{out}}(r,k_2)\bar{G}^{\text{in}}(r,k_3)G^{\text{out}}(r,k_4)\ , \\
\mathcal{I}^{(4)}_{0,2} &= \lambda\frac{1}{n_{k_{13},-2}}\int_{\text{ext}} \bar{G}^{\text{out}}(r,k_1)G^{\text{in}}(r,k_2)\bar{G}^{\text{out}}(r,k_3)G^{\text{in}}(r,k_4)\ , \\
\mathcal{I}^{(4)}_{1,0} &= -\frac{\lambda}{2}\frac{1}{n_{k_{234}}}\int_{\text{ext}} \bar{G}^{\text{in}}(r,k_1)G^{\text{out}}(r,k_2)\bar{G}^{\text{out}}(r,k_3)G^{\text{out}}(r,k_4)\ , \\
\mathcal{I}^{(4)}_{0,1} &= -\frac{\lambda}{2}\frac{1}{\bar{n}_{k_{134}}}\int_{\text{ext}} \bar{G}^{\text{out}}(r,k_1)G^{\text{in}}(r,k_2)\bar{G}^{\text{out}}(r,k_3)G^{\text{out}}(r,k_4)\ ,
\end{aligned}
\tag{4.53}
$$

where we have used $n_{k,1} = n_k$ and $n_{k,-1} = \bar{n}_k$ and suppressed the momentum dependence in $\mathcal{I}^{(4)}_{r,s}$ to shorten the expressions. Here, one could notice that the diagrams with either all the Future sources or all the Past sources vanish,

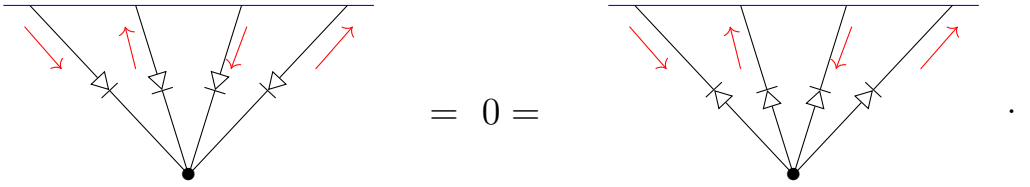

This is nothing but the SK collapse condition and the KMS condition at four-point functions. There are two equivalent ways to see why these diagrams vanish:

- On the RNSK contour: The underlying reason why the SK collapse rules and the KMS relations hold lies in the analyticity properties of the ingoing propagator. Specifically, the integrand is analytic, and its integral over the RNSK radial contour vanishes. To illustrate this, consider an analytic function $F(r)$ integrated over the radial RNSK contour:

$$\oint dr\ F(r)\ , \tag{4.54}$$

  where r runs over the full RNSK radial contour.

Breaking the full contour integral into different parts, we see

$$\begin{aligned}\oint dr\ F(r) &= \lim_{\epsilon\to 0}\left[\int_{\infty+i\epsilon}^{r_+ +i\epsilon} F(r) + \cancel{\int_{r_+ +i\epsilon}^{r_+ -i\epsilon} F(r)} + \int_{r_+ -i\epsilon}^{\infty-i\epsilon} F(r)\right] \\ &= \lim_{\epsilon\to 0}\left[\int_{\infty+i\epsilon}^{r_+ +i\epsilon} F(r) - \int_{\infty-i\epsilon}^{r_+ -i\epsilon} F(r)\right] \\ &= \lim_{\epsilon\to 0}\left[\int_{\infty+i\epsilon}^{r_+ +i\epsilon} F(r) - \int_{\infty+i\epsilon}^{r_+ +i\epsilon} F(r)\right] = 0\ .\end{aligned} \tag{4.55}$$

- From exterior field theory: The reason for the SK collapse and KMS condition lies behind the disappearance of corresponding effective vertices. These vertices vanish because they contain the inverse of the Bose-Einstein factor evaluated at $k^0 = 0$, i.e. $\frac{1}{n_{k^0}}\Big|_{k^0} = 0$.

Next, we come to the exchange diagrams contributing to the six-point influence phase $S_{(6)}$. Here, we will restrict ourselves to single exchange diagrams only that correspond to a single bulk-to-bulk propagator in an algebraic expression. The corresponding term in the on-shell action is given by:

$$\begin{aligned}S_{(6)} = -\frac{\lambda^2}{4}\int_{k_{1,2,3,4,5,6}} \oint_{\zeta,\zeta'} &\bar{\Phi}_{(0)}(\zeta,k_1)\Phi_{(0)}(\zeta,k_2)\bar{\Phi}_{(0)}(\zeta,k_3) \\ &\times \mathbb{G}(\zeta|\zeta',k_{456})\Phi_{(0)}(\zeta',k_4)\bar{\Phi}_{(0)}(\zeta',k_5)\Phi_{(0)}(\zeta',k_6)\ .\end{aligned} \tag{4.56}$$

Again, performing the RNSK radial integral to obtain the exterior radial integral using Eqs. (C.1) and (C.4) and the details are given in the Appendix D (for instance, see Eqs. after (D.6)). But here, we directly draw the diagrams and then write the corresponding expressions using the Feynman rules given above. For simplicity, we only illustrate two diagrams that contribute to $S_{(6)}$, while noting that other diagrams can be similarly derived using the same Feynman rules. Below are these diagrams:

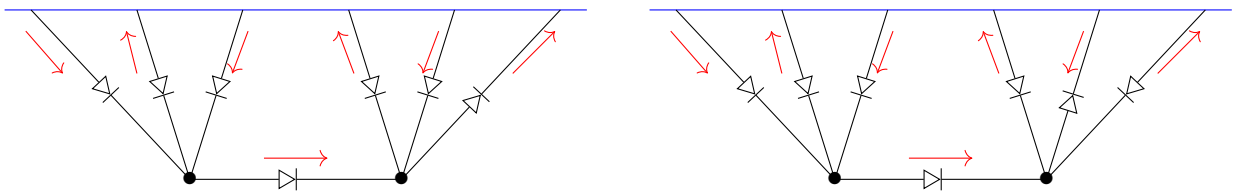

(a) $\mathcal{I}^{(6)}_{3,2}$ (b) $\mathcal{I}^{(6)}_{2,3}$

Figure 4.2: Two particular Witten diagrams that contribute to $S_{(6)}$.

and the terms corresponding to these diagrams are:

$$\begin{aligned}\mathcal{I}^{(6)}_{3,2} &= \frac{\lambda^2}{2}\frac{1}{n_{k_6}}\int_{\rm ext}\mathbb{G}_{\rm ret}(r|r',k_{123}) \\ &\qquad\times\left[\bar{G}^{\rm in}(r,k_1)G^{\rm in}(r,k_2)\bar{G}^{\rm in}(r,k_3)G^{\rm in}(r',k_4)\bar{G}^{\rm in}(r',k_5)G^{\rm out}(r',k_6)\right]\ , \\ \mathcal{I}^{(6)}_{2,3} &= \frac{\lambda^2}{2}\frac{1}{\bar{n}_{k_5}}\int_{\rm ext}\mathbb{G}_{\rm ret}(r|r',k_{123}) \\ &\qquad\times\left[\bar{G}^{\rm in}(r,k_1)G^{\rm in}(r,k_2)\bar{G}^{\rm in}(r,k_3)G^{\rm in}(r',k_4)\bar{G}^{\rm out}(r',k_5)G^{\rm in}(r',k_6)\right]\ .\end{aligned} \tag{4.57}$$

Similarly, higher-point exchange diagrams contributing to the higher-point influence phase can be built using the Feynman rules described above. This concludes our analysis of exterior diagrammatics, and we now shift focus to constructing solutions explicitly within the gradient expansion.

4.4 The Gradient Expansion

In this section, we solve the free complex Klein-Gordon equation by expressing the field in the gradient expansion. To derive the *fluctuation-dissipation relations* (FDRs), we only need to assume that the field Φ is independent of the boundary space coordinates $\mathbf{x}$. This is equivalent to setting its Fourier counterpart $\mathbf{k}=0$ in momentum space. Under this assumption, the free complex Klein-Gordon equation (4.5) reduces to the explicit form given below:

$$\begin{aligned}&\frac{d}{d\zeta}\left[r^{d-1}\frac{d\Phi}{d\zeta}\right]+\frac{\beta k^0}{2}\left[r^{d-1}\frac{d\Phi}{d\zeta}+\frac{d}{d\zeta}\left(r^{d-1}\Phi\right)\right] \\ &\qquad-\frac{\beta\mu_q}{2}\left[r\,r_+^{d-2}\frac{d\Phi}{d\zeta}+\frac{d}{d\zeta}\left(r\,r_+^{d-2}\Phi\right)\right]=0\ ,\end{aligned} \tag{4.58}$$

where we have used the explicit expression for the gauge field $\mathcal{A}_v$ with r_+ as outer horizon size, given in Eq. (3.1).

Note: We have omitted the subscript (0), which indicates that we are working at zeroth order in the coupling λ, as this will be clear from the context. We will continue this convention throughout the remainder of the section.

We begin by writing the most general solution (at $\mathbf{k}=0$) as a gradient expansion in frequency k^0. Instead of expanding around zero frequency (i.e, $k^0\sim 0$), we find it technically simpler to solve the field equations by expanding around the chemical

potential, i.e., for frequencies $k^0 \sim \mu_q$, up to second order, as

$$\Phi = \sum_{i=0}^{2} \left(\frac{\beta(k^0 - \mu_q)}{2} \right)^i \phi_i(\zeta) \ . \tag{4.59}$$

This type of expansion is natural when studying quasiparticle dynamics near the Fermi surface, where relevant excitations occur close to the chemical potential. Although our system does not contain fermions, we adopt this expansion purely for technical convenience.

Later, we will consider the small chemical potential limit ($\mu_q \to 0$). In that limit, the expansion around chemical potential (i.e, $k^0 \sim \mu_q$) effectively becomes an expansion around $k^0 \sim 0$. However, it is important to emphasize that these are distinct regimes: expanding in small $(k^0 - \mu_q)$ is not the same as expanding around $k^0 = 0$ at fixed μ_q. In particular, for arbitrary or large values of μ_q, the behaviour of the system near $k^0 = \mu_q$ might differ from that near $k^0 = 0$. A more detailed analysis in the regime of arbitrary chemical potential is left for future work.

Upon using this expansion (4.59) in the field equations (4.58), we can obtain the field equations at arbitrary orders. Subsequently, the field equations at zeroth order in the $\beta(k^0 - \mu_q)$ expansion,

$$\frac{d}{d\zeta}\left[r^{d-1} \frac{d\phi_0}{d\zeta} + \beta\mu_q \left(r^{d-1} - r\, r_+^{d-2} \right) \phi_0 \right] = \frac{\beta\mu_q}{2} \left(r^{d-1} - r\, r_+^{d-2} \right)' \phi_0 \ , \tag{4.60}$$

and at the first order in the $\beta(k^0 - \mu_q)$ expansion,

$$\begin{aligned} \frac{d}{d\zeta}\left[r^{d-1} \frac{d\phi_1}{d\zeta} + \beta\mu_q \left(r^{d-1} - r\, r_+^{d-2} \right) \phi_1 + 2\, r^{d-1} \phi_0 \right] \\ = \left[r^{d-1} \right]' \phi_0 + \frac{\beta\mu_q}{2} \left[r^{d-1} - r\, r_+^{d-2} \right]' \phi_1 \ , \end{aligned} \tag{4.61}$$

and at the second order in the $\beta(k^0 - \mu_q)$ expansion,

$$\begin{aligned} \frac{d}{d\zeta}\left[r^{d-1} \frac{d\phi_2}{d\zeta} + \beta\mu_q \left(r^{d-1} - r\, r_+^{d-2} \right) \phi_2 + 2\, r^{d-1} \phi_1 \right] \\ = \left[r^{d-1} \right]' \phi_1 + \frac{\beta\mu_q}{2} \left[r^{d-1} - r\, r_+^{d-2} \right]' \phi_2 \ , \end{aligned} \tag{4.62}$$

where $'$ denotes the derivative w.r.t ζ variable in all above-mentioned equations.

Next, to simplify further, we perform an expansion in small chemical potential (or equivalently, small charge) by taking $\mu_q \sim 0$, up to first order, as:

$$\phi_i = \sum_{j=0}^{1} (\beta\mu_q)^j \, \phi_{i,j}(\zeta) \ . \tag{4.63}$$

Taken together, Eqs. (4.59) and (4.63) define what we will refer to as the *near-μ_q gradient expansion in the small charge regime*. Note that these are nested expansions: we first expand in frequency near μ_q, and then expand each coefficient ϕ_i in powers of μ_q.

As discussed in the previous sections (e.g., see §4.1.1), it suffices to evaluate the ingoing solution, since the most general solution can be constructed using the CPT isometry. To determine the ingoing boundary-to-bulk Green's function $G^{\rm in}$, we will solve the field equations (4.58) under the following ingoing boundary conditions:

$$G^{\rm in}\big|_{r\to\infty} = 1 \ , \qquad\qquad \left.\frac{dG^{\rm in}}{d\zeta}\right|_{r_+} = 0 \ . \tag{4.64}$$

Under the restriction that the ingoing Green's function $G^{\rm in}$ is independent of the boundary space coordinates $\mathbf{x}$,[9] the $G^{\rm in}$ can be solved in the expansion near the chemical potential along with the small charge expansion. Here, we will only present the answer for $G^{\rm in}$ without going into the details of obtaining it.

Thus, the ingoing boundary-to-bulk Green's function in the near-μ_q gradient expansion in the small charge regime is,

$$G^{\rm in} = \sum_{i=0}^{2}\sum_{j=0}^{1} G^{\rm in}_{i,j}(\zeta) \left(\frac{\beta(k^0-\mu_q)}{2}\right)^i (\beta\mu_q)^j \ , \tag{4.65}$$

with the coefficients $G^{\rm in}_{i,j}$ explicitly given below

$$\begin{aligned} &G^{\rm in}_{0,0} = 1 \ , \qquad\qquad G^{\rm in}_{0,1} = \frac{1}{2}\mathbb{F}_2(r) \ , \qquad\qquad G^{\rm in}_{1,0} = \mathbb{F}_1(r) \ , \\ &G^{\rm in}_{2,0} = \int_{\zeta_c}^{\zeta} \frac{d\bar\zeta}{\bar r^{d-1}} \int_{\zeta_h}^{\bar\zeta} d\hat\zeta \left[\hat r^{d-1}\right]' \mathbb{F}_1(\hat r) - 2\int_{\zeta_c}^{\zeta} d\bar\zeta \left(\mathbb{F}_1(r) - \frac{r_+^{d-1}}{r^{d-1}}\mathbb{F}_1(r_+)\right) \ , \end{aligned} \tag{4.66}$$

[9] Since our goal is to derive FDRs, the boundary spatial directions $\mathbf{x}$ do not play a role.

where we have defined

$$\mathbb{F}_n(r) \equiv \int_{\zeta_c}^{\zeta} d\bar{\zeta} \left[\left(\frac{r_+}{\bar{r}} \right)^{d-n} - 1 \right] , \qquad \zeta_h \equiv \zeta(r_+) , \qquad \zeta_c \equiv \zeta(r_c) . \tag{4.67}$$

The $\mathbb{F}_n$ is analytic on the radial RNSK contour as long as $n < d$. The other remaining terms are written below:

$$\begin{aligned} &G^{\text{in}}_{1,1} + \int_{\zeta_c}^{\zeta} d\bar{\zeta} \left(1 - \frac{\bar{r}\, r_+^{d-2}}{\bar{r}^{d-1}} \right) \mathbb{F}_1(\bar{r}) + \int_{\zeta_c}^{\zeta} d\bar{\zeta} \left(\mathbb{F}_2(r) - \frac{r_+^{d-1}}{r^{d-1}} \mathbb{F}_2(r_+) \right) = \\ &\quad + \frac{1}{2} \int_{\zeta_c}^{\zeta} \frac{d\bar{\zeta}}{\bar{r}^{d-1}} \int_{\zeta_h}^{\bar{\zeta}} d\hat{\zeta} \left[\hat{r}^{d-1} \right]' \mathbb{F}_2(\hat{r}) + \frac{1}{2} \int_{\zeta_c}^{\zeta} \frac{d\bar{\zeta}}{\bar{r}^{d-1}} \int_{\zeta_h}^{\bar{\zeta}} d\hat{\zeta} \left[\hat{r}^{d-1} - \hat{r}\, r_+^{d-2} \right]' \mathbb{F}_1(\hat{r}) , \end{aligned} \tag{4.68}$$

and

$$\begin{aligned} &G^{\text{in}}_{2,1} + \int_{\zeta_c}^{\zeta} d\bar{\zeta} \left[1 - \left(\frac{r_+}{\bar{r}} \right)^{d-2} \right] G^{\text{in}}_{2,0}(\bar{r}) + 2 \int_{\zeta_c}^{\zeta} d\bar{\zeta} \left(G^{\text{in}}_{1,1}(\bar{r}) - \frac{r_+^{d-1}}{\bar{r}^{d-1}} G^{\text{in}}_{1,1}(r_+) \right) \\ &= \int_{\zeta_c}^{\zeta} d\bar{\zeta} \frac{1}{\bar{r}^{d-1}} \int_{\zeta_h}^{\bar{\zeta}} d\hat{\zeta} \left[\hat{r}^{d-1} \right]' G^{\text{in}}_{1,1}(\hat{r}) + \frac{1}{2} \int_{\zeta_h}^{\bar{\zeta}} d\bar{\zeta} \frac{1}{\bar{r}^{d-1}} \int_{\bar{\zeta}_h}^{\zeta} d\hat{\zeta} \left[\hat{r}^{d-1} - \hat{r}\, r_+^{d-2} \right]' G^{\text{in}}_{2,0}(\hat{r}) . \end{aligned} \tag{4.69}$$

It can be readily checked that the ingoing Green's function given in Eq. (4.65), along with the coefficients mentioned above, solves the Klein-Gordon equation with ingoing boundary conditions. Similarly, the ingoing boundary-to-bulk conjugate Green's function can be obtained by replacing $q \to -q$.

We will now express the field in the near-μ_q gradient expansion in the small charge regime. The approach involves first constructing the ingoing solution and then applying the CPT isometry (4.9) to obtain the full solution up to first order in both expansions. We find it helpful to represent the solution (4.14) in the following form,

$$\Phi = G^{\text{in}}_{\text{q}}(k) \left[J_a(k) + \left(n_k + \frac{1}{2} \right) J_d(k) \right] - e^{\beta\mu_q[\mathfrak{D}-1]} e^{-\beta k^0(\zeta-1)} G^{\text{in}}_{-\text{q}}(-k) n_k \; J_d(k) , \tag{4.70}$$

where we suppressed the radial dependence from the ingoing Green's function and also defined the sources in *average-difference* basis as,

$$J_a \equiv \frac{1}{2} \left(J_{\text{R}} + J_{\text{L}} \right) , \qquad J_d \equiv J_{\text{R}} - J_{\text{L}} . \tag{4.71}$$

In what follows, we retain only the leading-order terms in the nested expansion (4.65), keeping contributions up to linear order in both k^0 and μ_q, while discarding higher-order and mixed terms such as $\mathcal{O}((k^0)^2)$, $\mathcal{O}(\mu_q^2)$, and $\mathcal{O}(k^0\mu_q)$. This truncation isolates the dominant behaviour in the small frequency and small charge regime, and is sufficient for

our purposes. The resulting solution, keeping only the terms specified above, is given by:

$$\begin{aligned}\Phi = &\left[J_a + \left(\zeta - \frac{1}{2} + \mathbb{F}_1\right) J_d\right] + \frac{\beta k^0}{2}\left[\mathbb{F}_1 J_a - \left(\zeta(\zeta-1) + \left[\zeta - \frac{1}{2}\right]\mathbb{F}_1\right) J_d\right] \\ &+ \frac{\beta\mu_q}{2}\left[\left(\mathbb{F}_2 - \mathbb{F}_1\right) J_a + \left(\zeta(\zeta-1) + \left[\zeta - \frac{1}{2}\right]\mathbb{F}_2 + \left(\zeta - \frac{1}{2} + \mathbb{F}_2\right)\mathbb{F}_1\right) J_d\right] \ .\end{aligned} \tag{4.72}$$

To conclude the discussion on gradient expansion, we provide the solution in position space as well. This form will be significant when we evaluate the non-linear FDRs in the next section.

In position-space coordinates, the solution can be written as

$$\begin{aligned}\Phi = &\left[J_a + \left(\zeta - \frac{1}{2} + \mathbb{F}_1\right) J_d\right] + \frac{i\beta}{2}\left[\mathbb{F}_1 \partial_t J_a - \left(\zeta(\zeta-1) + \left[\zeta - \frac{1}{2}\right]\mathbb{F}_1\right) \partial_t J_d\right] \\ &+ \frac{\beta\mu_q}{2}\left[\left(\mathbb{F}_2 - \mathbb{F}_1\right) J_a + \left(\zeta(\zeta-1) + \left[\zeta - \frac{1}{2}\right]\mathbb{F}_2 + \left(\zeta - \frac{1}{2} + \mathbb{F}_2\right)\mathbb{F}_1\right) J_d\right] \ ,\end{aligned} \tag{4.73}$$

where we have replaced $k^0 \mapsto i\partial_t$ to obtain the above result.

4.4.1 On-shell action in gradient expansion

Using the gradient expansion solutions from Eqs. (4.72) and (4.73), we proceed to compute the on-shell action (or influence phase), starting with the quadratic (free) contribution $S_{(2)}$, given as

$$S_{(2)} = -\int d^d x \sqrt{-g}\ \Phi_{(0)}\left(\overline{\mathbb{D}\Phi_{(0)}}\right)\Big|_{\zeta=0}^{\zeta=1} . \tag{4.74}$$

Upon transitioning to momentum space, the on-shell action at quadratic order in the *average-difference* basis is found to be:

$$S_{(2)} = \int \frac{d^d k}{(2\pi)^d}\left[\widehat{\mathcal{J}}_{ad}\ \bar{J}_d(-k) J_a(k) + \widehat{\mathcal{J}}_{da}\ \bar{J}_a(-k) J_d(k) + \widehat{\mathcal{J}}_{dd}\ \bar{J}_d(-k) J_d(k)\right] \ , \tag{4.75}$$

with $\widehat{\mathcal{J}}_{ad}$, $\widehat{\mathcal{J}}_{da}$ and $\widehat{\mathcal{J}}_{dd}$ are the boundary Green's functions given below,[10]

$$\widehat{\mathcal{J}}_{ad} = K_{\rm ret}(k) \ , \qquad \widehat{\mathcal{J}}_{da} = K_{\rm adv}(k) \ , \qquad \widehat{\mathcal{J}}_{dd} = K_{\rm kel} \ , \tag{4.76}$$

where $K_{\rm ret}$, $K_{\rm adv}$ and $K_{\rm kel}$ denote the two-point retarded, advanced and Keldysh boundary correlators respectively. The retarded and advanced components only capture spectral information and do not depend on the occupation number n_k, as opposed to the Keldysh

[10]Here, the hat notation $\widehat{\mathcal{J}}$ denotes that $\mathcal{J}$ has been integrated over the radial direction and thus no longer depends on the radial coordinate, i.e. $\widehat{\mathcal{J}} \equiv \oint d\zeta \sqrt{-g}\ \mathcal{J}$.

component that explicitly involves n_k. The absence of $\widehat{\mathcal{J}}_{aa}$ follows from the Schwinger-Keldysh collapse condition. It is worth noting that the on-shell action expressed in the average-difference basis naturally produces boundary retarded correlators. The final term, $\widehat{\mathcal{J}}_{dd}$, representing the effects of fluctuations, as expected from the two-point KMS condition, is given by

$$\widehat{\mathcal{J}}_{dd} = \frac{1}{2}\coth\left(\frac{\beta(k^0-\mu_q)}{2}\right)\left[\widehat{\mathcal{J}}_{ad}-\widehat{\mathcal{J}}_{da}\right] \ . \tag{4.77}$$

where $K_{\rm kel}$ denotes the two-point Keldysh boundary correlator.

With the quadratic order on-shell action established and its coefficients identified, we now focus on the quartic on-shell action $S_{(4)}$. It receives contributions from the contact diagram illustrated in figure 4.1. Using the contact term from the second line of Eq. (4.39) and considering terms up to linear order in both ∂_t and μ_q while discarding higher-order and mixed terms such as $\mathcal{O}((\partial_t)^2)$, $\mathcal{O}(\mu_q^2)$, and $\mathcal{O}(\mu_q\partial_t)$, we obtain the following expression,

$$\begin{aligned} S_{(4)} &= -\lambda\int d^dx \oint d\zeta\sqrt{-g}\frac{|\Phi_{(0)}|^4}{4} \\ &= -\lambda\int d^dx\int_{\rm ext}\mathcal{L}_0 - \lambda\int d^dx\int_{\rm ext}\mathcal{L}_1 + \mathcal{O}((\beta\partial_t)^2) + \mathcal{O}((\beta\mu_q)^2) + \mathcal{O}(\beta^2\mu_q\partial_t) \ , \end{aligned} \tag{4.78}$$

where the terms $\mathcal{L}_0$ and $\mathcal{L}_1$ represent the non-derivative and first-derivative contributions to $S_{(4)}$, respectively. Note that the quartic on-shell action has been expressed in position space using Eq. (4.73).

The explicit form of the non-derivative contribution $\mathcal{L}_0$ is given by

$$\mathcal{L}_0 = \sum_{r,s=0}^{2}\mathcal{G}_{r,s}\ \left[\bar{J}_a\right]^r\left[J_a\right]^s\left[\bar{J}_d\right]^{2-r}\left[J_d\right]^{2-s} \ , \tag{4.79}$$

and we express the first-derivative contribution to the quartic on-shell action $\mathcal{L}_1$ as

$$\begin{aligned} \mathcal{L}_1 = &\sum_{r=0}^{1}\sum_{s=0}^{2}\left\{\mathcal{G}_{\dot{r},s}\left(\partial_t\bar{J}_a\right)+\mathcal{H}_{\dot{r},s}\left(\partial_t\bar{J}_d\right)\right\}\left[\bar{J}_a\right]^r\left[J_a\right]^s\left[\bar{J}_d\right]^{1-r}\left[J_d\right]^{2-s} \\ &+\sum_{r=0}^{2}\sum_{s=0}^{1}\left\{\mathcal{G}_{r,\dot{s}}\left(\partial_t J_a\right)+\mathcal{H}_{r,\dot{s}}\left(\partial_t J_d\right)\right\}\left[\bar{J}_a\right]^r\left[J_a\right]^s\left[\bar{J}_d\right]^{2-r}\left[J_d\right]^{1-s} \end{aligned} \ , \tag{4.80}$$

where the coefficients for all terms are provided in Appendix D.1, and relationships among them due to charge conjugation as outlined below:

$$\mathcal{G}_{r,s} = \mathcal{G}_{s,r}\Big|_{q\to -q} , \qquad \mathcal{G}_{r,\dot{s}} = \mathcal{G}_{\dot{s},r} , \qquad \mathcal{H}_{r,\dot{s}} = \mathcal{H}_{\dot{s},r} . \tag{4.81}$$

Note that since we are working only up to linear order in both ∂_t and μ_q while discarding higher-order and mixed terms such as $\mathcal{O}((\partial_t)^2)$, $\mathcal{O}(\mu_q^2)$, and $\mathcal{O}(\mu_q\partial_t)$, the term $\mathcal{L}_1$ cannot contain any μ-dependent contributions. However, if we go beyond this order, $\mathcal{L}_1$ would acquire μ-dependent terms, and the relationship given in Eq. (4.81) would be modified accordingly.

We have outlined the on-shell action (influence phase) to the leading order in the gradient expansion, highlighting the identification of several coefficients. The subsequent step is to examine how the coefficients of the quartic influence phase are related, in a manner analogous to the quadratic case discussed in Eq. (4.77), albeit in the high-temperature limit. The next section will clarify how these relationships pave the way for the emergence of holographic non-linear FDRs at finite density under small charge expansion.

Chapter 5

Holographic Fluctuation-Dissipation Theorems

This chapter is based on the results of [72] written by the author.

In the previous chapter, we examined interactions in the RNSK geometry and how it gives rise to exterior field theory. In this chapter, we now use those insights to derive fluctuation-dissipation theorems for holographic systems at finite density. Our central question is:

Do fluctuation-dissipation theorems hold in holographic theories at finite temperature and finite density? If so, what form do they take?

To address this question, we first begin with a brief review of the fluctuation-dissipation theorem. We then discuss its realization in zero-density holographic systems, following the work [47], and finally present our results on the finite-density case as developed in [72].

5.1 Review of FDT

Thermal systems are present throughout physics, from everyday objects like a cup of coffee to exotic objects like black holes. The behaviour of these systems is governed by various constraints on observable quantities. A key example is the *Fluctuation-Dissipation Theorem* (FDT), which fundamentally links the strength of fluctuations to the dissipation coefficient. In other words, the way a system responds to small external disturbances

(dissipation) is directly related to the fluctuations it exhibits in thermal equilibrium. The FDT connects macroscopic description to microscopic description by explaining how irreversible dissipation arises from time-symmetric fluctuations.

A simple illustration of the FDT can be found in classical Brownian motion. It is a random, erratic movement of tiny particles suspended in a fluid (like pollen in air), caused by continuous collisions with the molecules of the fluid. The dynamics of a Brownian particle is described by Langevin's equation:

$$\ddot{q} + \gamma \dot{q} = \mathfrak{f}\, \eta(t) \ , \tag{5.1}$$

where γ is the damping (or dissipation) coefficient, η represents the thermal noise[1] and $\mathfrak{f}$ measures the fluctuation strength. The relationship between these coefficients, as given by the following linear FDT:

$$\frac{2}{\beta}\gamma = \mathfrak{f} \ , \tag{5.2}$$

where β denotes the inverse temperature.

The origin of FDT lies in the thermal nature of the bath [101]. This theorem, though powerful, is also very intuitive because the mechanisms causing dissipation are inherently linked to the fluctuations observed. A common classical argument is that the thermal fluctuations causing noise in the bath are also responsible for dissipation. In Brownian motion, for instance, random kicks from the environment not only hinder the particle's motion but also simultaneously generate noise. Then the FDT precisely asserts that, on average, the random kicks from the fluctuating force balance out the energy lost through dissipation.

Another way to understand FDTs is through considering the role of the Kubo-Martin-Schwinger (KMS) conditions [73, 74], which encode thermal equilibrium in quantum systems. These conditions follow from the thermal density matrix $\hat{\rho}_\beta = e^{-\beta H}$ and relate various correlators of operators in thermal states.

To see how the KMS condition emerges, consider a thermal two-point function in the

[1] *Thermal noise* refers to the random fluctuations that arise due to the thermal motion of particles.

time domain:

$$\begin{aligned}
\langle A(t-i\beta)\ B(0)\rangle_\beta &= \mathrm{Tr}\big\{\hat{\rho}_\beta\ A(t-i\beta)\ B(0)\big\}\ , \\
&= \mathrm{Tr}\big\{e^{-\beta H}\ e^{iH(t-i\beta)}\ A(0)\ e^{-iH(t-i\beta)}\ B(0)\big\}\ , \\
&= \mathrm{Tr}\big\{e^{iHt}\ A(0)\ e^{-iHt}\ e^{-\beta H}\ B(0)\big\}\ , \\
&= \mathrm{Tr}\big\{e^{-\beta H}\ B(0)\ e^{iHt}\ A(0)\ e^{-iHt}\big\}\ , \\
&= \mathrm{Tr}\big\{e^{-\beta H}\ B(0)\ A(t)\big\}\ , \\
&= \langle B(0)\ A(t)\rangle_\beta\ .
\end{aligned} \tag{5.3}$$

where we have used the Heisenberg time evolution $A(t) = e^{iHt}\ A(0)\ e^{-iHt}$ and the cyclicity of the trace: $\mathrm{Tr}\big(A\ B\ C\big) = \mathrm{Tr}\big(C\ A\ B\big)$. Thus, the KMS condition in the time domain takes the form:

$$\langle A(t-i\beta)\ B(0)\rangle_\beta = \langle B(0)\ A(t)\rangle_\beta\ , \tag{5.4}$$

where the subscript β denotes the thermal state. In the frequency domain, this becomes:

$$e^{-\beta\omega}\ \langle A(\omega)\ B(0)\rangle_\beta = \langle B(0)\ A(\omega)\rangle_\beta\ , \tag{5.5}$$

where ω is the Fourier conjugate variable to time t.

This exponential relation (5.5) between correlators with different operator orderings lies at the heart of the fluctuation-dissipation relation. It ensures that fluctuations and responses are not independent but are intimately connected by the structure of thermal equilibrium.

To understand it better, let us start by defining two different types of thermal Wightman functions, as given below:

$$G^{>}(t) := \langle A(t)\ B(0)\rangle_\beta\ , \qquad\qquad G^{<}(t) := \langle B(0)\ A(t)\rangle_\beta\ . \tag{5.6}$$

Once these functions are defined, we can write down the commutator and anti-commutator as follows:

$$\begin{aligned}
\langle [A(t), B(0)]\rangle_\beta &:= G^{>}(t) - G^{<}(t)\ , \\
\langle \{A(t), B(0)\}\rangle_\beta &:= G^{>}(t) + G^{<}(t)\ .
\end{aligned} \tag{5.7}$$

As seen from the Eqs (5.4) and (5.5), the KMS condition in terms of two-point Wightman function is given by,

$$G^{>}(t) = G^{<}(t - i\beta) \ , \qquad\qquad G^{>}(\omega) = e^{\beta\omega}\, G^{<}(\omega) \ . \tag{5.8}$$

Again, writing the commutator and anti-commutator defined in Eq. (5.7), and using the above-mentioned KMS conditions, we find:

$$\begin{aligned} \langle [A(\omega), B(-\omega)] \rangle &= G^{>}(\omega) - G^{<}(\omega) = G^{>}(\omega)(1 - e^{-\beta\omega}) \ , \\ \langle \{A(\omega), B(-\omega)\} \rangle &= G^{>}(\omega) + G^{<}(\omega) = G^{>}(\omega)(1 + e^{-\beta\omega}) \ . \end{aligned} \tag{5.9}$$

Dividing the above equations gives the following fluctuation-dissipation relation:

$$\boxed{\langle \{A(\omega), B(-\omega)\} \rangle = \coth\left(\frac{\beta\omega}{2}\right) \langle [A(\omega), B(-\omega))] \rangle \ .} \tag{5.10}$$

Here,

- The **anti-commutator** gives the thermal fluctuations,
- The **commutator** gives the dissipative response,
- The factor $\coth(\beta\omega/2)$ encodes thermal weighting.

In the high-temperature limit $\beta \to 0$, this reduces to

$$\omega \, \langle \{A(\omega), B(-\omega)\} \rangle = \frac{2}{\beta} \, \langle [A(\omega), B(-\omega))] \rangle \ , \tag{5.11}$$

which is nothing but the familiar classical form of the linear FDT as given in Eq. (5.2) before. For textbook treatments of FDT via linear response theory, see [75, 79]. Although tangential to the main theme of the thesis, it is worth noting that the linear FDT can also be understood as an algebraic consequence rooted in the structure of von Neumann algebras.[2]

[2]In the algebraic perspective, the formulation of KMS relations/states depends on the type of von Neumann algebra involved. In particular, local QFTs are generically type-III, so there is no global trace or ordinary density matrix. Nevertheless, Tomita–Takesaki theory supplies a modular Hamiltonian, a modular automorphism group, and a precise notion of KMS states. Whenever a KMS state exists in this sense, the linear FDT follows as an algebraic consequence. What remains less clear — at least to our knowledge — is the extent to which this algebraic framework constrains the structure of non-linear FDTs.

On the other hand, *non-linear* FDTs [102] emerge from higher-point KMS conditions, often supplemented by principles such as microscopic time-reversibility. These relations are typically formulated using effective descriptions such as non-linear Langevin equations and can involve *out-of-time-ordered* (OTO) correlators. These correlators are sensitive to microscopic reversibility and quantum chaos, and are useful for diagnosing non-linear response. For detailed studies on this front, see [103–106].

At this stage, it is important to clarify a conceptual subtlety that frequently leads to confusion in the literature.

KMS relations and FDRs are not the same.

KMS relations constrain microscopic correlation functions and encode the thermal periodicity of operators. FDRs, by contrast, relate macroscopic dissipative transport coefficients to fluctuation strengths in the hydrodynamic, long-wavelength limit. These are qualitatively different layers of description: KMS symmetry governs the complete microscopic theory, whereas FDRs emerge only after coarse-graining. In this sense, they "live" in different spaces, and treating them interchangeably can be conceptually misleading.

This distinction is clearly illustrated in the existing literature. In Refs. [102, 104], certain higher-point KMS relations — often written in column-vector representation — are referred to as non-linear FDRs. However, these objects remain purely non-linear KMS constraints. Later developments [105, 106] demonstrate that extracting genuine non-linear FDRs requires additional dynamical input beyond KMS, and even with full knowledge of the microscopic KMS relations, deriving non-linear FDRs can be technically challenging.

From this perspective, the situation in holography becomes even more interesting. There is no a priori guarantee that non-linear FDRs should exist in generic interacting QFTs, much less at finite density. Even in neutral holographic systems, non-linear FDRs were established only recently [47], and their derivation relied crucially on the detailed structure of the grSK geometry. At non-zero chemical potential, no general proof of non-linear FDRs is currently known. While KMS symmetry undoubtedly holds for any thermal holographic state, it does not automatically imply the existence of non-linear FDRs. In this light, the question of whether such relations persist at finite density is both natural and non-trivial.

Despite these conceptual challenges, holography offers a promising framework for addressing them. Strongly coupled quantum systems interacting with black hole horizons provide first-principles access to both fluctuations and dissipation. This makes it possible — at least in principle — to derive non-linear FDRs in the presence of strongly coupled baths. It is precisely this holographic path that we now turn to.

5.2 Review of Holographic FDTs at zero-density

Black holes are thermal systems characterised by a well-defined temperature, and as such, they are expected to exhibit typical thermal properties. For example, they obey the laws of thermodynamics, captured in the form of black hole mechanics. As discussed earlier, all thermal systems satisfy fluctuation-dissipation theorems, and consequently, black holes — and more broadly, thermal holographic systems — should exhibit analogous FDTs. However, since these holographic systems are typically strongly coupled and thus extracting FDTs directly is difficult. Fortunately, holography maps such systems to weakly coupled classical gravitational configurations, making it possible to derive FDTs through gravitational techniques.

One of the simplest and most intuitive contexts in which FDTs arise is in the study of Brownian motion. In this case, the motion of a particle in a thermal medium is governed by a Langevin-type equation, where the FDT relates the dissipative and stochastic coefficients of the equation. This naturally leads us to ask:

How to construct an effective Langevin-like equation describing Brownian motion in a holographic setup, and thereby derive FDTs from gravity?

This question gains further motivation from the perspective of the *fluid-gravity correspondence* [107, 108] and has been explored in several works involving holographic descriptions of Brownian motion (see, e.g., [56, 109–113]). In the context of real-time holography, and specifically the grSK geometry, a comprehensive discussion of non-linear Langevin dynamics and the corresponding non-linear FDTs can be found in [60].

The basic idea is to model the Brownian particle (e.g. Heavy quark) as the endpoint of a fundamental string in a black hole background. One end of the string is fixed at the asymptotic boundary, representing the particle, while the rest of the string extends into

the bulk, interacting with the black hole horizon. The dynamics of this string capture the response of the particle to the strongly coupled medium.

Solving the string equations of motion and evaluating the on-shell action yields a generating functional for the boundary theory for the particle's dynamics. Interpreting this functional as an effective action for the Brownian particle allows one to derive a stochastic equation of motion via a Hubbard-Stratonovich transformation [114–116]. Comparing the dissipative and noise terms then provides direct access to the FDTs in the theory [60]. However, this analysis was restricted to a Brownian particle, leaving a generalization to fields as the next natural step.

The authors of [47] provided the first derivation of non-linear FDTs entirely within a field-theoretic framework by integrating out holographic bath degrees of freedom using the grSK prescription. Their derivation relied on analyzing Hawking radiation and its interaction with ingoing modes near the horizon. Before reviewing their analysis in the next subsection §5.2.1, we briefly outline the setup and key steps involved in deriving the FDTs.

To illustrate, they considered a non-linear generalisation of the Langevin equation for a Brownian field Φ of the form:

$$\left(-K\partial_t^2 + D\nabla^2 + \gamma\partial_t\right)\Phi + \sum_{k=1}^{n-1}\frac{\eta^k}{k!}\left(\theta_k + \bar{\theta}_k\partial_t\right)\Phi^{n-k} = \mathfrak{f}\,\eta \ , \tag{5.12}$$

where $K, D, \theta_k, \bar{\theta}_k$ are some unknown coefficients. These coefficients were shown to satisfy the following non-linear FDTs,

$$\frac{2}{\beta}\bar{\theta}_k + \theta_{k+1} + \frac{1}{4}\theta_{k-1} = 0 \ , \tag{5.13}$$

where θ_k and $\bar{\theta}_k$ correspond to non-linear generalization of fluctuation and dissipation coefficients.[3] Importantly, Eq. (5.13) provides a non-linear FDT valid to arbitrary order, capturing the full structure of fluctuations and dissipation in the zero-density holographic system.

The key steps behind deriving these holographic non-linear FDTs can be summarised as follows:

[3]The explicit expressions for θ_k and $\bar{\theta}_k$ can be found in the section 6 of [47].

1. One probes the grSK geometry with a self-interacting real scalar field and construct the on-shell action in the average-difference basis (see §5.2.1 for details).

2. Applying inverse Martin-Siggia-Rose (MSR) trick [117] then yields a classical Langevin equation, from which fluctuation and dissipation coefficients (θ_k, $\bar{\theta}_k$) and their relations can be extracted. These relations can also be directly read off from the on-shell action, as we will discuss in §5.2.1.

5.2.1 Real scalar field at zero-density

Let us begin by consider a self-interacting real scalar field ϕ in the zero-density case (i.e., in the grSK geometry), with the action given by:

$$S = -\oint_{\text{grSK}} \left(\frac{1}{2}(\partial_M \phi)^2 + \frac{g}{4!}\phi^4 \right) , \tag{5.14}$$

where g is the coupling constant. Note that while [47] considers general ϕ^n interactions, we restrict ourselves to the quartic case for simplicity.[4] In what follows, we adopt the same notation and conventions as used for the complex scalar field system in chapter 4, and will not elaborate on them unless ambiguity arises.

We now present the solution for this system. The zeroth-order (in coupling g) solution for the real scalar field ϕ, to linear order in the gradient expansion (with $\mathbf{k} = 0$), is:

$$\phi_{(0)} = \left[J_a + \left(\zeta - \frac{1}{2} + \mathbb{F}_1 \right) J_d \right] + \frac{i\beta}{2} \left[\mathbb{F}_1 \partial_t J_a - \left(\zeta(\zeta - 1) + \left[\zeta - \frac{1}{2} \right] \mathbb{F}_1 \right) \partial_t J_d \right] , \tag{5.15}$$

where we recall the $\mathbb{F}_1$ is defined in Eq. (4.67), and the corresponding expression of quartic on-shell action is,

$$S^{\phi}_{(4)} = -\frac{g}{4!} \oint_{\text{grSK}} d\zeta d^d x \sqrt{-g}\ \phi^4_{(0)} , \tag{5.16}$$

where the superscript indicates that we are working with the real scalar field ϕ. Upon evaluating the radial contour integrals in the grSK geometry, the quartic on-shell action

[4] This simplification is for convenience; the analysis can be extended to general ϕ^n interactions.

becomes up to linear order in derivatives,

$$S^{\phi}_{(4)} = -g\int d^dx\Bigg\{\sum_{k=1}^{4}\Theta_k\frac{J_a^{4-k}}{(4-k)!}\frac{(iJ_d)^k}{k!}+\sum_{k=1}^{3}\bar{\Theta}^{(a)}_k\ (\partial_t J_a)\frac{J_a^{3-k}}{(3-k)!}\frac{(iJ_d)^k}{k!} + \sum_{k=1}^{3}\bar{\Theta}^{(d)}_k\frac{J_a^{4-k}}{(4-k)!}\frac{(iJ_d)^{k-1}}{(k-1)!}\partial_t(iJ_d)\Bigg\}+\mathcal{O}\left((\beta\partial_t)^2\right)\ , \tag{5.17}$$

where the zeroth-order coefficients in the gradient-expansion are:

$$\Theta_k = \frac{1}{i^k}\oint_{\text{grSK}} d\zeta\ \sqrt{-g}\left(\zeta-\frac{1}{2}+\mathbb{F}_1\right)^k\ , \tag{5.18}$$

where we recall that $\mathbb{F}_1$ id defined in Eq. (4.67).

The first-order coefficients in the gradient expansion are given by:

$$\begin{aligned}\bar{\Theta}^{(a)}_k &= \frac{1}{i^{k-1}}\frac{\beta}{2}\oint_{\text{grSK}} d\zeta\ \sqrt{-g}\ \mathbb{F}_1\left(\zeta-\frac{1}{2}+\mathbb{F}_1\right)^k\ ,\\ \bar{\Theta}^{(d)}_k &= -\frac{1}{i^{k-1}}\frac{\beta}{2}\oint_{\text{grSK}} d\zeta\ \sqrt{-g}\ \left[\zeta(\zeta-1)+\left(\zeta-\frac{1}{2}\right)\mathbb{F}_1\right]\left(\zeta-\frac{1}{2}+\mathbb{F}_1\right)^{k-1}\ ,\end{aligned} \tag{5.19}$$

where the superscripts (a) and (d) indicate that the time derivative ∂_t acts on the average source J_a and the difference source J_d, respectively.

By performing integration by parts in Eq. (5.17) and ignoring total derivative terms, we can shift the derivatives from J_a onto J_d, yielding

$$S^{\phi}_{(4)} = -g\int d^dx\Bigg\{\sum_{k=1}^{4}\Theta_k\frac{J_a^{4-k}}{(4-k)!}\frac{(iJ_d)^k}{k!}+\sum_{k=1}^{3}\left(\bar{\Theta}^{(d)}_k-\bar{\Theta}^{(a)}_k\right)\frac{J_a^{4-k}}{(4-k)!}\frac{(iJ_d)^{k-1}}{(k-1)!}\partial_t(iJ_d)\Bigg\}\ . \tag{5.20}$$

Now, we define $\bar{\Theta}_k \equiv \left(\bar{\Theta}^{(a)}_k-\bar{\Theta}^{(d)}_k\right)$ to simplify the above expression,

$$S^{\phi}_{(4)} = -g\int d^dx\Bigg\{\sum_{k=1}^{4}\Theta_k\frac{J_a^{4-k}}{(4-k)!}\frac{(iJ_d)^k}{k!}-\sum_{k=1}^{3}\bar{\Theta}_k\frac{J_a^{4-k}}{(4-k)!}\frac{(iJ_d)^{k-1}}{(k-1)!}\partial_t(iJ_d)\Bigg\}\ . \tag{5.21}$$

Then, it is not hard to check that the coefficients are related by the following equation,

$$\frac{2}{\beta}\bar{\Theta}_k+\Theta_{k+1}+\frac{1}{4}\Theta_{k-1}=0\ , \tag{5.22}$$

where we note that these relations hold even before performing the radial grSK integral,

i.e., they are valid at the level of the integrands. In fact, they reproduce the same FDRs derived in [47] for a system at zero density.[5]

That said, it is important to emphasize that the coefficients $\{\Theta_k, \bar{\Theta}_k\}$ appearing here are not identical to those defined in Eq. (5.12), namely $\{\theta_k, \bar{\theta}_k\}$, but are proportional to them.[6] The explicit computation of these coefficients requires evaluating a radial grSK integral, as detailed in Appendix (E.1) of [47]. Making use of those results, we obtain the following expressions for Θ_k:

$$\begin{aligned} \Theta_1 &= \frac{1}{i}\frac{1}{d}\left(r_c^d - r_h^d\right) \ , \qquad \Theta_2 = -\frac{1}{i^2}\frac{r_h^d}{\pi i}\log\frac{r_c}{r_h} \ , \\ \Theta_3 &= \frac{1}{i^3}\left(\frac{r_c^d}{4d} - \frac{r_h^d}{2d}\right) \ , \quad \Theta_4 = \frac{1}{i^4}\left(-\frac{r_h^d}{2\pi i}\log\frac{r_c}{r_h} + \frac{1}{2\pi i}\frac{r_h^d}{d}\frac{6}{\pi^2}\zeta(3) + \mathcal{O}\left(\frac{1}{r_c^d}\right)\right) \ . \end{aligned} \tag{5.23}$$

The remaining $\bar{\Theta}_k$ terms can be obtained using the non-linear FDRs given in Eq. (5.22).

These non-linear FDRs can also be represented diagrammatically. For example, in the case of $k = 2$, Eq. (5.22) yields the following schematic representation,

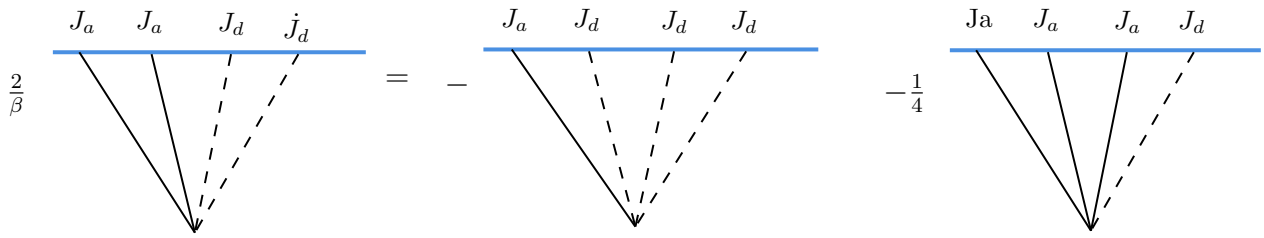

Figure 5.1: Schematic representation of a non-linear FDR for the case of $k = 2$. Solid and dashed lines represent boundary-to-bulk propagators that terminate on average J_a and difference J_d boundary sources, respectively.

Here, solid lines denote average sources (J_a), dashed lines denote difference sources (J_d), and dots indicate time derivatives. Similar diagrammatic representations can be constructed for other cases ($k \neq 2$), rendering the structure of the non-linear FDRs manifest in terms of effective vertices.

We now conclude our discussion of FDRs at zero density with a brief motivation to study their counterparts at finite density.

To the best of our knowledge, this remains the only available method for deriving FDTs in strongly coupled thermal baths. However, to build greater confidence in these

[5] Throughout this work, we use the terms FDT and FDR interchangeably and will continue to do so for consistency.

[6] The proportionality factors can be determined explicitly, but since they do not affect our discussion, we will not elaborate on them here.

results, it is important to explore other settings where such relations may hold. A natural next step is to extend this analysis to finite-density holographic baths and investigate whether analogous FDRs emerge.

At the outset, it is not obvious that such FDTs should persist in these systems. Finite-density holographic theories introduce qualitatively new features — such as charged black hole backgrounds, multiple horizons, and chemical potentials — that might affect affect the dynamics of fluctuations and dissipation relative to the zero-density case. This leads us to the following central question:

Do fluctuation-dissipation theorems exist in finite-density holographic systems? If so, what form do they take, and how do they differ from the zero-density case?

We now turn to this question in the next section.

5.3 Holographic FDTs at small but finite density

We begin this section by revisiting the setup and results discussed in chapter 4. Recall, we considered a self-interacting complex scalar field propagating in the RNSK geometry, with the action given by

$$S = -\oint_{\text{RNSK}} \left(|D_M \Phi|^2 + \frac{\lambda}{2!2!} |\Phi|^4 \right) . \tag{5.24}$$

We employed perturbation theory to study the dynamics of this theory and computed the on-shell bulk action, which corresponds to the Schwinger-Keldysh generating functional for the dual boundary theory.

The on-shell action S_{os} can be expanded in powers of the coupling constant λ as:

$$S_{\text{os}} = S_{(2)} + S_{(4)} + S_{(6)} + \dots , \tag{5.25}$$

where the subscript denotes the number of boundary sources involved in each term. To streamline the notation, we expressed the general $2n$-point contribution to the on-shell action as:

$$S_{(2n)} = \int_{k_{1,2,\dots,2n}} \sum_{r,s=0}^{n} \mathcal{I}_{r,s}^{(2n)}(k_1, \dots, k_{2n}) \prod_{i=1}^{r} \bar{J}_{\bar{F}}(k_i) \prod_{j=1}^{s} J_{\bar{F}}(k_j) \prod_{l=r+1}^{n} \bar{J}_{\bar{P}}(k_l) \prod_{m=s+1}^{n} J_{\bar{P}}(k_m) , \tag{5.26}$$

where the coefficients $\mathcal{I}^{(2n)}_{r,s}$ are determined from the Feynman rules of the exterior field theory derived from the bulk, as see in Eqs. (4.53) and (4.57).

Our goal now is to extract the relationships between fluctuation and dissipation coefficients — that is, to identify holographic FDTs for this system. To do this, it is convenient to work in the average-difference basis of the SK formalism. This basis is particularly important because the average field maps to the classical stochastic variable under a inverse MSR transformation, while the difference field corresponds to the noise source.[7]

However, it is worth emphasizing that both the on-shell action (or SK generating functional) and the corresponding stochastic equation contain the same physical information, simply packaged differently. Therefore, instead of performing the MSR transformation, we can equivalently analyze the on-shell action directly and look for relations among various terms — these relations are the sought-after holographic FDTs.

We begin with the simplest case: the quadratic part of the SK effective action in average-difference basis as given in Eq. (4.75),

$$S_{(2)} = \int \frac{d^d k}{(2\pi)^d} \left[K_{\rm ret}\ \bar{J}_d(-k) J_a(k) + K_{\rm adv}\ \bar{J}_a(-k) J_d(k) + K_{\rm kel}\ \bar{J}_d(-k) J_d(k) \right] \ . \tag{5.27}$$

This part contains two-point correlations and, as seen earlier, yields the KMS relation. At finite density, the two-point KMS relation takes the following form:

$$\begin{aligned} \frac{K_{\rm kel}}{2} &= \frac{1}{4} \coth\left(\frac{\beta(k^0 - \mu_q)}{2}\right) \left[K_{\rm ret} - K_{\rm adv}\right] \ , \\ &= \frac{i}{2} \coth\left(\frac{\beta(k^0 - \mu_q)}{2}\right) {\rm Im}\left[K_{\rm ret}\right] \ . \end{aligned} \tag{5.28}$$

Here, $K_{\rm ret}$ and $K_{\rm adv}$ are the retarded and advanced propagators, and $K_{\rm kel}$ is the Keldysh (or symmetric) propagator, which captures the fluctuations. This relation is the finite-density generalisation of the linear fluctuation-dissipation theorem. To understand this, recall that ${\rm Im}\left[K_{\rm ret}\right]$ corresponds to the spectral function at finite temperature, while $K_{\rm kel}$ represents twice the anti-commutator (refer to [79, 98] for details). Commutators present in response functions naturally measure dissipation and transport, whereas anti-commutators capture fluctuations [104]. Consequently, Eq. (5.28) provides a correct description of the linear fluctuation-dissipation relation in finite-density systems.

[7] For details on this mapping, see [47].

In the zero-density case ($\mu = 0$), and assuming the field is real, the two-point KMS condition in the high-temperature limit ($\beta \to 0$) takes the form of linear FDT, which can be diagrammatically described as,

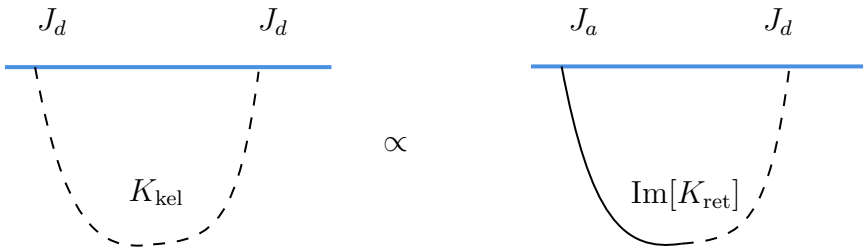

Figure 5.2: Schematic representation of the linear FDT. Solid and dashed lines correspond to average J_a and difference J_d sources, respectively.

In what follows, we explore how the fluctuation-dissipation paradigm extends to higher-point functions, and whether non-linear FDRs persist in strongly coupled systems at finite density. This question captures the novelty of our work.

Just as we analyzed the quadratic on-shell action in the linear FDT case, we now turn to the next non-vanishing term: the quartic term in the on-shell action. Due to the parity structure of the action, only even-order terms contribute, making the quartic term the natural next step.

This quartic contribution to the on-shell action arises from the contact Witten diagrams, depicted in figure 4.1. Each diagram contributes a specific term to the on-shell action, written explicitly using Feynman rules in the Past-Future (PF) basis as shown in Eq. (4.53). However, to extract FDRs, it is more appropriate to express the on-shell action in the average-difference basis.

Unlike the quadratic case, the quartic expressions become significantly more involved. Fortunately, since the FDRs only require terms up to first order in derivatives, we can simplify our analysis by keeping only the leading derivative expansion. As shown in Eq. (4.78), the quartic on-shell action up to linear order in near-μ_q gradient and charge expansion while discarding mixed terms, can be written as:

$$S_{(4)} \approx -\lambda \int d^d x \int_{\text{ext}} \mathcal{L}_0 - \lambda \int d^d x \int_{\text{ext}} \mathcal{L}_1 \ , \tag{5.29}$$

where the terms $\mathcal{L}_0$ and $\mathcal{L}_1$ represent the non-derivative and first-derivative contributions

to $S_{(4)}$, respectively. The $\mathcal{L}_0$ and $\mathcal{L}_1$ are given by

$$\begin{aligned}
\mathcal{L}_0 &= \sum_{r,s=0}^{2} \mathcal{G}_{r,s} \ \left[\bar{J}_a\right]^r [J_a]^s \left[\bar{J}_d\right]^{2-r} [J_d]^{2-s} \ , \\
\mathcal{L}_1 &= \sum_{r=0}^{1}\sum_{s=0}^{2} \left\{ \mathcal{G}_{\dot{r},s} \left(\partial_t \bar{J}_a\right) + \mathcal{H}_{\dot{r},s} \left(\partial_t \bar{J}_d\right) \right\} \left[\bar{J}_a\right]^r [J_a]^s \left[\bar{J}_d\right]^{1-r} [J_d]^{2-s} \\
&\quad + \sum_{r=0}^{2}\sum_{s=0}^{1} \left\{ \mathcal{G}_{r,\dot{s}} \left(\partial_t J_a\right) + \mathcal{H}_{r,\dot{s}} \left(\partial_t J_d\right) \right\} \left[\bar{J}_a\right]^r [J_a]^s \left[\bar{J}_d\right]^{2-r} [J_d]^{1-s} \ ,
\end{aligned} \tag{5.30}$$

where all of the above-mentioned terms/coefficients are given in Appendix D.1 (see Eqs. (D.15), (D.19) and (D.20)). These terms/coefficients are not all independent. Their interrelations arise from:

- the *reality* of the on-shell action ,
- the *underlying KMS symmetry*, which gives rise to non-linear fluctuation-dissipation relations.

Importantly, these relations connect terms with and without derivatives (i.e., dissipation vs. fluctuation), and terms with different combinations of average $(J_a, \bar{J}_a)$ and difference $(J_d, \bar{J}_d)$ sources. This structure becomes more transparent in the Witten diagram representation, where different diagram topologies naturally encode these dependencies.

Without further ado, we now write down the non-linear FDRs among the quartic coefficients:

$$\begin{aligned}
&\mathcal{G}_{\dot{0},0} - \mathcal{H}_{\dot{1},0} - i\beta\mathcal{G}_{0,0} + \frac{i\beta}{24}\left(\mathcal{G}_{2,0} + \mathcal{G}_{1,1} + \mathcal{G}_{0,2}\right) = 0 \ , \\
&-\frac{1}{3}\left(\mathcal{G}_{\dot{0},2} + \mathcal{G}_{\dot{1},1}\right) + \mathcal{H}_{\dot{1},2} + \frac{i\beta}{6}\left(\mathcal{G}_{2,0} + \mathcal{G}_{1,1} + \mathcal{G}_{0,2}\right) = 0 \ , \\
&-\frac{1}{3}\left(\mathcal{G}_{\dot{1},0} + \mathcal{G}_{\dot{0},1}\right) + \frac{1}{5}\mathcal{H}_{\dot{0},2} + \frac{2}{5}\mathcal{H}_{\dot{1},1} - \frac{i\beta}{16}\left(\mathcal{G}_{1,2} + \mathcal{G}_{2,1}\right) + \frac{i\beta}{4}\left(\mathcal{G}_{0,1} + \mathcal{G}_{1,0}\right) = 0 \ .
\end{aligned} \tag{5.31}$$

where the terms containing time derivatives correspond to dissipation coefficients, while those without derivatives represent the fluctuation strength and coefficient β (inverse temperature) acts as the thermal weighting factor. Hence, these are the non-linear FDRs at finite density, derived from the structure of the on-shell action. It is important to emphasize, however, that these relations have been obtained by working only to linear order in the small chemical potential. Going beyond this approximation may modify these relations, a question we leave for future work.

These relations can be further understood using the inverse Martin-Siggia-Rose (MSR) formalism [117], where one transforms the influence functional into a stochastic field theory. In that language:

- The *average source* J_a is identified with the classical stochastic field.
- The *difference source* iJ_d corresponds to the stochastic noise.

For the purposes of this work, we focus on the on-shell action and postpone a detailed derivation of the corresponding stochastic field equations to future work.

The non-linear relations we have derived represent a new class of holographic FDRs valid at finite density. Unlike the well-studied two-point correlators with linear FDT, these relations govern the dynamics of higher-order correlators in strongly coupled systems with chemical potential and describe how non-linear fluctuations and dissipative responses are interrelated. The fact that such relations are encoded in the dynamics of bulk gravity further underscores holography as a powerful organising principle for understanding fluctuations in strongly coupled systems.

The holographic FDRs at finite density presented here constitute one of the novel contributions of this work. To our knowledge, this is the first time such relations have been explicitly derived. Naturally, this raises the question of whether they can be independently verified through other means. Unfortunately, strongly coupled field theories at finite density generally lack non-holographic tools that allow for computing such relations. This very limitation highlights the power and utility of holography in accessing non-perturbative regimes.

That said, an important consistency check is to consider the zero-density limit ($\mu \to 0$), in which the dual black hole background becomes neutral. One would expect to recover previously known results in this limit. However, the system we study here differs from the one examined in earlier zero-density analyses (e.g, the system we reviewed in §5.2.1). In particular, our zero-density limit involves two coupled scalar fields with cross-interactions, as opposed to a single self-interacting scalar field considered in [47]. Thus, the check is less straightforward than it may appear.

A meaningful first step is to derive the holographic FDRs for two cross-interacting scalar fields at zero density. This itself constitutes a new result and is worth pursuing independently. Once obtained, these FDRs can be compared to those in [47] (or system

presented in §5.2.1). However, the outcome of such a comparison is not obvious *a priori*, given the structural differences between the two setups. As such, the question is exploratory in nature and could lead to new insights into how FDRs behave in the presence of multiple interacting fields.

5.4 Zero-density limit

The zero-density limit of our setup corresponds to a self-interacting complex scalar field propagating in the grSK geometry instead of the RNSK geometry, with the action given by,

$$S = -\oint_{\text{grSK}} \left(|\partial_M \Phi|^2 + \frac{\lambda}{2!2!} |\Phi|^4 \right) . \tag{5.32}$$

This new setup can equivalently be described in terms of real degrees of freedom by replacing the complex field Φ with a pair of real scalar fields $\{\phi, \varphi\}$ defined as,

$$\Phi \equiv \frac{\phi + i\varphi}{\sqrt{2}} . \tag{5.33}$$

The action in terms of the ϕ–φ variables then becomes,

$$S = -\oint_{\text{grSK}} \left(\frac{1}{2}(\partial\phi)^2 + \frac{1}{2}(\partial\varphi)^2 + \frac{\lambda}{16}\phi^4 + \frac{\lambda}{16}\varphi^4 + \frac{\lambda}{8}\phi^2\varphi^2 \right) . \tag{5.34}$$

Inserting the perturbative solution[8] into the bare action yields the *on-shell action* S_{os} in the following form:

$$\begin{aligned} S_{\text{os}} = &-\frac{1}{2}\int_{\partial\mathcal{M}} \phi_{(0)} \left(\partial_A \phi_{(0)}\right) - \frac{1}{2}\int_{\partial\mathcal{M}} \varphi_{(0)} \left(\partial_A \varphi_{(0)}\right) \\ &+ \lambda \oint_{\mathcal{M}} \left[\frac{1}{8} \left((\phi - \phi_{(0)})\phi + i\varphi_{(0)}\phi - i\phi_{(0)}\varphi + (\varphi - \varphi_{(0)})\varphi \right) (\phi^2 + \varphi^2) \right. \\ &\left. - \frac{1}{16}\phi^4 - \frac{1}{16}\varphi^4 - \frac{1}{8}\phi^2\varphi^2 \right] , \end{aligned} \tag{5.35}$$

where $\partial\mathcal{M}$ denotes the boundary of the bulk manifold $\mathcal{M}$. In deriving the above expression, we have used the field equations of the ϕ–φ system and imposed appropriate boundary conditions to simplify the on-shell action.

[8] The notation for the perturbative expansion of $\phi - \varphi$ system is similar to that of Φ, as given in Eq. (4.29).

Expanding the on-shell action $S_{\rm os}$ in powers of λ, we obtain:

$$S_{\rm os} = S_{(2)} + S_{(4)} + \dots \ , \tag{5.36}$$

where the subscripts indicate the number of boundary sources in each term. In particular, the quadratic and quartic contributions are given by:

$$\begin{aligned} S_{(2)} &= -\frac{1}{2}\int_{\partial\mathcal{M}} \phi_{(0)}\left(\partial_A \phi_{(0)}\right) - \frac{1}{2}\int_{\partial\mathcal{M}} \varphi_{(0)}\left(\partial_A \varphi_{(0)}\right) \ , \\ S_{(4)} &= -\oint_{\rm grSK}\left(\frac{\lambda}{16}\phi_{(0)}^4 + \frac{\lambda}{16}\varphi_{(0)}^4 + \frac{\lambda}{8}\phi_{(0)}^2\varphi_{(0)}^2\right) \ . \end{aligned} \tag{5.37}$$

Again, these terms correspond to the free and contact contributions at tree-level in the Feynman diagram expansion.

Since the chemical potential vanishes in the zero-density case, we can directly write down the gradient-expanded solution for the zeroth-order complex field Φ (with $\mathbf{k} = 0$) by setting $\mu = 0$. As previously noted, the only non-trivial component we require is the ingoing solution $G^{\rm in}$, which, after setting $\mu = 0$, takes the form:

$$G^{\rm in} = \sum_i G_i^{\rm in}(\zeta)\left(\frac{\beta k^0}{2}\right)^i \ , \tag{5.38}$$

with coefficients explicitly given by:

$$\begin{aligned} &G_0^{\rm in} = 1 \ , \quad G_1^{\rm in} = \mathbb{F}_1(r) \ , \\ &G_2^{\rm in} = \int_{\zeta_c}^{\zeta}\frac{d\bar{\zeta}}{\bar{r}^{d-1}}\int_{\zeta_h}^{\bar{\zeta}} d\hat{\zeta}\left[\hat{r}^{d-1}\right]'\mathbb{F}_1(\hat{r}) - 2\int_{\zeta_c}^{\zeta} d\bar{\zeta}\left(\mathbb{F}_1(r) - \frac{r_+^{d-1}}{r^{d-1}}\mathbb{F}_1(r_+)\right) \ , \end{aligned} \tag{5.39}$$

where we again define,

$$\mathbb{F}_n(r) \equiv \int_{\zeta_c}^{\zeta} d\bar{\zeta}\left[\left(\frac{r_+}{\bar{r}}\right)^{d-n} - 1\right] \ , \qquad \zeta_h \equiv \zeta(r_+), \qquad \zeta_c \equiv \zeta(r_c) \ , \tag{5.40}$$

where r_+ now denotes the horizon size of the grSK geometry. The outgoing solution is obtained via CPT conjugation discussed in chapter 4 (See Eq. (4.9) for the mapping) by setting $\mu_q = 0$.

Using this, the full solution for the zeroth-order complex field at zero density is:

$$\Phi_{(0)}\Big|_{\mu=0} = G_q^{\text{in}}(k)\left[J_a(k) + \left(n_k + \frac{1}{2}\right) J_d(k)\right] - e^{-\beta k^0(\zeta-1)} G_{-q}^{\text{in}}(-k) n_k J_d(k) \ , \tag{5.41}$$

where we have suppressed the radial dependence of the Green's functions.

To conclude the discussion on the gradient expansion, we present the solution up to linear order in derivatives, which will be useful when we evaluate the non-linear FDRs in the upcoming text.

$$\Phi_{(0)}\Big|_{\mu=0} = \left[J_a + \left(\zeta - \frac{1}{2} + \mathbb{F}_1\right) J_d\right] + \frac{i\beta}{2}\left[\mathbb{F}_1\, \partial_t J_a - \left(\zeta(\zeta-1) + \left(\zeta - \frac{1}{2}\right)\mathbb{F}_1\right)\partial_t J_d\right] \ , \tag{5.42}$$

where we have replaced $k^0 \mapsto i\partial_t$.

As far as the quadratic influence phase $S_{(2)}$ is concerned, the calculation is straightforward. One can simply take the result from the non-zero chemical potential case and set $\mu = 0$. The two-point KMS condition is satisfied and gives rise to two familiar linear FDTs — one for each real scalar field in the complex field.

However, the interesting structure emerges in the quartic influence phase $S_{(4)}$, where cross-interactions — i.e., couplings between the two real scalar fields — first appear. By taking the $\mu \to 0$ limit of Eq. (5.29), we obtain,

$$S_{(4)}\big|_{\mu=0} = -\lambda \int d^d x \int_{\text{ext}} \mathcal{L}_0 - \lambda \int d^d x \int_{\text{ext}} \mathcal{L}_1 + \mathcal{O}\left((\beta\partial_t)^2\right) \ , \tag{5.43}$$

where $\mathcal{L}_0$ and $\mathcal{L}_1$ denote the non-derivative and first-derivative contributions in the zero chemical potential limit, respectively. From here on, we will omit the explicit notation indicating $\mu = 0$, as it will be clear from the context.

The non-derivative part is given by:

$$\mathcal{L}_0 = \sum_{r,s=0}^{2} \mathcal{G}_{r,s} \left[\bar{J}_a\right]^r \left[J_a\right]^s \left[\bar{J}_d\right]^{2-r} \left[J_d\right]^{2-s} \ , \tag{5.44}$$

with independent components:

$$\begin{aligned} &\mathcal{G}_{0,0} = \frac{1}{4}\left(\zeta + \mathbb{F}_1\right) + \left(\zeta + \mathbb{F}_1\right)^3 \ , \qquad \mathcal{G}_{0,1} = \frac{1}{8} + \frac{3}{2}\left(\zeta + \mathbb{F}_1\right)^2 \ , \\ &\mathcal{G}_{0,2} = \frac{1}{2}\left(\zeta + \mathbb{F}_1\right) \ , \quad \mathcal{G}_{1,1} = 2\left(\zeta + \mathbb{F}_1\right) \ , \quad \mathcal{G}_{1,2} = \frac{1}{2} \ , \quad \mathcal{G}_{2,2} = 0 \ . \end{aligned} \tag{5.45}$$

Here, all the remaining coefficients are related by the following relation:

$$\mathcal{G}_{r,s} = \mathcal{G}_{s,r} \ . \tag{5.46}$$

The first-derivative contribution, $\mathcal{L}_1$, remains unchanged from the $\mu \neq 0$ case (See Eqs. (5.30) and Eqs. (D.19) and (D.20)), as it does not contain any μ-dependent terms to begin with. Note that this holds only because we are working to linear order in the small chemical potential expansion.

Thus, it can be readily checked that these coefficients are related by what we call FDRs at zero density for the system of complex field with quartic interactions (similar to the $\phi - \varphi$ system described above). The relations which directly follow from taking the $\mu \to 0$ limit are as follows:

$$\begin{aligned}
&\mathcal{G}_{\dot{0},0} - \mathcal{H}_{\dot{1},0} - i\beta\mathcal{G}_{0,0} + \frac{i\beta}{24}\mathcal{G}_{1,1} + \frac{i\beta}{12}\mathcal{G}_{0,2} = 0 \ , \\
&-\frac{1}{3}\left(\mathcal{G}_{\dot{0},2} + \mathcal{G}_{\dot{1},1}\right) + \mathcal{H}_{\dot{1},2} + \frac{i\beta}{6}\mathcal{G}_{1,1} + \frac{i\beta}{3}\mathcal{G}_{0,2} = 0 \ , \\
&-\frac{2}{3}\left(\mathcal{G}_{\dot{1},0} + \mathcal{G}_{\dot{0},1}\right) + \frac{2}{5}\mathcal{H}_{\dot{0},2} + \frac{4}{5}\mathcal{H}_{\dot{1},1} - \frac{i\beta}{4}\mathcal{G}_{1,2} + i\beta\,\mathcal{G}_{0,1} = 0 \ .
\end{aligned} \tag{5.47}$$

Apart from these relations, we expect additional relations to emerge in the zero-density limit. We leave a systematic exploration of these to future work. For now, our goal is to compare the fluctuation and dissipation coefficients $\mathcal{G}_{r,s}$, $\mathcal{G}_{\dot{r},s}$, and $\mathcal{H}_{\dot{r},s}$ introduced in this section with the coefficients $(\Theta_k, \bar{\Theta}_k)$ that appeared earlier in §5.2.1.

Since both sets of coefficients arise in the zero-density case, it is natural to ask: how are they related? We will shortly demonstrate this connection explicitly, but let us first introduce the idea at a general level by examining how the coefficients $\mathcal{G}_{r,s}$ and related quantities can be expressed in terms of $(\Theta_k, \bar{\Theta}_k)$.

To begin, we consider a prototypical example by taking a coefficient $\mathcal{G}_{1,1}$ defined in Eq. (5.45). We now convert the exterior integral to the grSK integral, as shown below–

$$\begin{aligned}
\int_{\text{ext}} \mathcal{G}_{1,1} &= 2\int_{\text{ext}} (\zeta + \mathbb{F}_1) \\
&= \int_{\text{ext}} \left[\left(\zeta + \frac{1}{2} + \mathbb{F}_1\right)^2 - \left(\zeta - \frac{1}{2} + \mathbb{F}_1\right)^2\right] \\
&= \oint_{\text{grSK}} \left(\zeta - \frac{1}{2} + \mathbb{F}_1\right)^2 = i^2\Theta_2 \ ,
\end{aligned} \tag{5.48}$$

where in the last line we used the definition of Θ_2 from Eq. (5.18). This computation illustrates that the coefficient $\mathcal{G}_{1,1}$, once integrated over the exterior region, directly relates to Θ_2. where we have used the definition given in Eq. (5.18).

To streamline notation going forward, we define,

$$\widetilde{F} \equiv \int_{\text{ext}} F(\zeta) \ , \tag{5.49}$$

where the 'tilde' denotes integration over the exterior region. Then, the result from Eq. (5.48) simply becomes,

$$\widetilde{\mathcal{G}}_{1,1} = i^2 \Theta_2 \ . \tag{5.50}$$

Using this logic, we can now compare other coefficients in a similar fashion. Without going into the details, we first quote the results of the comparison of zero-derivative terms as,

$$\begin{aligned} &\widetilde{\mathcal{G}}_{0,0} = \frac{i^4}{4}\Theta_4 \ , \qquad \widetilde{\mathcal{G}}_{0,1} = \frac{i^3}{2}\Theta_3 \ , \\ &\widetilde{\mathcal{G}}_{0,2} = \frac{i^2}{4}\Theta_2 \ , \qquad \widetilde{\mathcal{G}}_{1,1} = i^2\,\Theta_2 \ , \qquad \widetilde{\mathcal{G}}_{1,2} = \frac{i}{2}\Theta_1 \ , \end{aligned} \tag{5.51}$$

where Θ_k is defined in Eq. (5.18) and explicit expressions are given in Eq. (5.23).

Next, we quote the comparison of first-derivative terms as,

$$\begin{aligned} &\widetilde{\mathcal{G}}_{\dot{0},2} = \frac{i}{2}\bar{\Theta}_1^{(a)} \ , \qquad \widetilde{\mathcal{G}}_{\dot{1},1} = i\bar{\Theta}_1^{(a)} \ , \\ &\widetilde{\mathcal{G}}_{\dot{1},0} = \frac{i^2}{2}\bar{\Theta}_2^{(a)} \ , \qquad \widetilde{\mathcal{G}}_{\dot{0},1} = i^2\bar{\Theta}_2^{(a)} \ , \qquad \widetilde{\mathcal{G}}_{\dot{0},0} = \frac{i^3}{2}\bar{\Theta}_3^{(a)} \ , \end{aligned} \tag{5.52}$$

and

$$\begin{aligned} &\widetilde{\mathcal{H}}_{\dot{1},2} = \frac{i}{2}\bar{\Theta}_1^{(d)} \ , \quad \widetilde{\mathcal{H}}_{\dot{0},2} = \frac{i^2}{2}\bar{\Theta}_2^{(d)} \ , \qquad \widetilde{\mathcal{H}}_{\dot{1},1} = i^2\bar{\Theta}_2^{(d)} \ , \\ &\widetilde{\mathcal{H}}_{\dot{0},1} = i^3\bar{\Theta}_3^{(d)} \ , \quad \widetilde{\mathcal{H}}_{\dot{1},0} = \frac{i^3}{2}\bar{\Theta}_3^{(d)} \ , \qquad \widetilde{\mathcal{H}}_{\dot{0},0} = \frac{i^4}{2}\bar{\Theta}_4^{(d)} \ , \end{aligned} \tag{5.53}$$

where we have used the expressions for coefficients $\bar{\Theta}_k^{(a)}$ and $\bar{\Theta}_k^{(d)}$ are defined in Eq. (5.19). These relations provide a precise dictionary between the two sets of coefficients — those arising in the complex scalar field setup and those in the real scalar field setup — in the zero-density limit.

Consistency Check: To validate this dictionary, let us consider a particular fluctuation-dissipation relation in the $\mu \to 0$ limit. For example, consider the first equation in Eq. (5.47):

$$\mathcal{G}_{\dot{0},0} - \mathcal{H}_{\dot{1},0} - i\beta\mathcal{G}_{0,0} + \frac{i\beta}{24}\mathcal{G}_{1,1} + \frac{i\beta}{12}\mathcal{G}_{0,2} = 0 \ . \tag{5.54}$$

Plugging in the relations from Eqs. (5.51), (5.52), and (5.53), we find that this becomes the following Θ-based expression:

$$\frac{2}{\beta}\bar{\Theta}_3 + \Theta_4 + \frac{1}{4}\Theta_2 = 0 \ , \tag{5.55}$$

where we have used the identity $\bar{\Theta}_k = \bar{\Theta}_k^{(a)} - \bar{\Theta}_k^{(d)}$. As noted in Eq. (5.22), this is nothing but FDRs for real scalar setup at zero density.

One can perform similar checks for other FDRs and confirm that they are consistent with the non-linear FDRs expressed in Eq. (5.22). This establishes the equivalence between the two descriptions at zero density, at least for the set of relations we have obtained, namely those in Eq. (5.47).

We now conclude our discussion of the comparison between the zero-density FDRs derived here and those obtained in the earlier work [47], and proceed to summarize the main insights of this section.

To summarise, we have shown that:

- Non-linear fluctuation-dissipation relations exist in holographic systems at small but finite density.
- These relations are encoded in the structure of the on-shell gravitational action.
- They reduce to known results at zero density, thereby passing a non-trivial consistency check,
- And they represent a step forward in connecting bulk gravity with non-linear stochastic dynamics in strongly coupled quantum systems at finite density.

Having resolved the question posed at the beginning of this work, we now conclude the thesis with a summary of results and a discussion of future directions.

Chapter 6

Conclusion

We will now conclude with a summary of results and future directions.

6.1 Summary

In this work, we have studied fluctuations in strongly coupled quantum field theories at finite density. We have achieved this using the real-time (Schwinger-Keldysh) formalism within the holographic framework. Our first goal was to construct a gravitational setting that captures the physics of finite-density holographic systems. Once this setup was established, we focused on understanding the nature of fluctuations in these systems. In particular, we asked whether such fluctuations are related to dissipation. This question is natural, since fluctuation-dissipation theorems are expected in any thermal system.

In chapter 2, we reviewed the Schwinger-Keldysh formalism and established the basic conventions used throughout this work. This framework is well-suited for describing non-equilibrium quantum systems, where fluctuations naturally arise. We then introduced its gravitational counterpart, called the grSK geometry [47, 58]. This geometry is constructed by glueing two copies of the black hole exterior. It provides the correct bulk dual for real-time dynamics in the boundary theory.

To incorporate finite density, we extended the grSK construction to charged black holes, leading to our prescription called RNSK geometry [49], as detailed in chapter 3. The RNSK geometry represents a CFT evolving in real time at finite temperature and chemical potential. In this geometry, we showed that outgoing Hawking modes arise from CPT-transformed ingoing quasi-normal modes. This generalises the neutral black hole

case, where time reversal alone relates the two. We also gave a detailed explanation of why CPT is needed, including examples involving spinor fields. As a check, we verified that the resulting boundary generating functional satisfies the Kubo-Martin-Schwinger (KMS) condition, confirming the correct statistical structure. However, at first, this validation was limited to free fields, namely free Dirac spinors [49].

A full understanding of KMS and fluctuation-dissipation dynamics requires going beyond free theory to include interactions. In chapter 4, we considered a self-interacting complex scalar field in the RNSK background and used perturbation theory to analyze its dynamics. We developed a framework for an exterior field theory, confined outside the outer horizon, to describe scattering in a charged black hole background in the presence of Hawking radiation [72]. This extended recent works [70, 71] by implementing a real-time Witten diagrammatic approach to compute boundary correlators in finite-density holographic CFTs. Importantly, the existence of an exterior field theory in this setting is far from trivial — especially in the presence of derivative interactions. Then, such a construction exists for charged black holes and remains well-defined underscores the novelty and robustness of framework of exterior field theory.

In Chapter 5, we presented the main result of this thesis using the exterior field theory framework. We derived both linear and non-linear fluctuation-dissipation relations (FDRs) for boundary correlators in the small-density regime [72]. These FDRs are valid at small but finite chemical potential and represent a extension of previous results of FDRs at zero-density [47]. These relations crucially rely on the RNSK geometry, and their derivation highlights the power of this gravitational setup. To our knowledge, this is the first derivation of non-linear FDRs for a holographic system at small but finite density. In addition, we analyzed non-linear FDRs for a system of two interacting real scalar fields in the zero-density limit. We showed that our results reduce smoothly to known relations in the $\mu_q \to 0$ limit, providing a non-trivial check of our methods and reaffirming consistency with previous work [47].

Although a complete understanding of holographic FDRs at arbitrary density remains an open question, this work makes a significant step toward that goal. It provides a systematic and well-controlled framework for studying fluctuation and dissipation in strongly coupled quantum systems using real-time holography. This sets the stage for future investigations of non-equilibrium dynamics in holography.

6.2 Future directions

There are several directions in which the results of this work can be extended. First and foremost, it would be interesting to investigate the fate of fluctuation-dissipation relations beyond the small-density regime. In particular, how to generalize our analysis of non-linear FDTs to the regime of arbitrary, and potentially large, chemical potential. While this is primarily a computational rather than conceptual challenge, the physics in this regime is expected to be qualitatively different. At large density, the fluctuation spectrum becomes increasingly skewed — albeit differently for bosons and fermions. This opens the door to discovering new forms of fluctuation-dissipation relations that are unique to strongly coupled high-density matter.

Another important direction is to understand the behaviour of the RNSK geometry in the extremal limit – that is, as the boundary temperature $T \to 0$. This regime is of particular interest because thermal fluctuations that dominate at high temperatures tend to obscure quantum effects. As a result, the extremal limit can unveil features associated with quantum criticality and non-trivial infrared (IR) structure. In the bulk, extremal black holes often exhibit AdS_2 near-horizon geometries, reflecting emergent scaling symmetries and IR fixed points in the dual field theory. It would also be interesting to explore possible connections to the Schwarzian dynamics of Jackiw–Teitelboim (JT) gravity, as discussed in [118].

From a technical standpoint, an important next step is the explicit evaluation of the radial integrals appearing in the exterior field theory. In higher dimensions, this is hindered by the fact that bulk propagators are only known perturbatively in a boundary derivative expansion. However, for the BTZ black hole ($d = 2$), the bulk-to-boundary propagators are known exactly in terms of hypergeometric functions [47, 119]. This makes the BTZ geometry an ideal testbed to validate our methods more precisely and perform explicit computations beyond the derivative expansion.

In this work, we focused on the tree-level on-shell action, which corresponds to the leading order in the large-N expansion of the boundary theory. A natural next step is to include loop corrections in the bulk, which encode $1/N$ effects on the boundary. A fundamental question is whether the exterior field theory we have constructed survives in the presence of such loop effects. Preliminary results in the neutral case [120] suggest

that it does, but for charged black holes, this remains an open problem. Addressing it could also shed light on how FDTs are modified at sub-leading orders and clarify the interplay between quantum and statistical fluctuations in holographic systems.

Once loop effects are under control, we can study transport phenomena in more realistic systems. For instance, we can investigate how fluctuations affect conductivity in the presence of a holographic Fermi surface. Here, the leading contribution to charge transport arises from loop diagrams in the bulk, as discussed in [41]. From the gravitational perspective, this also opens the door to studying renormalization in black hole spacetimes, including questions about thermal masses and running coupling constants.

Finally, it would be interesting to explore whether our results admit cosmological analogues, along the lines of [121, 122]. In particular, one could apply the methods developed in this work to the study of correlators in de Sitter spacetime using the Schwinger–Keldysh formalism, following the spirit of recent works such as [123–125]. Such an investigation could offer new insights into the structure of cosmological correlators and clarify the role of fluctuations during the early stages of the universe. It may also help illuminate how real-time holographic techniques generalize to spacetimes with cosmological horizons.

Appendix A

Clifford algebra

In this appendix, we describe our conventions for the Gamma matrices and Clifford algebra used in chapter §3. Our notation and setup closely follow those introduced in [48]. We then see how bulk Gamma matrices can be written in terms of boundary Gamma matrices. Here, we choose to write Clifford algebra in the basis given in [48], which differs from the standard one given in [96, 126–129]. However, none of the results depend on a particular basis of these gamma matrices.

To start the discussion of spinors in our context, we first move to the discussion of Clifford algebra. In $(d+1)$-dimensions, the Clifford algebra consists of an identity matrix $\mathbb{1}$, the $(d+1)$ generators called Gamma matrices Γ^a and all anti-symmetric product of these generators. Let us first begin with the Gamma matrices Γ^a that satisfy the Clifford algebra, given by,

$$\left\{\Gamma^a,\, \Gamma^b\right\} = 2\,\eta^{ab}\,\mathbb{1}, \tag{A.1}$$

where $\eta^{ab} = \mathrm{diag}\,(-1,\, +1, \ldots,\, +1)$ is the flat metric in mostly positive signature. Here, the single time–like Gamma matrix $\Gamma^{(v)}$ squares to $-\mathbb{1}$, while the other space–like Gamma matrices, i.e. $\Gamma^{(\zeta)}$ and $\Gamma^{(i)}$, are idempotent or squares to $\mathbb{1}$. In what follows, our convention is to take $\Gamma^{(v)}$ to be *anti*–Hermitian matrix and all the rest to be Hermitian matrices. Recall that in a $(d+1)$–dimensional spacetime, the gamma matrices are $2^k \times 2^k$ dimensional, where

$$k = \left\lfloor \frac{d+1}{2} \right\rfloor. \tag{A.2}$$

As a result, Dirac spinors in the bulk also have 2^k components. Thus, the number of spinor components in the bulk and boundary can differ depending on the spacetime dimension. We adopt the following conventions to handle this mismatch. Bulk spinors are always taken to be Dirac spinors. On the boundary, if the spacetime dimension is odd ($d = 2n + 1$), the boundary spinors are Dirac spinors of dimension 2^n. If the boundary dimension is even ($d = 2n$), we use Weyl spinors — chiral or anti-chiral — each of dimension 2^{n-1}. With these conventions, the bulk spinors always have twice as many components as the boundary spinors, ensuring consistency in dimensional reduction.

To write the gamma matrices explicitly, we focus on the case where the boundary dimension is even, i.e., $d = 2n$. In this case, the boundary spinors are Weyl spinors that transform under the covariant Pauli (or Sigma) matrices $(\Sigma^{(\mu)}, \overline{\Sigma}^{(\mu)})$. The corresponding bulk gamma matrices are given by:

$$\Gamma^{(\zeta)} = \begin{pmatrix} \mathbb{1} & 0 \\ 0 & -\mathbb{1} \end{pmatrix}, \qquad \Gamma^{(\mu)} = \begin{pmatrix} 0 & \Sigma^{(\mu)} \\ -\overline{\Sigma}^{(\mu)} & 0 \end{pmatrix}, \tag{A.3}$$

where the Sigma matrices are defined as

$$\Sigma^{(\mu)} = \left(\mathbb{1}, \sigma^{(i)}\right) ; \qquad \overline{\Sigma}^{(\mu)} = \left(\mathbb{1}, -\sigma^{(i)}\right) , \tag{A.4}$$

with $\sigma^{(i)}$ denoting the standard Pauli matrices. These satisfy the usual algebra:

$$\left\{\sigma^{(i)}, \sigma^{(j)}\right\} = 2\,\delta^{(i)(j)}\,\mathbb{1}. \tag{A.5}$$

It is straightforward to verify that the bulk gamma matrices defined above satisfy the Clifford algebra. Since all the Sigma matrices are Hermitian, this implies that $\Gamma^{(v)}$ is anti-Hermitian, while all the other gamma matrices are Hermitian.

Finally, the lightcone combinations of gamma matrices, $\mathbb{\Gamma}$ and $\mathbb{\Gamma}^\dagger$, as well as the constant bulk-to-boundary matrix S_0, take the following forms:

$$\mathbb{\Gamma} = \frac{1}{2}\left(\Gamma^{(v)} + \Gamma^{(\zeta)}\right) = \frac{1}{2}\begin{pmatrix} \mathbb{1} & \Sigma^{(v)} \\ -\overline{\Sigma}^{(v)} & -\mathbb{1} \end{pmatrix} = \frac{1}{2}\begin{pmatrix} \mathbb{1} & \mathbb{1} \\ -\mathbb{1} & -\mathbb{1} \end{pmatrix}, \qquad S_0 = \begin{pmatrix} \mathbb{1} \\ -\mathbb{1} \end{pmatrix}. \tag{A.6}$$

Similarly, when the boundary dimension is odd, i.e., $d = 2n - 1$, the bulk Gamma

matrices for the Dirac spinor can be chosen as,

$$\Gamma^{(\zeta)} = \begin{pmatrix} \mathbb{1} & 0 \\ 0 & -\mathbb{1} \end{pmatrix}, \qquad \Gamma^{(\mu)} = \begin{pmatrix} 0 & \gamma^{(\mu)} \\ \gamma^{(\mu)} & 0 \end{pmatrix}. \tag{A.7}$$

where $\gamma^{(\mu)}$ denotes the boundary gamma matrices.

In these odd-dimensional cases, the matrices $\mathbb{\Gamma}$, $\mathbb{\Gamma}^\dagger$ and S_0 then take the following form,

$$\mathbb{\Gamma} = \frac{1}{2} \begin{pmatrix} \mathbb{1} & \gamma^{(v)} \\ \gamma^{(v)} & -\mathbb{1} \end{pmatrix}, \qquad S_0 = \begin{pmatrix} \mathbb{1} \\ \gamma^{(v)} \end{pmatrix}. \tag{A.8}$$

Appendix B

Bulk-to-Bulk Green's function

Derivation of bulk-to-bulk Green's function. This appendix is based on [72] written by the author.

In this appendix, we derive the bulk-to-bulk propagators for a complex scalar field in the grSK geometry. Our approach closely follows the techniques developed in [41, 130], and more recently applied to the grSK geometry in [70]. We emphasize this connection, as we adopt the same notation as in [70], but our convention for Green's functions differs by an overall sign.

In this appendix, we will discuss the derivation of bulk-to-bulk Green's functions for a complex field in the grSK geometry. Our derivation will closely follow the techniques used in [41, 130] and recently implemented in the grSK geometry [70]. This we want to emphasize because we are using same notation but different convention for Green's function

The bulk-to-bulk Green's function solves the following equation,[1]

$$\begin{aligned}\left\{\left(\frac{d}{d\zeta}+\frac{\beta p^0}{2}\right)\left[r^{d-1}\left(\frac{d}{d\zeta}+\frac{\beta p^0}{2}\right)\right]-r^{d-1}\left[\left(\frac{\beta p^0}{2}\right)^2-f\left(\frac{\beta \mathbf{p}}{2}\right)^2\right]\right.\\ \left.+\beta q r^{d-1}\mathcal{A}_v\left(\frac{d}{d\zeta}+\frac{i\beta}{4}rf\right)\right\}\mathbb{G}_{\mathrm{q}}(\zeta|\zeta_0,p)=\frac{i\beta}{2}\delta(\zeta-\zeta_0)\ ,\end{aligned} \tag{B.1}$$

with the following bi-normalisable boundary conditions,

$$\lim_{\zeta\to 0}\mathbb{G}_{\mathrm{q}}(\zeta|\zeta_0,p)=\lim_{\zeta\to 1}\mathbb{G}_{\mathrm{q}}(\zeta|\zeta_0,p)=0\ . \tag{B.2}$$

[1] Comparing it to the equation present in [70] (see Eq. (2.28) in [70]), there is overall sign difference.

Using the notation used by the authors [70] and bi-normalisability of the Green's function, our ansatz for the bulk-bulk Green's function is given below,

$$\mathbb{G}_{\rm q}(\zeta|\zeta_0,p)=\frac{1}{W_{\rm q}(\zeta_0,p)}g_{\rm L}(\zeta_>,p)g_{\rm R}(\zeta_<,p)\ . \tag{B.3}$$

where $g_{\rm L}$ and $g_{\rm R}$ represent boundary-bulk Green's functions from the left and the right boundary, respectively, while $W_{\rm q}$ denotes the undetermined Wronskian. The symbols $\zeta_<$ and $\zeta_>$ are defined by,

$$\zeta_{<(>)}\equiv\begin{cases}\zeta & \text{if } \zeta \text{ comes before (after) } \zeta_0 \text{ on the RNSK contour}\\ \zeta_0 & \text{if } \zeta_0 \text{ comes before (after) } \zeta \text{ on the RNSK contour}\ .\end{cases} \tag{B.4}$$

Since the bulk-to-bulk Green's function has to solve the free field equation away from the sources, it is clear that it has to be proportional to the boundary-to-bulk Green's functions. Left and right-normalisability then fixes this combination of the boundary-to-bulk Green's functions to be $g_{\rm L}(\zeta_>,k)g_{\rm R}(\zeta_<,k)$. The other factors in the above expression must be fixed using the jump condition coming from the delta function source in the field equation. The jump condition is obtained by integrating the Eq. (B.1), given as follows,

$$\left[r^{d-1}\frac{d}{d\zeta}\mathbb{G}_{\rm q}(\zeta|\zeta_0,p)\right]_{\zeta_0^-}^{\zeta_0^+}=\frac{i\beta}{2}\ . \tag{B.5}$$

Now, we put our ansatz (B.3) into the jump condition (B.5) to obtain the Wronskian $W_{\rm q}$ as,[2]

$$\begin{aligned}W_{\rm q}(\zeta,p)&=\frac{2}{i\beta}r^{d-1}\left[g_{\rm R}(\zeta,p)\frac{dg_{\rm L}(\zeta,p)}{d\zeta}-g_{\rm L}(\zeta,p)\frac{dg_{\rm R}(\zeta,p)}{d\zeta}\right]\\&=g_{\rm L}(\zeta,p)g_{\rm R}^{\Pi^*}(\zeta,p)-g_{\rm R}(\zeta,p)g_{\rm L}^{\Pi^*}(\zeta,p)\ ,\end{aligned} \tag{B.6}$$

where we have defined left and right conjugate Green's functions[3] as,

$$g_{\rm R(L)}^{\Pi^*}\equiv -r^{d-1}\mathbb{D}_+g_{\rm R(L)}=-r^{d-1}\frac{2}{i\beta}\left(\frac{d}{d\zeta}+\frac{\beta p^0}{2}+\frac{\beta q}{2}\mathcal{A}_v\right)g_{\rm R(L)}\ . \tag{B.7}$$

[2]Again, note the sign difference in the Wronskian as compared to [70].

[3]By conjugate Green's function, we mean the Green's function corresponding to the conjugate field in question.

Let's now apply the above differential operator to the Wronskian given above to get,

$$\frac{2}{i\beta}\left(\frac{d}{d\zeta}+\beta p^0+\beta q\mathcal{A}_v\right)W_{\rm q}(\zeta,p)=g_{\rm R}\mathbb{D}_+\left[r^{d-1}\mathbb{D}_+g_{\rm L}\right]-g_{\rm L}\mathbb{D}_+\left[r^{d-1}\mathbb{D}_+g_{\rm R}\right]=0\ . \tag{B.8}$$

The second equality holds upon using EOM obeyed by $g_{\rm R}$ and $g_{\rm L}$. Hence, it implies that,

$$e^{\beta p^0\zeta+iq\mathbb{A}}W_{\rm q}(\zeta,p)=\text{constant along the RNSK radial contour}\ . \tag{B.9}$$

Determining the Wronskian

The retarded 2-point boundary correlator $K^{\rm in}$ is obtained by taking the boundary limit of the ingoing boundary-bulk conjugate Green's function [62], as shown below–

$$\lim_{\zeta\to0,1}r^{d-1}\mathbb{D}_+G^{\rm in}_{\rm q}(\zeta,p)=\lim_{r\to\infty}r^{d-1}\mathbb{D}_+G^{\rm in}_{\rm q}(\zeta,p)\Big|_{\rm ren}=K^{\rm in}_{\rm q}(p)\ , \tag{B.10}$$

where subscript 'ren' denotes the standard holographic renormalisation [53]. Henceforth, we will stop writing this subscript as it is to be assumed in every boundary limit.

Similarly, the boundary limits of the outgoing boundary-bulk conjugate Green's function give,

$$\begin{aligned}
&\lim_{\zeta\to0}r^{d-1}\mathbb{D}_+G^{\rm out}_{\rm q}(\zeta,p)=\lim_{r\to\infty}r^{d-1}\mathbb{D}_+G^{\rm in}_{-\rm q}(\zeta,-p)=K^{\rm in}_{-\rm q}(-p)\ ,\\
&\lim_{\zeta\to1}r^{d-1}\mathbb{D}_+G^{\rm out}_{\rm q}(\zeta,p)=e^{-\beta(p^0-q\mu)}\lim_{r\to\infty}r^{d-1}\mathbb{D}_+G^{\rm in}_{-\rm q}(\zeta,-p)=e^{-\beta(p^0-\mu q)}K^{\rm in}_{-\rm q}(-p)\ ,
\end{aligned} \tag{B.11}$$

where we have used the CPT isometry: $G^{\rm out}_{\rm q}(\zeta,k)=e^{-\beta k^0\zeta}e^{-iq\mathbb{A}}G^{\rm in}_{-\rm q}(\zeta,-k)$. Note that the difference between the left and right boundary limit of the outgoing conjugate Green's function as opposed to the same limit of the ingoing conjugate Green's function.

We now turn to the left and right conjugate Green's functions and their boundary limits. Using above-mentioned boundary limits, i.e. equations (B.10) and (B.11), we obtain the left boundary limits as,

$$\begin{aligned}
&\lim_{\zeta\to0}g^{\Pi^*}_{\rm R}\equiv-\lim_{\zeta\to0}r^{d-1}\mathbb{D}_+g_{\rm R}=-(1+n_p)\left[K^{\rm in}_{\rm q}(p)-K^{\rm in}_{-\rm q}(-p)\right]\ ,\\
&\lim_{\zeta\to0}g^{\Pi^*}_{\rm L}\equiv-\lim_{\zeta\to0}r^{d-1}\mathbb{D}_+g_{\rm L}=-n_p\left[K^{\rm in}_{\rm q}(p)-e^{\beta(p^0-\mu q)}K^{\rm in}_{-\rm q}(-p)\right]\ ,
\end{aligned} \tag{B.12}$$

and the corresponding right boundary limits as,

$$\begin{aligned}\lim_{\zeta\to 1} g_{\rm R}^{\Pi^*} &\equiv -\lim_{\zeta\to 0} r^{d-1}\mathbb{D}_+ g_{\rm R} = -(1+n_p)\left[K_{\rm q}^{\rm in}(p) - e^{-\beta(p^0-\mu q)}K_{-\rm q}^{\rm in}(-p)\right] \\ \lim_{\zeta\to 1} g_{\rm L}^{\Pi^*} &\equiv -\lim_{\zeta\to 0} r^{d-1}\mathbb{D}_+ g_{\rm L} = -n_p\left[K_{\rm q}^{\rm in}(p) - K_{-\rm q}^{\rm in}(-p)\right] \ .\end{aligned} \tag{B.13}$$

Using these boundary limits and boundary limits of the right and the left boundary-bulk Green's functions Eqs. (4.16) and (4.17), we obtain the constant in Eq. (B.9) at the left boundary,

$$\begin{aligned}\lim_{\zeta\to 0} e^{\beta p^0\zeta + iq\mathbb{A}} W_{\rm q}(\zeta,p) &= \lim_{\zeta\to 0}\left[g_{\rm L}(\zeta,p)g_{\rm R}^{\Pi^*}(\zeta,p) - g_{\rm R}(\zeta,p)g_{\rm L}^{\Pi^*}(\zeta,p)\right] \\ &= (1+n_p)\left[K_{\rm q}^{\rm in}(p) - K_{-\rm q}^{\rm in}(-p)\right] \ ,\end{aligned} \tag{B.14}$$

and at the right boundary also gives the same result as expected from Eq. (B.9). Since the above quantity is the same everywhere in the bulk, the expression of the Wronskian can be easily found to be given by,

$$W_{\rm q}(\zeta,p) = e^{-\beta p^0\zeta - iq\mathbb{A}}(1+n_p)\left[K_{\rm q}^{\rm in}(p) - K_{-\rm q}^{\rm in}(-p)\right] \ . \tag{B.15}$$

Binormalisable bulk-bulk Green's function

Now that we have expression for the Wronskian (B.15), the bi-normalisable bulk-bulk Green's function (B.3) can be explicitly written as,

$$\begin{aligned}\mathbb{G}_{\rm q}(\zeta|\zeta_0,p) &= \frac{e^{\beta p^0\zeta_0 + iq\mathbb{A}(\zeta_0)}}{(1+n_p)\left[K_{\rm q}^{\rm in}(p) - K_{-\rm q}^{\rm in}(-p)\right]} g_{\rm L}(\zeta_>,p)g_{\rm R}(\zeta_<,p) \\ &= \frac{e^{\beta p^0\zeta_0 + iq\mathbb{A}(\zeta_0)}}{(1+n_p)\left[K_{\rm q}^{\rm in}(p) - K_{-\rm q}^{\rm in}(-p)\right]} \\ &\times\left\{\Theta_{\rm SK}(\zeta>\zeta_0)g_{\rm L}(\zeta,p)g_{\rm R}(\zeta_0,p) + \Theta_{\rm SK}(\zeta<\zeta_0)g_{\rm R}(\zeta,p)g_{\rm L}(\zeta_0,p)\right\} \ .\end{aligned} \tag{B.16}$$

When we compare this binormalisable bulk-bulk Green's function to the one given in [48](see Eq. (A.31) in [48]), we can see a clear overall sign difference as expected. The bulk-bulk Green's function, when written ingoing-outgoing basis using the boundary-bulk

Green's functions given in Eq. (4.15), we obtain,

$$\mathbb{G}_{\rm q}(\zeta|\zeta_0,p) = \frac{1}{\left[K^{\rm in}_{\rm q}(p) - K^{\rm in}_{-\rm q}(-p)\right]} \times \Bigg\{ n_p e^{\beta p^0\zeta_0 + iq\mathbb{A}(\zeta_0)} G^{\rm in}_{\rm q}(\zeta,p)G^{\rm in}_{\rm q}(\zeta_0,p) + (1+n_p)e^{-\beta p^0\zeta - iq\mathbb{A}(\zeta)} G^{\rm in}_{-\rm q}(\zeta,-p)G^{\rm in}_{-\rm q}(\zeta_0,-p) - \left[\Theta_{\rm SK}(\zeta<\zeta_0)+n_p\right] G^{\rm in}_{\rm q}(\zeta,p)G^{\rm in}_{-\rm q}(\zeta_0,-p) - \left[\Theta_{\rm SK}(\zeta>\zeta_0)+n_p\right] e^{\beta p^0(\zeta_0-\zeta)} e^{iq[\mathbb{A}(\zeta_0)-\mathbb{A}(\zeta)]} G^{\rm in}_{-\rm q}(\zeta,-p)G^{\rm in}_{\rm q}(\zeta_0,p) \Bigg\} . \tag{B.17}$$

As expected, it resembles the bi-normalisable bulk-bulk Green's function for a real scalar field in the grSK geometry [71]. Once we have constructed the bi-normalisable Green's function, we now move to retarded and advanced Green's functions useful in describing the causal scattering processes in the bulk. Later, we will see that they are not completely independent but related by reciprocity.

B.1 Retarded and Advanced bulk-bulk Green's functions

After constructing bi-normalisable bulk-bulk Green's function, we can also construct bulk-to-bulk Green's functions that have specific causal properties, i.e., the retarded and the advanced bulk-to-bulk Green's functions. These Green's functions are normalisable at the left boundary and analytic in the upper half and the lower half of the frequency plane, respectively. Here, we will not provide a derivation of these Green's functions, as it is similar to the computation of the bi-normalisable bulk-to-bulk Green's function given above.[4] We just quote the end results for the retarded bulk-bulk Green's function here

[4] Again, readers are encouraged to look at [70, 71] for detailed analysis.

as,

$$\mathbb{G}_{\rm ret}(\zeta|\zeta_0,p) = \frac{1}{\left[K^{\rm in}_{\rm q}(p) - K^{\rm in}_{-\rm q}(-p)\right]} \times \Big\{ - e^{\beta p^0 \zeta_0 + iq\mathbb{A}(\zeta_0)} G^{\rm in}_{\rm q}(\zeta,p) G^{\rm in}_{\rm q}(\zeta_0,p) + \Theta_{\rm SK}(\zeta > \zeta_0) G^{\rm in}_{\rm q}(\zeta,p) G^{\rm in}_{-\rm q}(\zeta_0,-p) + \Theta_{\rm SK}(\zeta < \zeta_0) e^{\beta p^0(\zeta_0-\zeta)} e^{iq[\mathbb{A}(\zeta_0)-\mathbb{A}(\zeta)]} G^{\rm in}_{-\rm q}(\zeta,-p) G^{\rm in}_{\rm q}(\zeta_0,p) \Big\} \tag{B.18}$$

and the advanced bulk-bulk Green's function,

$$\mathbb{G}_{\rm adv}(\zeta|\zeta_0,p) = \frac{1}{\left[K^{\rm in}_{\rm q}(p) - K^{\rm in}_{-\rm q}(-p)\right]} \times \Big\{ e^{-\beta p^0 \zeta - iq\mathbb{A}(\zeta)} G^{\rm in}_{-\rm q}(\zeta,-p) G^{\rm in}_{-\rm q}(\zeta_0,-p) - \Theta_{\rm SK}(\zeta < \zeta_0) G^{\rm in}_{\rm q}(\zeta,p) G^{\rm in}_{-\rm q}(\zeta_0,-p) - \Theta_{\rm SK}(\zeta > \zeta_0) e^{\beta p^0(\zeta_0-\zeta)} e^{iq[\mathbb{A}(\zeta_0)-\mathbb{A}(\zeta)]} G^{\rm in}_{-\rm q}(\zeta,-p) G^{\rm in}_{\rm q}(\zeta_0,p) \Big\} \tag{B.19}$$

where there is again, but due to same reason, an overall sign difference in $\mathbb{G}_{\rm ret}$ and $\mathbb{G}_{\rm adv}$ as compared to [70].Note that we have suppressed the label q for the retarded and advanced Green's functions.

The reciprocity relation of the bi-normalisable bulk-bulk Green's function can be easily found from Eq. (B.17) as follows,

$$\mathbb{G}_{\rm q}(\zeta|\zeta_0,p) = \mathbb{G}_{-\rm q}(\zeta_0|\zeta,-p) \equiv \bar{\mathbb{G}}_{\rm q}(\zeta_0|\zeta,-p) \ , \tag{B.20}$$

where we have defined the bar as an action which changes the sign of charge: $q \mapsto -q$.

The bi-normalisable bulk-bulk Green's function can be written as a linear combination of retarded and advanced bulk-bulk Green's functions, given as,

$$\mathbb{G}(\zeta|\zeta_0,p) = -n_p \mathbb{G}_{\rm ret}(\zeta|\zeta_0,p) + (1+n_p)\mathbb{G}_{\rm adv}(\zeta|\zeta_0,p) \ , \tag{B.21}$$

and then the reciprocity at the level of retarded and advanced Green's functions is given

by,

$$\mathbb{G}_{\mathrm{adv}}(\zeta|\zeta_0, p) = \bar{\mathbb{G}}_{\mathrm{ret}}(\zeta_0|\zeta, -p) \ . \tag{B.22}$$

Appendix C

Monodromy integrals on the RNSK geometry

In this appendix, we examine the integration over the RNSK geometry, relevant to the on-shell action calculation. Specifically, the calculation involves a contour integral over the complexified radius, as depicted in Fig. (3.1). This integral can be simplified into a single exterior integral, defined in Eq. (4.51), with the discontinuities arising from the horizon cap. Here, we will outline these discontinuities and demonstrate how they are computed.

The discontinuity arises due to the non-analytic nature of the integrand, which originates from the outgoing propagators. These non-analyticities are introduced through terms such as ζ and $\mathbb{\Lambda}$. Notably, $e^{-iq\mathbb{\Lambda}}$ experiences a jump by $e^{\beta\mu q}$ across contour branches, and ζ increments by unity. These factors collectively explain the origin of the discontinuity.

To understand this, consider the evaluation of the following integral ,

$$\oint_{\zeta} \left[e^{\beta\mu q - iq\mathbb{\Lambda}(\zeta)}\right]^{\alpha} \prod_{i=1}^{\alpha} e^{\beta k_i^0(1-\zeta)} \mathcal{F}(\zeta) = \frac{-1}{n_{\sum k_i,\alpha}} \int_{\text{ext}} \left[e^{-iq\mathbb{\Lambda}(\zeta)}\right]^{\alpha} \prod_{i=1}^{\alpha} e^{-\beta k_i^0 \zeta} \mathcal{F}(\zeta) \ , \tag{C.1}$$

where $\mathcal{F}(\zeta)$ is an analytic function and recall the definition of $\int_{\text{ext}}$ and $n_{k,\alpha}$

$$\int_{\text{ext}} \equiv \int_{r_h}^{r_c} \mathrm{d}r \ r^{d-1} \ , \qquad\qquad n_{k,\alpha} = \frac{1}{e^{\beta(k^0 - \alpha\mu q)} - 1} \ . \tag{C.2}$$

This is the only type of discontinuity that arises in a single integral, representing the most

general form of a single discontinuity. It can be explicitly verified that this result yields the correct expressions for contact diagrams. However, as we move beyond contact diagrams – for example, to exchange diagrams – a greater number of bulk integrals appear, often accompanied by multiple bulk-to-bulk propagators. Therefore, it becomes necessary to extend this result to multi-discontinuities, starting with double discontinuities.

To de-clutter the expressions in more complicated integrals, we find it convenient to define $\mathbb{\Theta}$ as,

$$\mathbb{\Theta} \equiv -\frac{1}{\mu}\int_0^\zeta d\zeta' \mathcal{A}_v(\zeta') = \int_0^\zeta d\zeta' \left(\frac{r_+}{r}\right)^{d-2} \qquad \text{or} \qquad \mathbb{\Lambda} = i\beta\mu\mathbb{\Theta} \ , \tag{C.3}$$

where we note that the $\mathbb{\Theta}$ jumps by unity across the horizon cap.

Now we will come to the computation of exchange diagrams that contain bulk-to-bulk propagators. The simplest exchange diagrams consist of double integrals over the RNSK contour. The most general form of such an integral is given by,

$$\begin{aligned}\oint_{\zeta_1,\zeta_2} \prod_{i=1}^{2} e^{-\beta\mu q\alpha_i[1-\mathbb{\Theta}(\zeta_i)]} e^{\beta\kappa_i(1-\zeta_i)} \mathcal{F}(\zeta_1,\zeta_2)\mathbb{G}(\zeta_2|\zeta_1,p) \\ = \int_{\text{ext}} \prod_{i=1}^{2} e^{-\beta\mu q\alpha_i[1-\mathbb{\Theta}(\zeta_i)]} e^{\beta\kappa_i(1-\zeta_i)} \mathcal{F}(\zeta_1,\zeta_2)\mathbb{G}_{\text{dd}}(\zeta_2|\zeta_1,p) \ ,\end{aligned} \tag{C.4}$$

where $\mathcal{F}(\zeta)$ is again an analytic function and the the double-discontinuity $\mathbb{G}_{\text{dd}}$ is given by,

$$\begin{aligned}\mathbb{G}_{\text{dd}}(\zeta_2|\zeta_1,p) \equiv& \mathbb{G}(\zeta_2|\zeta_1,p) - e^{\beta(\mu q\alpha_1-\kappa_1)}\mathbb{G}(\zeta_2|\zeta_1+1,p) \\ &- e^{\beta(\mu q\alpha_2-\kappa_2)}\mathbb{G}(\zeta_2+1|\zeta_1,p) + e^{\beta(\mu q\alpha_1+\mu q\alpha_2-\kappa_1-\kappa_2)}\mathbb{G}(\zeta_2+1|\zeta_1+1,p) \ .\end{aligned} \tag{C.5}$$

The exponential factors in the above expression are simply the monodromy factors due to the branch cut extending from the horizon radius r_+ to the cut-off radius r_c on the complex r plane. We can now use the expression for the bulk-to-bulk propagator given in Eq. (B.17) to evaluate the integrand above explicitly. We will use the theta function identities. Using the following properties of step functions on the grSK/RNSK contour, we find,

$$\Theta_{\text{SK}}(\zeta+1>\zeta'+1) = \Theta_{\text{SK}}(\zeta<\zeta') \ , \tag{C.6}$$

and,

$$\Theta_{\rm SK}(\zeta + 1 > \zeta') = 1 \ , \qquad \Theta_{\rm SK}(\zeta > \zeta' + 1) = 0 \ , \tag{C.7}$$

where $\zeta, \zeta' < \zeta_h$ or both ζ and ζ' are on the left exterior contour.

Substituting the expressions for the bulk-bulk propagator and using relations of Heavyside step functions, the double-discontinuity obtained is as follows,

$$\begin{aligned} \mathbb{G}_{\rm dd}(\zeta|\zeta', p) = & \frac{-n_{p,1}}{(1 + n_{\kappa_1 - 1, \alpha_1 - 1})(1 + n_{\kappa_2, \alpha_2})} \mathbb{G}_{\rm ret}(\zeta|\zeta', p) \\ & + \frac{(1 + n_{p,1})}{(1 + n_{\kappa_1, \alpha_1})(1 + n_{\kappa_2 + p, \alpha_2 + 1})} \mathbb{G}_{\rm adv}(\zeta|\zeta', p) \ . \end{aligned} \tag{C.8}$$

We observe that the double-discontinuity formula reduces to the result in [70] in the $q \to 0$ limit. Though a generalisation to multi-discontinuities is possible, we focus on the double-discontinuity in this work.

Appendix D

Computations in $|\Phi|^4$ theory

In this appendix, we present the on-shell action for the $|\Phi|^4$ theory using a method similar to [70]. This approach circumvents the need to evaluate the boundary terms in the on-shell action explicitly. It leverages the fact that the boundary value of the higher-order solution vanishes, thereby simplifying the computation.

The bare action is given by

$$S_{\text{bare}} = -\oint d^{d+1}x\sqrt{-g}\left(|D_M\Phi|^2 + \frac{\lambda}{2!\,2!}\left(\bar{\Phi}\Phi\right)^2\right) . \tag{D.1}$$

Inserting the perturbative solution into the bare action yields the on-shell action in the following form.

$$S_{\text{os}} = -\int_{\partial\mathcal{M}} d\Sigma^A\ \Phi_{(0)}\overline{\left(D_A\Phi_{(0)}\right)} + \lambda\oint_{\mathcal{M}}\left[\frac{1}{2!}\left(\bar{\Phi}-\bar{\Phi}_{(0)}\right)\Phi\left(\bar{\Phi}\Phi\right) - \frac{1}{2!2!}\left(\bar{\Phi}\Phi\right)^2\right] , \tag{D.2}$$

where we have used the equations of motion and imposed the appropriate boundary conditions to significantly simplify the expression for the on-shell action. When expanded in terms of the coupling constant, the on-shell action is explicitly expressed as follows:

$$\begin{aligned} S_{(2)} &= -\int_{\partial\mathcal{M}} d\Sigma^A\ \Phi_{(0)}\overline{\left(D_A\Phi_{(0)}\right)} , \\ S_{(4)} &= -\frac{\lambda}{2!\,2!}\oint d^{d+1}x\sqrt{-g}\left(\bar{\Phi}_{(0)}\Phi_{(0)}\right)^2 , \\ S_{(6)} &= -\frac{\lambda^2}{2}\oint d^{d+1}x\sqrt{-g}\ \bar{\Phi}_{(0)}\Phi_{(1)}\bar{\Phi}_{(0)}\Phi_{(0)} , \end{aligned} \tag{D.3}$$

where the above terms represent both free and contact contributions at the tree level in

Feynman diagrams.

We find it convenient to express the on-shell action in the Past-Future (PF) basis, i.e. Eqs. (4.10) and (4.21). In this basis, SK collapse (unitarity) and KMS condition (thermality) are reflected in the vanishing of coefficients of all Fs and the Ps terms, respectively. Moreover, this basis exclusively involves retarded/advanced propagators in the correlators, ensuring the description of causal scattering processes.

Now, we turn to the explicit calculation of the on-shell action, starting from the contact term $S_{(4)}$ of the $|\Phi|^4$ theory.

Contact term: The contact term $S_{(4)}$ is given in the second line of the eq. (4.39). Passing into the boundary momentum variables, it can be written as,

$$\begin{aligned} S_{(4)} &= -\frac{\lambda}{4}\int_{k_{1,2,3,4}} \oint_\zeta \prod_{i=1}^{2} \bar{\Phi}_{(0)}(\zeta, k_i) \prod_{j=1}^{2} \Phi_{(0)}(\zeta, k_j) \\ &= -\frac{\lambda}{4}\int_{k_{1,2,3,4}} \oint_\zeta \prod_{i=1}^{2} \Big\{ -\bar{G}^{\text{in}}(\zeta, k_i)\bar{J}_{\bar{F}}(k_i) + e^{\beta(k_i^0+\mu q)}\bar{G}^{\text{out}}(\zeta, k_i)\bar{J}_{\bar{P}}(k_i)\Big\} \\ &\qquad \times \prod_{j=1}^{2} \Big\{ -G^{\text{in}}(\zeta, k_j)J_{\bar{F}}(k_j) + e^{\beta(k_j^0-\mu q)}G^{\text{out}}(\zeta, k_j)J_{\bar{P}}(k_j)\Big\} \end{aligned} \tag{D.4}$$

where we have written the solution in terms of ingoing and outgoing solution, as given in Eq. (4.8) and Eq. (4.19).

Taking into account the analyticity of G^{in} and $\bar{G}^{\text{in}}$ in the ζ coordinate and using momentum conservation, the RNSK radial integral leads us to the following observations:

1. SK collapse holds: The term with only $\bar{J}_{\bar{F}}$ and $J_{\bar{F}}$ vanishes.

2. KMS condition holds: The term with only $\bar{J}_{\bar{P}}$ and $J_{\bar{P}}$ vanishes.

As a result, seven of the original nine terms remain. The next step involves performing the RNSK integral to obtain a single exterior integral, using the Eq. (C.1) from the

previous appendix. Thus, we obtain the following,

$$
\begin{aligned}
S_{(4)} = -\lambda \int_{k_{1,2,3,4}} \int_{\text{ext}} \Bigg\{ & \frac{1}{2n_{k_4,1}} \bar{J}_{\bar{F}}(k_1) J_{\bar{F}}(k_2) \bar{J}_{\bar{F}}(k_3) J_{\bar{F}}(k_4) \bar{G}^{\text{in}}(\zeta, k_1) G^{\text{in}}(\zeta, k_2) \bar{G}^{\text{in}}(\zeta, k_3) G^{\text{out}}(\zeta, k_4) \\
& + \frac{1}{2\bar{n}_{k_3,1}} \bar{J}_{\bar{F}}(k_1) J_{\bar{F}}(k_2) \bar{J}_{\bar{F}}(k_3) J_{\bar{F}}(k_4) \bar{G}^{\text{in}}(\zeta, k_1) G^{\text{in}}(\zeta, k_2) \bar{G}^{\text{out}}(\zeta, k_3) G^{\text{in}}(\zeta, k_4) \\
& - \frac{1}{n_{k_{34},0}} \bar{J}_{\bar{F}}(k_1) J_{\bar{F}}(k_2) \bar{J}_{\bar{F}}(k_3) J_{\bar{F}}(k_4) \bar{G}^{\text{in}}(\zeta, k_1) G^{\text{in}}(\zeta, k_2) \bar{G}^{\text{out}}(\zeta, k_3) G^{\text{out}}(\zeta, k_4) \\
& - \frac{1}{n_{k_{24},2}} \bar{J}_{\bar{F}}(k_1) J_{\bar{P}}(k_2) \bar{J}_{\bar{F}}(k_3) J_{\bar{P}}(k_4) \bar{G}^{\text{in}}(\zeta, k_1) G^{\text{out}}(\zeta, k_2) \bar{G}^{\text{in}}(\zeta, k_3) G^{\text{out}}(\zeta, k_4) \\
& - \frac{1}{\bar{n}_{k_{13},2}} \bar{J}_{\bar{P}}(k_1) J_{\bar{F}}(k_2) \bar{J}_{\bar{P}}(k_3) J_{\bar{F}}(k_4) \bar{G}^{\text{out}}(\zeta, k_1) G^{\text{in}}(\zeta, k_2) \bar{G}^{\text{out}}(\zeta, k_3) G^{\text{in}}(\zeta, k_4) \\
& + \frac{1}{2n_{k_{234},1}} \bar{J}_{\bar{F}}(k_1) J_{\bar{P}}(k_2) \bar{J}_{\bar{P}}(k_3) J_{\bar{P}}(k_4) \bar{G}^{\text{in}}(\zeta, k_1) G^{\text{out}}(\zeta, k_2) \bar{G}^{\text{out}}(\zeta, k_3) G^{\text{out}}(\zeta, k_4) \\
& + \frac{1}{2\bar{n}_{k_{134},1}} \bar{J}_{\bar{P}}(k_1) J_{\bar{F}}(k_2) \bar{J}_{\bar{P}}(k_3) J_{\bar{P}}(k_4) \bar{G}^{\text{out}}(\zeta, k_1) G^{\text{in}}(\zeta, k_2) \bar{G}^{\text{out}}(\zeta, k_3) G^{\text{out}}(\zeta, k_4) \Bigg\} ,
\end{aligned}
\tag{D.5}
$$

as noted previously, these exterior integrals naturally exhibit Bose-Einstein factors. These seven terms correspond to the seven diagrams shown in Figure (4.1).

Exchange terms: Having addressed the contact term, the next step is to examine the exchange terms. In the case of $|\Phi|^4$ theory, the first exchange term originates from the six-point influence phase $S_{(6)}$, which appears at quadratic order in λ. The $S_{(6)}$ is given in the third line of Eq. (4.39) and is expressed in momentum space as

$$
S_{(6)} = -\frac{\lambda^2}{2} \int_{k_{1,2,3,4}} \oint_{\zeta,\zeta'} \bar{\Phi}_{(0)}(\zeta, k_1) \Phi_{(0)}(\zeta, k_2) \bar{\Phi}_{(0)}(\zeta, k_3) \mathbb{G}(\zeta|\zeta', k_4) \mathbb{J}_{(1)}(\zeta', k_4) \ . \tag{D.6}
$$

Upon using the expression of bulk source $\mathbb{J}_{(1)}$ from Eq. (4.35), we find,

$$
\begin{aligned}
S_{(6)} = -\frac{\lambda^2}{4} & \int_{k_{1,2,\ldots,6}} \oint_{\zeta,\zeta'} \\
& \times \bar{\Phi}_{(0)}(\zeta, k_1) \Phi_{(0)}(\zeta, k_2) \bar{\Phi}_{(0)}(\zeta, k_3) \mathbb{G}(\zeta|\zeta', k_{456}) \Phi_{(0)}(\zeta', k_4) \bar{\Phi}_{(0)}(\zeta', k_5) \Phi_{(0)}(\zeta', k_6) \ .
\end{aligned}
\tag{D.7}
$$

Using the expressions of zeroth-order solution equations (4.8), (4.19) and (B.17), we get,

$$
\begin{aligned}
S_{(6)} = &-\frac{\lambda^2}{4}\int_{k_{1,2,\ldots,6}}\oint_{\zeta,\zeta'}\left[-\bar{G}^{\rm in}(\zeta,k_1)\bar{J}_{\bar{F}}(k_1)+e^{\beta(k_1^0+\mu q)}\bar{G}^{\rm out}(\zeta,k_1)\bar{J}_{\bar{P}}(k_1)\right]\\
&\times\left[-G^{\rm in}(\zeta,k_2)J_{\bar{F}}(k_2)+e^{\beta(k_2^0-\mu q)}G^{\rm out}(\zeta,k_2)J_{\bar{P}}(k_2)\right]\left[-\bar{G}^{\rm in}(\zeta,k_3)\bar{J}_{\bar{F}}(k_3)+e^{\beta(k_3^0+\mu q)}\bar{G}^{\rm out}(\zeta,k_3)\bar{J}_{\bar{P}}(k_3)\right]\\
&\times\mathbb{G}(\zeta|\zeta',k_{456})\left[-G^{\rm in}(\zeta,k_4)J_{\bar{F}}(k_4)+e^{\beta(k_4^0-\mu q)}G^{\rm out}(\zeta,k_4)J_{\bar{P}}(k_4)\right]\\
&\times\left[-\bar{G}^{\rm in}(\zeta,k_5)\bar{J}_{\bar{F}}(k_5)+e^{\beta(k_5^0+\mu q)}\bar{G}^{\rm out}(\zeta,k_5)\bar{J}_{\bar{P}}(k_5)\right]\left[-G^{\rm in}(\zeta,k_6)J_{\bar{F}}(k_6)+e^{\beta(k_6^0-\mu q)}G^{\rm out}(\zeta,k_6)J_{\bar{P}}(k_6)\right] .
\end{aligned}
\tag{D.8}
$$

Once again, the SK collapse and KMS condition are evident, as all Fs and Ps terms vanish in the six-point influence phase $S_{(6)}$.

We proceed with the RNSK integral to express $S_{(6)}$ in terms of the exterior radial integrals. Here, we present the result for a single term of $S_{(6)}$, specifically the component with five Fs and one Ps, denoted as $S_{5\bar{F},1\bar{P}}$. This term comprises two independent contributions, as shown below–

$$
S_{5\bar{F},1\bar{P}} = S[\bar{F}\bar{F}\bar{F}\bar{F}\bar{P}] + S[\bar{F}\bar{F}\bar{F}\bar{P}\bar{F}] \ , \tag{D.9}
$$

where the notation is designed to clearly indicate whether the past source is from the field or its conjugate. Now, let us analyze the case where the past source is from the field, written as,

$$
\begin{aligned}
S[\bar{F}\bar{F}\bar{F}\bar{F}\bar{P}] = &\frac{\lambda^2}{4}\int_{k_{1,2,\ldots,6}}\bar{J}_{\bar{F}}(k_1)J_{\bar{F}}(k_2)\bar{J}_{\bar{F}}(k_3)J_{\bar{F}}(k_4)\bar{J}_{\bar{F}}(k_5)J_{\bar{P}}(k_6)\oint_{\zeta,\zeta'}\mathbb{G}(\zeta|\zeta',k_{456})\\
&\times\left[\bar{G}^{\rm in}(\zeta,k_1)G^{\rm in}(\zeta,k_2)\bar{G}^{\rm in}(\zeta,k_3)G^{\rm in}(\zeta',k_4)\bar{G}^{\rm in}(\zeta',k_5)e^{\beta(k_6^0-\mu q)}G^{\rm out}(\zeta',k_6)\right] .
\end{aligned}
\tag{D.10}
$$

Using double-discontinuity integral given in the Eq. (C.4) from the previous Appendix, we find,

$$
\begin{aligned}
S[\bar{F}\bar{F}\bar{F}\bar{F}\bar{P}] = &\frac{\lambda^2}{2}\int_{k_{1,2,\ldots,6}}\frac{1}{n_{k_6,1}}\bar{J}_{\bar{F}}(k_1)J_{\bar{F}}(k_2)\bar{J}_{\bar{F}}(k_3)J_{\bar{F}}(k_4)\bar{J}_{\bar{F}}(k_5)J_{\bar{P}}(k_6)\\
&\times\int_{\rm ext}\mathbb{G}_{\rm ret}(\zeta|\zeta',k_{456})\left[\bar{G}^{\rm in}(\zeta,k_1)G^{\rm in}(\zeta,k_2)\bar{G}^{\rm in}(\zeta,k_3)G^{\rm in}(\zeta',k_4)\bar{G}^{\rm in}(\zeta',k_5)G^{\rm out}(\zeta',k_6)\right] .
\end{aligned}
\tag{D.11}
$$

It is worth emphasizing that the result above was derived by leveraging the reciprocity

between the retarded and advanced bulk-bulk propagators.

Similarly, one could extend this approach to compute additional terms in the six-point influence phase. However, since the same principles apply, we restrict our focus to a single term in this appendix. By employing a similar analysis and multi-discontinuity integrals, exchange terms contributing to the higher-order influence phase can also be determined.

D.1 Explicit terms of quartic on-shell action $S_{(4)}$

In this section, we will explicitly compute the four-point influence phase at linear order in the gradient expansion. In time domain, we start with the solution itself given in Eq. (4.73), as,

$$\begin{aligned}\Phi = &\left[J_a + \left(\zeta - \frac{1}{2} + \mathbb{F}_1\right) J_d\right] + \frac{i\beta}{2}\left[\mathbb{F}_1 \partial_t J_a - \left(\zeta(\zeta-1) + \left[\zeta - \frac{1}{2}\right]\mathbb{F}_1\right)\partial_t J_d\right] \\ &+ \frac{\beta\mu_q}{2}\left[\left(\mathbb{F}_2 - \mathbb{F}_1\right) J_a + \left(\zeta(\zeta-1) + \left[\zeta - \frac{1}{2}\right]\mathbb{F}_2 + \left(\zeta - \frac{1}{2} + \mathbb{F}_2\right)\mathbb{F}_1\right) J_d\right] .\end{aligned} \tag{D.12}$$

Since we are only working up to linear order in derivatives while discarding the mixed terms (see the discussion around Eq. (4.78)), we can divide the following terms into two parts:

$$\begin{aligned}S_{(4)} &= -\lambda \int d^d x \oint d\zeta \sqrt{-g} \frac{|\Phi_{(0)}|^4}{4} \\ &= -\lambda \int d^d x \int_{\text{ext}} \mathcal{L}_0 - \lambda \int d^d x \int_{\text{ext}} \mathcal{L}_1 + \mathcal{O}((\beta\partial_t)^2) + \mathcal{O}((\beta\mu_q)^2) + \mathcal{O}(\beta^2 \mu_q \partial_t) \ ,\end{aligned} \tag{D.13}$$

where $\mathcal{L}_0$ and $\mathcal{L}_1$ are non-derivative and first derivative term.

As we can see now, we can make our lives easier by moving into position space. It will remove unnecessary notation and declutter the expressions.

Zeroth-derivative term $\mathcal{L}_0$: The $\mathcal{L}_0$ can be explicitly written as,

$$\mathcal{L}_0 = \sum_{r,s=0}^{2} \mathcal{G}_{r,s} \ \left[\bar{J}_a\right]^r \left[J_a\right]^s \left[\bar{J}_d\right]^{2-r} \left[J_d\right]^{2-s} \ . \tag{D.14}$$

where some of the terms are as follows

$$\begin{aligned}
&\mathcal{G}_{2,2} = 0 \ , \qquad \mathcal{G}_{1,1} = 2\left(\zeta + \mathbb{F}_1\right) \ , \qquad \mathcal{G}_{1,2} = \frac{1}{2} - \frac{\beta\mu_q}{2}\left(\zeta + \mathbb{F}_1\right) \ , \\
&\mathcal{G}_{2,1} = \frac{1}{2} + \frac{\beta\mu_q}{2}\left(\zeta + \mathbb{F}_1\right) \ , \qquad \mathcal{G}_{0,0} = \frac{1}{4}\left(\zeta + \mathbb{F}_1\right) + \left(\zeta + \mathbb{F}_1\right)^3 \ , \\
&\mathcal{G}_{0,2} = \frac{1}{2}\left(\zeta + \mathbb{F}_1\right) - \frac{3\,\beta\mu_q}{4}\left(\zeta + \mathbb{F}_1\right)^2 \ , \qquad \mathcal{G}_{2,0} = \frac{1}{2}\left(\zeta + \mathbb{F}_1\right) + \frac{3\,\beta\mu_q}{4}\left(\zeta + \mathbb{F}_1\right)^2 \ , \\
&\mathcal{G}_{0,1} = \frac{1}{8} + \frac{3}{2}\left(\zeta + \mathbb{F}_1\right)^2 - \frac{\beta\mu_q}{8}\left(\zeta + \mathbb{F}_1\right) - \beta\mu_q\left(\zeta + \mathbb{F}_1\right)^3 \ , \\
&\mathcal{G}_{1,0} = \frac{1}{8} + \frac{3}{2}\left(\zeta + \mathbb{F}_1\right)^2 + \frac{\beta\mu_q}{8}\left(\zeta + \mathbb{F}_1\right) + \beta\mu_q\left(\zeta + \mathbb{F}_1\right)^3 \ .
\end{aligned} \tag{D.15}$$

Note that the following is true,

$$\mathcal{G}_{r,s} = \mathcal{G}_{s,r}\Big|_{q\to -q} \ , \tag{D.16}$$

Note that the above statement is quite general as will see later.

First-derivative term $\mathcal{L}_1$: In the first derivative term, the time derivative can appear on any of the four sources. Thus, we can explicitly write $\mathcal{L}_1$ as,

$$\begin{aligned}
\mathcal{L}_1 = &\sum_{r=0}^{1}\sum_{s=0}^{2}\mathcal{G}_{\dot{r},s}\left(\partial_t \bar{J}_a\right)\left[\bar{J}_a\right]^r\left[J_a\right]^s\left[\bar{J}_d\right]^{1-r}\left[J_d\right]^{2-s} + \sum_{r=0}^{2}\sum_{s=0}^{1}\mathcal{G}_{r,\dot{s}}\left(\partial_t J_a\right)\left[\bar{J}_a\right]^r\left[J_a\right]^s\left[\bar{J}_d\right]^{2-r}\left[J_d\right]^{1-s} \\
&+ \sum_{r=0}^{1}\sum_{s=0}^{2}\mathcal{H}_{\dot{r},s}\left(\partial_t \bar{J}_d\right)\left[\bar{J}_a\right]^r\left[J_a\right]^s\left[\bar{J}_d\right]^{1-r}\left[J_d\right]^{2-s} + \sum_{r=0}^{2}\sum_{s=0}^{1}\mathcal{H}_{r,\dot{s}}\left(\partial_t J_d\right)\left[\bar{J}_a\right]^r\left[J_a\right]^s\left[\bar{J}_d\right]^{2-r}\left[J_d\right]^{1-s}
\end{aligned} \tag{D.17}$$

which in concise form is given by,

$$\begin{aligned}
\mathcal{L}_1 = &\sum_{r=0}^{1}\sum_{s=0}^{2}\left\{\mathcal{G}_{\dot{r},s}\left(\partial_t \bar{J}_a\right) + \mathcal{H}_{\dot{r},s}\left(\partial_t \bar{J}_d\right)\right\}\left[\bar{J}_a\right]^r\left[J_a\right]^s\left[\bar{J}_d\right]^{1-r}\left[J_d\right]^{2-s} \\
&+ \sum_{r=0}^{2}\sum_{s=0}^{1}\left\{\mathcal{G}_{r,\dot{s}}\left(\partial_t J_a\right) + \mathcal{H}_{r,\dot{s}}\left(\partial_t J_d\right)\right\}\left[\bar{J}_a\right]^r\left[J_a\right]^s\left[\bar{J}_d\right]^{2-r}\left[J_d\right]^{1-s}
\end{aligned} \tag{D.18}$$

where independent set of the terms are as follows:

$$\begin{aligned}
&\mathcal{G}_{\dot{1},2} = 0 \ , \qquad \mathcal{G}_{\dot{0},2} = \frac{i\beta}{4}\mathbb{F}_1 \ , \qquad \mathcal{G}_{\dot{1},1} = \frac{i\beta}{2}\mathbb{F}_1 \ , \\
&\mathcal{G}_{\dot{1},0} = \frac{i\beta}{2}\mathbb{F}_1(\mathbb{F}_1 + \zeta) \ , \qquad \mathcal{G}_{\dot{0},1} = i\beta\mathbb{F}_1(\mathbb{F}_1 + \zeta) \ , \\
&\mathcal{G}_{\dot{0},0} = \frac{i\beta}{4}\mathbb{F}_1\left(\frac{1}{4} + 3(\mathbb{F}_1 + \zeta)^2\right) \ .
\end{aligned} \tag{D.19}$$

Now, we turn to the independent terms involving $\dot{J}_d$ and they are explicitly given as,

$$
\begin{aligned}
\mathcal{H}_{\dot{1},2} &= -\frac{i\beta}{4}\left(\mathbb{F}_1 + 2\zeta\right) \ , \\
\mathcal{H}_{\dot{0},2} &= \frac{i\beta}{8}\Bigg\{ -2(\mathbb{F}_1+\zeta)(\mathbb{F}_1+3\zeta)\Bigg\}, \\
\mathcal{H}_{\dot{1},1} &= \frac{i\beta}{4}\Bigg\{ -2(\mathbb{F}_1+\zeta)(\mathbb{F}_1+3\zeta)\Bigg\}, \\
\mathcal{H}_{\dot{0},1} &= \frac{i\beta}{8}\Bigg\{ (-\mathbb{F}_1 - 4\mathbb{F}_1^3 - 2\zeta - 24\mathbb{F}_1^2\zeta - 36\mathbb{F}_1\zeta^2 - 16\zeta^3\Bigg\}, \\
\mathcal{H}_{\dot{1},0} &= \frac{i\beta}{16}\Bigg\{ (-\mathbb{F}_1 - 4\mathbb{F}_1^3 - 2\zeta - 24\mathbb{F}_1^2\zeta - 36\mathbb{F}_1\zeta^2 - 16\zeta^3\Bigg\}, \\
\mathcal{H}_{\dot{0},0} &= \frac{i\beta}{32}\Bigg\{ -2(\mathbb{F}_1+\zeta)(3\mathbb{F}_1 + 4\mathbb{F}_1^3 + 7\zeta + 28\mathbb{F}_1^2\zeta + 44\mathbb{F}_1\zeta^2 + 20\zeta^3)\Bigg\} \ ,
\end{aligned}
\tag{D.20}
$$

where all the remaining terms can be obtained from the following relation,

$$
\mathcal{G}_{r,\dot{s}} = \mathcal{G}_{\dot{s},r} \ , \qquad \mathcal{H}_{r,\dot{s}} = \mathcal{H}_{\dot{s},r} \ . \tag{D.21}
$$

Bibliography

[1] M. Ammon and J. Erdmenger, *Gauge/gravity duality: Foundations and applications*, Cambridge University Press, Cambridge (4, 2015), 10.1017/CBO9780511846373.

[2] J. Zaanen, Y. Liu, Y.-W. Sun and K. Schalm, *Holographic Duality in Condensed Matter Physics*, Cambridge University Press (2015), 10.1017/CBO9781139942492.

[3] S.A. Hartnoll, A. Lucas and S. Sachdev, *Holographic Quantum Matter*, MIT Press (2018), [1612.07324].

[4] J.M. Maldacena, *The Large N limit of superconformal field theories and supergravity*, *Adv. Theor. Math. Phys.* **2** (1998) 231 [hep-th/9711200].

[5] S.S. Gubser, I.R. Klebanov and A.M. Polyakov, *Gauge theory correlators from noncritical string theory*, *Phys. Lett. B* **428** (1998) 105 [hep-th/9802109].

[6] E. Witten, *Anti-de Sitter space and holography*, *Adv. Theor. Math. Phys.* **2** (1998) 253 [hep-th/9802150].

[7] O. Aharony, S.S. Gubser, J.M. Maldacena, H. Ooguri and Y. Oz, *Large N field theories, string theory and gravity*, *Phys. Rept.* **323** (2000) 183 [hep-th/9905111].

[8] H. Năstase, *Introduction to the AdS/CFT Correspondence*, Cambridge University Press (2015), 10.1017/CBO9781316090954.

[9] M. Natsuume, *AdS/CFT Duality User Guide*, vol. 903 of *Lecture Notes in Physics*, Springer (Tokyo) (2015), 10.1007/978-4-431-55441-7.

[10] E. Witten, *Anti-de Sitter space, thermal phase transition, and confinement in gauge theories*, *Adv. Theor. Math. Phys.* **2** (1998) 505 [hep-th/9803131].

[11] G. Policastro, D.T. Son and A.O. Starinets, *The Shear viscosity of strongly coupled N=4 supersymmetric Yang-Mills plasma*, *Phys. Rev. Lett.* **87** (2001) 081601 [hep-th/0104066].

[12] G. Policastro, D.T. Son and A.O. Starinets, *From AdS / CFT correspondence to hydrodynamics*, *JHEP* **09** (2002) 043 [hep-th/0205052].

[13] P. Kovtun, D.T. Son and A.O. Starinets, *Viscosity in strongly interacting quantum field theories from black hole physics*, *Phys. Rev. Lett.* **94** (2005) 111601 [hep-th/0405231].

[14] J. Casalderrey-Solana and D. Teaney, *Heavy quark diffusion in strongly coupled N=4 Yang-Mills*, *Phys. Rev.* **D74** (2006) 085012 [hep-ph/0605199].

[15] J. Casalderrey-Solana and D. Teaney, *Transverse Momentum Broadening of a Fast Quark in a N=4 Yang Mills Plasma*, *JHEP* **04** (2007) 039 [hep-th/0701123].

[16] D.T. Son and A.O. Starinets, *Viscosity, Black Holes, and Quantum Field Theory*, *Ann. Rev. Nucl. Part. Sci.* **57** (2007) 95 [0704.0240].

[17] D. Mateos, *String Theory and Quantum Chromodynamics*, *Class. Quant. Grav.* **24** (2007) S713 [0709.1523].

[18] S. Bhattacharyya, V.E. Hubeny, R. Loganayagam, G. Mandal, S. Minwalla, T. Morita et al., *Local Fluid Dynamical Entropy from Gravity*, *JHEP* **06** (2008) 055 [0803.2526].

[19] J. Casalderrey-Solana, H. Liu, D. Mateos, K. Rajagopal and U. Achim Wiedemann, *Gauge/String Duality, Hot QCD and Heavy Ion Collisions*, Cambridge University Press (2014), 10.1017/9781009403504, [1101.0618].

[20] M. Blake, Y. Gu, S.A. Hartnoll, H. Liu, A. Lucas, K. Rajagopal et al., *Snowmass White Paper: New ideas for many-body quantum systems from string theory and black holes*, 2203.04718.

[21] A.S.T. Pires, *AdS/CFT Correspondence in Condensed Matter*, Morgan & Claypool, San Rafael (2014), 10.1088/978-1-627-05309-9.

[22] A. Amoretti, *Condensed Matter Applications of AdS/CFT: Focusing on strange metals*, Ph.D. thesis, Genoa U., 2016.

[23] L.D. Landau, *The Theory of a Fermi Liquid*, *Zh. Eksp. Teor. Fiz.* **30** (1956) 1058.

[24] C.M. Varma, Z. Nussinov and W. Van Saarloos, *Singular or non-fermi liquids*, *Physics Reports* **361** (2002) 267.

[25] S.-S. Lee, *Recent Developments in Non-Fermi Liquid Theory*, *Ann. Rev. Condensed Matter Phys.* **9** (2018) 227 [1703.08172].

[26] C.M. Varma, P.B. Littlewood, S. Schmitt-Rink, E. Abrahams and A.E. Ruckenstein, *Phenomenology of the normal state of cu-o high-temperature superconductors*, *Phys. Rev. Lett.* **63** (1989) 1996.

[27] P.A. Lee, *From high temperature superconductivity to quantum spin liquid: progress in strong correlation physics*, *Reports on Progress in Physics* **71** (2007) 012501.

[28] T. Senthil, *Critical fermi surfaces and non-fermi liquid metals*, *Phys. Rev. B* **78** (2008) 035103.

[29] S. Sachdev, *Quantum Phase Transitions*, Cambridge University Press (4, 2011), 10.1017/cbo9780511973765.

[30] D.V. Else and T. Senthil, *Strange metals as ersatz fermi liquids*, *Physical Review Letters* **127** (2021) .

[31] P.W. Phillips, N.E. Hussey and P. Abbamonte, *Stranger than metals*, *Science* **377** (2022) .

[32] R. Mahajan, M. Barkeshli and S.A. Hartnoll, *Non-Fermi liquids and the Wiedemann-Franz law*, *Phys. Rev. B* **88** (2013) 125107 [1304.4249].

[33] T. Faulkner, H. Liu, J. McGreevy and D. Vegh, *Emergent quantum criticality, Fermi surfaces, and AdS(2)*, *Phys. Rev. D* **83** (2011) 125002 [0907.2694].

[34] T. Faulkner, N. Iqbal, H. Liu, J. McGreevy and D. Vegh, *Strange metal transport realized by gauge/gravity duality*, *Science* **329** (2010) 1043.

[35] T. Faulkner, N. Iqbal, H. Liu, J. McGreevy and D. Vegh, *From Black Holes to Strange Metals*, 1003.1728.

[36] N. Iqbal, H. Liu, M. Mezei and Q. Si, *Quantum phase transitions in holographic models of magnetism and superconductors*, *Phys. Rev. D* **82** (2010) 045002 [1003.0010].

[37] T. Faulkner and J. Polchinski, *Semi-Holographic Fermi Liquids*, *JHEP* **06** (2011) 012 [1001.5049].

[38] N. Iqbal, H. Liu and M. Mezei, *Semi-local quantum liquids*, *JHEP* **04** (2012) 086 [1105.4621].

[39] D. Vegh, *Holographic Fermi Surfaces Near Quantum Phase Transitions*, 1112.3318.

[40] N. Iqbal, H. Liu and M. Mezei, *Lectures on holographic non-Fermi liquids and quantum phase transitions*, in *Theoretical Advanced Study Institute in Elementary Particle Physics: String theory and its Applications: From meV to the Planck Scale*, pp. 707–816, 10, 2011, DOI [1110.3814].

[41] T. Faulkner, N. Iqbal, H. Liu, J. McGreevy and D. Vegh, *Charge transport by holographic Fermi surfaces*, *Phys. Rev. D* **88** (2013) 045016 [1306.6396].

[42] J. Polchinski, *Effective field theory and the Fermi surface*, in *Theoretical Advanced Study Institute (TASI 92): From Black Holes and Strings to Particles*, pp. 0235–276, 6, 1992 [hep-th/9210046].

[43] J. Polchinski, *Low-energy dynamics of the spinon gauge system*, *Nucl. Phys. B* **422** (1994) 617 [cond-mat/9303037].

[44] S.-S. Lee, *A Non-Fermi Liquid from a Charged Black Hole: A Critical Fermi Ball*, *Phys. Rev. D* **79** (2009) 086006 [0809.3402].

[45] S.-S. Lee, *Low energy effective theory of Fermi surface coupled with U(1) gauge field in 2+1 dimensions*, *Phys. Rev. B* **80** (2009) 165102 [0905.4532].

[46] H. Liu, J. McGreevy and D. Vegh, *Non-Fermi liquids from holography*, *Phys. Rev. D* **83** (2011) 065029 [0903.2477].

[47] C. Jana, R. Loganayagam and M. Rangamani, *Open quantum systems and Schwinger-Keldysh holograms*, *JHEP* **07** (2020) 242 [2004.02888].

[48] R. Loganayagam, K. Ray and A. Sivakumar, *Fermionic Open EFT from Holography*, 2011.07039.

[49] R. Loganayagam, K. Ray, S.K. Sharma and A. Sivakumar, *Holographic KMS relations at finite density*, *JHEP* **03** (2021) 233 [2011.08173].

[50] R. Loganayagam, M. Rangamani and J. Virrueta, *Holographic open quantum systems: toy models and analytic properties of thermal correlators*, *JHEP* **03** (2023) 153 [2211.07683].

[51] R.P. Feynman and F.L. Vernon, Jr., *The Theory of a general quantum system interacting with a linear dissipative system*, *Annals Phys.* **24** (1963) 118.

[52] D.T. Son and A.O. Starinets, *Minkowski space correlators in AdS / CFT correspondence: Recipe and applications*, *JHEP* **09** (2002) 042 [hep-th/0205051].

[53] K. Skenderis and B.C. van Rees, *Real-time gauge/gravity duality*, *Phys. Rev. Lett.* **101** (2008) 081601 [0805.0150].

[54] K. Skenderis and B.C. van Rees, *Real-time gauge/gravity duality: Prescription, Renormalization and Examples*, *JHEP* **05** (2009) 085 [0812.2909].

[55] C.P. Herzog and D.T. Son, *Schwinger-Keldysh propagators from AdS/CFT correspondence*, *JHEP* **03** (2003) 046 [hep-th/0212072].

[56] D.T. Son and D. Teaney, *Thermal Noise and Stochastic Strings in AdS/CFT*, *JHEP* **07** (2009) 021 [0901.2338].

[57] G.W. Gibbons and S.W. Hawking, *Action Integrals and Partition Functions in Quantum Gravity*, *Phys. Rev. D* **15** (1977) 2752.

[58] P. Glorioso, M. Crossley and H. Liu, *A prescription for holographic Schwinger-Keldysh contour in non-equilibrium systems*, 1812.08785.

[59] S.W. Hawking, *Particle Creation by Black Holes*, *Commun. Math. Phys.* **43** (1975) 199.

[60] B. Chakrabarty, J. Chakravarty, S. Chaudhuri, C. Jana, R. Loganayagam and A. Sivakumar, *Nonlinear Langevin dynamics via holography*, *JHEP* **01** (2020) 165 [1906.07762].

[61] S. Colin-Ellerin, X. Dong, D. Marolf, M. Rangamani and Z. Wang, *Real-time gravitational replicas: Formalism and a variational principle*, *JHEP* **05** (2021) 117 [2012.00828].

[62] J.K. Ghosh, R. Loganayagam, S.G. Prabhu, M. Rangamani, A. Sivakumar and V. Vishal, *Effective field theory of stochastic diffusion from gravity*, *JHEP* **05** (2021) 130 [2012.03999].

[63] Y. Bu, T. Demircik and M. Lublinsky, *All order effective action for charge diffusion from Schwinger-Keldysh holography*, *JHEP* **05** (2021) 187 [2012.08362].

[64] T. He, R. Loganayagam, M. Rangamani and J. Virrueta, *An effective description of momentum diffusion in a charged plasma from holography*, *JHEP* **01** (2022) 145 [2108.03244].

[65] T. He, R. Loganayagam, M. Rangamani, A. Sivakumar and J. Virrueta, *The timbre of Hawking gravitons: an effective description of energy transport from holography*, *JHEP* **09** (2022) 092 [2202.04079].

[66] T. He, R. Loganayagam, M. Rangamani and J. Virrueta, *An effective description of charge diffusion and energy transport in a charged plasma from holography*, *JHEP* **03** (2023) 161 [2205.03415].

[67] C. Pantelidou and B. Withers, *Thermal three-point functions from holographic Schwinger-Keldysh contours*, *JHEP* **04** (2023) 050 [2211.09140].

[68] R. Loganayagam, M. Rangamani and J. Virrueta, *Holographic thermal correlators: a tale of Fuchsian ODEs and integration contours*, *JHEP* **07** (2023) 008 [2212.13940].

[69] R. Loganayagam and O. Shetye, *Influence phase of a dS observer. Part I. Scalar exchange*, *JHEP* **01** (2024) 138 [2309.07290].

[70] R. Loganayagam and G. Martin, *An exterior EFT for Hawking radiation*, *JHEP* **06** (2025) 184 [2403.10654].

[71] G. Martin and S.K. Sharma, *Open EFT for Interacting Fermions from Holography*, 2403.10604.

[72] S.K. Sharma, *Holographic Fluctuation-Dissipation Relations in Finite Density Systems*, 2501.17852.

[73] R. Kubo, *Statistical mechanical theory of irreversible processes. 1. General theory and simple applications in magnetic and conduction problems*, *J. Phys. Soc. Jap.* **12** (1957) 570.

[74] P.C. Martin and J.S. Schwinger, *Theory of many particle systems. 1.*, *Phys. Rev.* **115** (1959) 1342.

[75] J. Rammer, *Quantum field theory of non-equilibrium states* (2007).

[76] F.M. Haehl, R. Loganayagam and M. Rangamani, *Schwinger-Keldysh formalism. Part I: BRST symmetries and superspace*, *JHEP* **06** (2017) 069 [1610.01940].

[77] J.S. Schwinger, *Brownian motion of a quantum oscillator*, *J. Math. Phys.* **2** (1961) 407.

[78] L. Keldysh, *Diagram technique for nonequilibrium processes*, *Zh. Eksp. Teor. Fiz.* **47** (1964) 1515.

[79] A. Kamenev, *Field Theory of Non-Equilibrium Systems*, Cambridge University Press (2011), 10.1017/CBO9781139003667.

[80] M.L. Bellac, *Thermal Field Theory*, Cambridge Monographs on Mathematical Physics, Cambridge University Press (3, 2011), 10.1017/CBO9780511721700.

[81] F. Gelis, *Quantum Field Theory*, Cambridge University Press (7, 2019), 10.1017/9781108691550.

[82] M.E. Peskin and D.V. Schroeder, *An Introduction to quantum field theory*, Addison-Wesley, Reading, USA (1995), 10.1201/9780429503559.

[83] M. Srednicki, *Quantum field theory*, Cambridge University Press (1, 2007), 10.1017/CBO9780511813917.

[84] H.-P. Breuer and F. Petruccione, *The Theory of Open Quantum Systems*, Oxford University Press (1, 2007), 10.1093/acprof:oso/9780199213900.001.0001.

[85] Rivas and S.F. Huelga, *Open Quantum Systems: An Introduction*, Springer Berlin Heidelberg (2012), 10.1007/978-3-642-23354-8.

[86] G.C. Giecold, *Fermionic Schwinger-Keldysh Propagators from AdS/CFT*, *JHEP* **10** (2009) 057 [0904.4869].

[87] B. Chakrabarty and A. P. M., *Open effective theory of scalar field in rotating plasma*, *JHEP* **08** (2021) 169 [2011.13223].

[88] A. Sivakumar, *Real Time Correlations and Complexified Horizons*, 2410.18188.

[89] Y. Bu and B. Zhang, *Schwinger-Keldysh effective action for a relativistic Brownian particle in the AdS/CFT correspondence*, *Phys. Rev. D* **104** (2021) 086002 [2108.10060].

[90] N. Ceplak, K. Ramdial and D. Vegh, *Fermionic pole-skipping in holography*, *JHEP* **07** (2020) 203 [1910.02975].

[91] N.D. Birrell and P.C.W. Davies, *Quantum Fields in Curved Space*, Cambridge Monographs on Mathematical Physics, Cambridge University Press, Cambridge, UK (1982), 10.1017/CBO9780511622632.

[92] L.E. Parker and D. Toms, *Quantum Field Theory in Curved Spacetime: Quantized Field and Gravity*, Cambridge Monographs on Mathematical Physics, Cambridge University Press (8, 2009), 10.1017/CBO9780511813924.

[93] M. Henningson and K. Sfetsos, *Spinors and the AdS / CFT correspondence*, *Phys. Lett. B* **431** (1998) 63 [hep-th/9803251].

[94] W. Mueck and K.S. Viswanathan, *Conformal field theory correlators from classical field theory on anti-de Sitter space. 2. Vector and spinor fields*, *Phys. Rev.* **D58** (1998) 106006 [hep-th/9805145].

[95] M. Henneaux, *Boundary terms in the AdS / CFT correspondence for spinor fields*, in *International Meeting on Mathematical Methods in Modern Theoretical Physics (ISPM 98)*, pp. 161–170, 9, 1998 [hep-th/9902137].

[96] N. Iqbal and H. Liu, *Real-time response in AdS/CFT with application to spinors*, *Fortsch. Phys.* **57** (2009) 367 [0903.2596].

[97] K.-c. Chou, Z.-b. Su, B.-l. Hao and L. Yu, *Equilibrium and Nonequilibrium Formalisms Made Unified*, *Phys. Rept.* **118** (1985) 1.

[98] S. Chaudhuri, C. Chowdhury and R. Loganayagam, *Spectral Representation of Thermal OTO Correlators*, *JHEP* **02** (2019) 018 [1810.03118].

[99] U. Moitra, S.K. Sake and S.P. Trivedi, *Near-Extremal Fluid Mechanics*, *JHEP* **02** (2021) 021 [2005.00016].

[100] A. Almheiri, T. Hartman, J. Maldacena, E. Shaghoulian and A. Tajdini, *The entropy of Hawking radiation*, *Rev. Mod. Phys.* **93** (2021) 035002 [2006.06872].

[101] R. Kubo, *The fluctuation-dissipation theorem*, *Rept. Prog. Phys.* **29** (1966) 255.

[102] E. Wang and U. Heinz, *Generalized fluctuation-dissipation theorem for nonlinear response functions*, *Phys. Rev. D* **66** (2002) 025008.

[103] N. Tsuji, T. Shitara and M. Ueda, *Out-of-time-order fluctuation-dissipation theorem*, *Phys. Rev. E* **97** (2018) 012101 [1612.08781].

[104] F.M. Haehl, R. Loganayagam, P. Narayan, A.A. Nizami and M. Rangamani, *Thermal out-of-time-order correlators, KMS relations, and spectral functions*, *JHEP* **12** (2017) 154 [1706.08956].

[105] B. Chakrabarty, S. Chaudhuri and R. Loganayagam, *Out of Time Ordered Quantum Dissipation*, *JHEP* **07** (2019) 102 [1811.01513].

[106] B. Chakrabarty and S. Chaudhuri, *Out of time ordered effective dynamics of a quartic oscillator*, *SciPost Phys.* **7** (2019) 013 [1905.08307].

[107] M. Rangamani, *Gravity and Hydrodynamics: Lectures on the fluid-gravity correspondence*, *Class. Quant. Grav.* **26** (2009) 224003 [0905.4352].

[108] V.E. Hubeny, S. Minwalla and M. Rangamani, *The fluid/gravity correspondence*, in *Theoretical Advanced Study Institute in Elementary Particle Physics: String theory and its Applications: From meV to the Planck Scale*, pp. 348–383, 2012 [1107.5780].

[109] J. de Boer, V.E. Hubeny, M. Rangamani and M. Shigemori, *Brownian motion in AdS/CFT*, *JHEP* **07** (2009) 094 [0812.5112].

[110] G.C. Giecold, E. Iancu and A.H. Mueller, *Stochastic trailing string and Langevin dynamics from AdS/CFT*, *JHEP* **07** (2009) 033 [0903.1840].

[111] J. Casalderrey-Solana and D. Teaney, *Transverse Momentum Broadening of a Fast Quark in a N=4 Yang Mills Plasma*, *JHEP* **04** (2007) 039 [hep-th/0701123].

[112] S. Chakrabortty, S. Chakraborty and N. Haque, *Brownian motion in strongly coupled, anisotropic Yang-Mills plasma: A holographic approach*, *Phys. Rev. D* **89** (2014) 066013 [1311.5023].

[113] P. Banerjee and B. Sathiapalan, *Holographic Brownian Motion in 1+1 Dimensions*, *Nucl. Phys. B* **884** (2014) 74 [1308.3352].

[114] J. Hubbard, *Calculation of partition functions*, *Phys. Rev. Lett.* **3** (1959) 77.

[115] R.L. Stratonovich, *On a Method of Calculating Quantum Distribution Functions*, *Soviet Physics Doklady* **2** (1957) 416.

[116] H. Kleinert, *Hubbard-Stratonovich Transformation: Successes, Failure, and Cure*, *arXiv e-prints* (2011) arXiv:1104.5161 [1104.5161].

[117] P.C. Martin, E.D. Siggia and H.A. Rose, *Statistical Dynamics of Classical Systems*, *Phys. Rev. A* **8** (1973) 423.

[118] L. Daguerre, *Boundary correlators and the Schwarzian mode*, *JHEP* **01** (2024) 118 [2310.19885].

[119] D. Birmingham, *Choptuik scaling and quasinormal modes in the AdS / CFT correspondence*, *Phys. Rev. D* **64** (2001) 064024 [hep-th/0101194].

[120] R. Loganayagam, G. Martin and S.K. Sharma, *Loops Outside a Black Hole*, 2509.03656.

[121] T. Colas, *Open Effective Field Theories for cosmology*, in *58th Rencontres de Moriond on Cosmology*, 5, 2024 [2405.09639].

[122] S.A. Salcedo, T. Colas, L. Dufner and E. Pajer, *An Open System Approach to Gravity*, 2507.03103.

[123] C. Sleight and M. Taronna, *From dS to AdS and back*, *JHEP* **12** (2021) 074 [2109.02725].

[124] V. Schaub, *Spinors in (Anti-)de Sitter Space*, *JHEP* **09** (2023) 142 [2302.08535].

[125] S. Bhattacharya and N. Joshi, *Decoherence and entropy generation at one loop in the inflationary de Sitter spacetime for Yukawa interaction*, *JCAP* **04** (2024) 078 [2307.13443].

[126] J. Polchinski, *String theory. Vol. 2: Superstring theory and beyond*, Cambridge Monographs on Mathematical Physics, Cambridge University Press (12, 2007), 10.1017/CBO9780511618123.

[127] P. West, *Introduction to strings and branes*, Cambridge University Press (7, 2012).

[128] D.Z. Freedman and A. Van Proeyen, *Supergravity*, Cambridge Univ. Press, Cambridge, UK (5, 2012).

[129] T. Ortin, *Gravity and Strings*, Cambridge Monographs on Mathematical Physics, Cambridge University Press, 2nd ed. ed. (7, 2015), 10.1017/CBO9781139019750.

[130] P. Arnold and D. Vaman, *4-point correlators in finite-temperature AdS/CFT: Jet quenching correlations*, *JHEP* **11** (2011) 033 [1109.0040].